General Disclaimer

One or more of the Following Statements may affect this Document

- This document has been reproduced from the best copy furnished by the organizational source. It is being released in the interest of making available as much information as possible.

- This document may contain data, which exceeds the sheet parameters. It was furnished in this condition by the organizational source and is the best copy available.

- This document may contain tone-on-tone or color graphs, charts and/or pictures, which have been reproduced in black and white.

- This document is paginated as submitted by the original source.

- Portions of this document are not fully legible due to the historical nature of some of the material. However, it is the best reproduction available from the original submission.

Produced by the NASA Center for Aerospace Information (CASI)

FINAL REPORT

ME-NSG-3109

SPECKLE TECHNIQUES FOR DETERMINING STRESSES IN MOVING OBJECTS

by

E. A. Murphree

T. F. Wilson

W. F. Ranson

W. F. Swinson

Technical Report to

NASA

Auburn University
Engineering Experiment Station
Auburn, Alabama 36830

(NASA-CR-157549) SPECKLE TECHNIQUES FOR DETERMINING STRESSES IN MOVING OBJECTS Final Report (Auburn Univ.) 151 p HC A08/MF A01 CSCL 20K

N78-30607

Unclas

G3/39 28615

FINAL REPORT

ME-NSG-3109

SPECKLE TECHNIQUES FOR DETERMINING STRESSES IN MOVING OBJECTS

by

E. A. Murphree

T. F. Wilson

W. F. Ranson

W. F. Swinson

Technical Report to

NASA

Auburn University
Engineering Experiment Station
Auburn, Alabama 36830

PREFACE

This final report under NASA NSG 3109 ME grant is composed of two parts.

Part I discusses theory relative to measuring inplane displacements using speckle interferometry. From the inplane displacement field, strains and stresses can be determined. This approach is potentially preferred over holographic techniques for evaluating stresses in rotating turbine or compressor blades because of the relative ease in collecting data, because the rigid body motion requirements are relaxed and because data interpretation is simpler.

Part II discusses theory relative to measuring derivatives of displacement fields by shearing speckle interferometry. The derivatives of displacements are closer to and in some cases are the strain fields. Therefore, stresses can be calculated directly. Again this approach 's potentially preferred over holographic techniques as noted above.

PART I

DETERMINATION OF IN-PLANE DISPLACEMENTS USING SPECKLE INTERFEROMETRY

TABLE OF CONTENTS

LIST OF TABLES. viii

LIST OF FIGURES ix

LIST OF SYMBOLS xi

I. INTRODUCTION. 1

II. DOUBLE EXPOSURE SPECKLE INTERFEROMETRY. 7

Basic Phenomena
Theory of Speckle Interferometry - Double Exposure - Single Beam Analysis
Optical Fourier Fringe Interpretation
Point-by-Point Data Interpretation
Experimental Verification

III. TIME AVERAGE SPECKLE INTERFEROMETRY 50

Basic Phenomena
Theory of Speckle Interferometry - Time Averaging - Single Beam Analysis
Optical Fourier Fringe Interpretation
Point-by-Point Data Interpretation
Numerical Example - Vibrating Cantilever Beam

IV. CONCLUSION. 71

REFERENCES. 72

LIST OF TABLES

1. Example 1 - Cantilever Beam - Point-by-Point Interpretation for Vertical Displacement. 33

2. Example 1 - Cantilever Beam - Whole Field Interpretation for Vertical Displacement. 34

3. Example 1 - Cantilever Beam - Theoretical Results for Vertical Displacements. 35

4. Example 2 - Pressure Vessel - Point-by-Point Interpretation for Horizontal Displacement. 46

5. Example 2 - Pressure Vessel - Whole Field Interpretation for Horizontal Displacement. 46

6. Example 2 - Pressure Vessel - Theoretic Results for Horizontal Displacement 47

7. Zero Values for $J_o(x)$. 56

8. Ratio of Amplitude/Tip Deflection. 60

LIST OF FIGURES

1. Illumination Conditions for Out of Plane Measurement - Dual Beam. 4

2. Illumination Conditions for In-plane Measurement - Dual Beam. 4

3. Effect of Aperture Opening on Speckle Size (150X). 8

4. Arrangement for Analysis of the Specklegram - Point-by-Point Interpretation. 10

5. Arrangement for Transform Analysis of the Specklegram. 12

6. Arrangement for Single Beam Analysis 13

7. Arrangement for Fringe Interpretation - Whole Field Technique. 20

8. Technique for Determining P, Z, X and θ. 23

9. Experimental Setup for Taking a Specklegram. 24

10. Schematic of Experimental Setup for Recording Specklegram. . . 25

11. Whole-Field Fringe Analyzer. 26

12. Example 1 - Cantilever Beam. 28

13. Fixed end Condition for Cantilever Beam. 30

14. Method of Load Application and Measurement of δ. 30

15. Schematic of Experimental Setup for Example 1. 31

16. Vertical Displacement for Example 1 as Determined from Theory, Point-by-Point and Whole Field, δ = .003 inches. . . . 36

17. Vertical Displacement for Example 1 as Determined from Theory, Point-by-Point and Whole Field, δ = .006 inches. . . . 37

18. Diffraction Halo and Fringes for Cantilever Beam, δ = .003 inches. 38

19. Fringes from Whole Field Interpretation for Cantilever Beam, δ = .003 inches. 39

20. Fringes from Whole Field Interpretation for Cantilever Beam, δ = .006 inches. 40

21. Example 2 - Pressure Vessel 42

22. Dimensions for Pressure Vessel 44

23. Fringes from Whole Field Interpretation for Pressure Vessel, ΔP = 400 psi 48

24. Horizontal Displacement for Example 2 as Determined from Theory, Point-by-Point and Whole Field, ΔP = 400 psi 49

25. Numerical Example - Vibrating Cantilever Beam. 63

26. Fringe Spacing as a Function of In-Plane Displacement 64

27. Variation of Fringe Order along the Beam for the First Mode of Vibration. 65

28. Variation of Fringe Order along the Beam for the Second Mode of Vibration 66

29. Fringe Location on Cantilever Beam for First Mode of Vibration 67

30. Fringe Location on Cantilever Beam for Second Mode of Vibration. 67

31. In-Plane Displacement as a Function of Fringe Spacing for the Numerical Example. 68

32. Fringe Spacing Along the Beam for the First Mode of Vibration. 69

33. Fringe Spacing Along the Beam for the Second Mode of Vibration 70

LIST OF SYMBOLS

$\overline{A}$	amplitude factor
a	photographic film constant
b	photographic film constant
$\overline{E}$	complex light amplitude
$\overline{E}^*$	complex conjugate of $\overline{E}$
E	modulus of elasticity
$F[A^2]$	Fourier Transform of A^2
G	amplitude transmission in the transform plane
G^*	complex conjugate of G
g	amplitude transmission
H and D	Hurter-Driffield
$J_o(x)$	zero-order Bessel Function
l	length of cantilever beam
M	magnification factor
p, P	distance from center line to aperture
ΔP	pressure change
R	radius of cylinder
ΔR	change in radius
u	displacement of the object
u_f	displacement in the film plane
t	thickness of cylinder
$\overline{X}$	distance between fringes
z	distance between spherical mirror and transform plane

δ	deflection
ε_r	radial strain
θ	phase angle of the light source
$\Delta\theta$	relative change in the phase angle
λ	wavelength of the light source
ν	Poisson's ratio
ω	frequency
ω_r	natural frequency
ρ	density

I. INTRODUCTION

Conventional methods of measuring surface strains and displacements utilize strain gages, dial gages and various other mechanical and electrical sensing devices. The major limitation to these systems is the information obtained is for a limited region only. In order to determine the displacement or strain field for the entire object, a large number of separate measurements must be obtained which is generally time consuming, costly and, in some instances, critical areas may be missed.

In recent years, optical techniques employing a coherent light source (laser) for detecting and measuring the components of surface displacement and strain have come into use. The primary advantage of these techniques is that the entire displacement or strain field can be determined completely. The majority of these techniques fall into three categories: Moire' gauging, holography and laser speckle interferometry. The method employed in this report is laser speckle interferometry.

Moire' technique consists of attaching or projecting a grid pattern on an object, then photographing the surface of the object before and after deformation, and observing the interference fringes produced by the overlapping grid pattern [1, 2]*. This particular method has the disadvantage that, somehow, a fine grid pattern must

---

* Numbers in the brackets refer to the references listed at the end.

be generated and superimposed on the test surface and the photographic system used to record the image must be of a high sensitivity to be capable of resolving the grid system.

Ennos [3] measured in-plane surface strain using holographic interferometry. The principal advantage of this method is the fact that it is a very sensitive method of measurement, and the whole surface of the structure can be investigated at the same time, rather than a point-by-point. Although well suited for measuring normal movements, there is no general way of eliminating the effect of normal movements from in-plane movements. Also, holographic techniques have the disadvantage that they require several separate views of the holographic fringe patterns of the surface, which requires a considerable amount of data reduction to separate out the in-plane displacement field.

Laser speckle interferometry is a relatively new experimental technique which shows promise of alleviating many difficult problems in experimental mechanics. The method utilizes simple high-resolution photographs of the surface which is illuminated by coherent light. The result is a real-time or permanently stored whole-field record of interference fringes which yields a map of displacements in the object. Suggestions for the direct use of coherent light, in displacement metrology and contour mapping first appeared in 1968 [4]. Burch and Tokarski [5] showed that if two identical speckle patterns are superimposed on a photographic plate translated laterally by a short distance between exposures, then the diffraction halo generated by the processed plate will consist of a pattern of parallel straight fringes

similar to Young's fringes. The diffraction halo observed through a small area of the recorded image will correspond to the local displacement at the corresponding point on the object and the direction of the fringes will be orthogonal to the direction of the local displacement vector. Also, Burch and Tokarski [5] showed that by optically illuminating the developed photographic plate with a converging spherical wave, the entire surface could be analyzed at one time to determine the displacement field of the surface.

Leendertz [6] developed a technique utilizing laser speckle effect for measuring either normal or in-plane components of displacement over an entire surface at one time. For measurement of normal (out-of-plane) displacement two surfaces are coherently illuminated and two separate speckle patterns are obtained (Figure 1). For measurement of the in-plane components of displacement, a surface is illuminated by two beams of coherent laser light, symmetrically disposed about the normal to the surface as illustrated schematically in Figure 2. These two speckle patterns are superimposed and the resultant speckle pattern is recorded on film. The intensity distribution of the resultant speckle pattern depends on the relative phases of the component patterns. Then one or both speckle patterns is changed and again the resultant speckle pattern is recorded on the same photographic film. By measuring correlation between the resultant pattern at two different times, a change of relative phase is detected, which in turn gives a measure of surface displacements. These correlation fringes are observed either in real-time or by combining two transparences having resultant speckle pattern at two different times and illuminating it in a Fourier filter system. A major drawback of

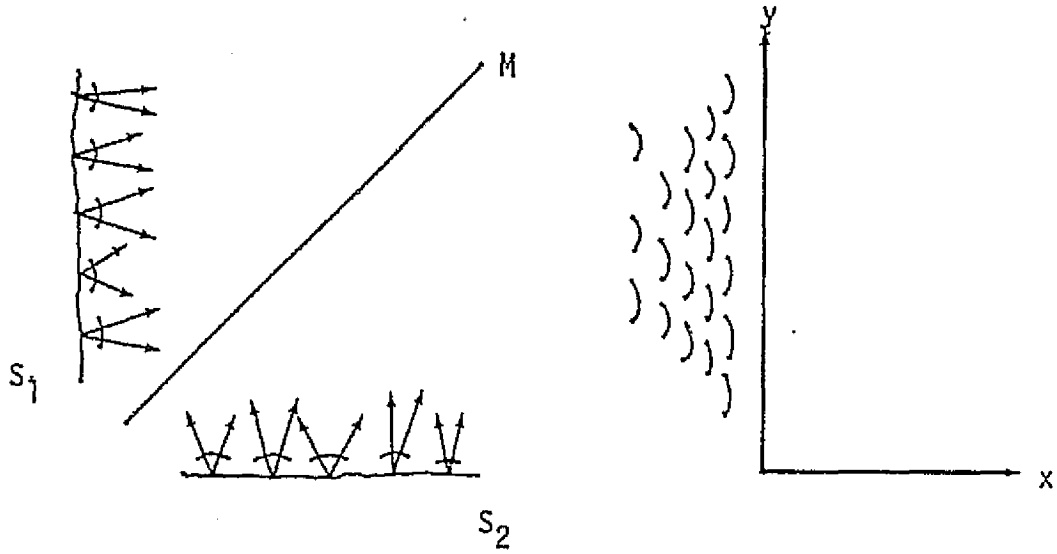

Figure 1. Illumination Conditions for Out of Plane Measurement - Dual Beam

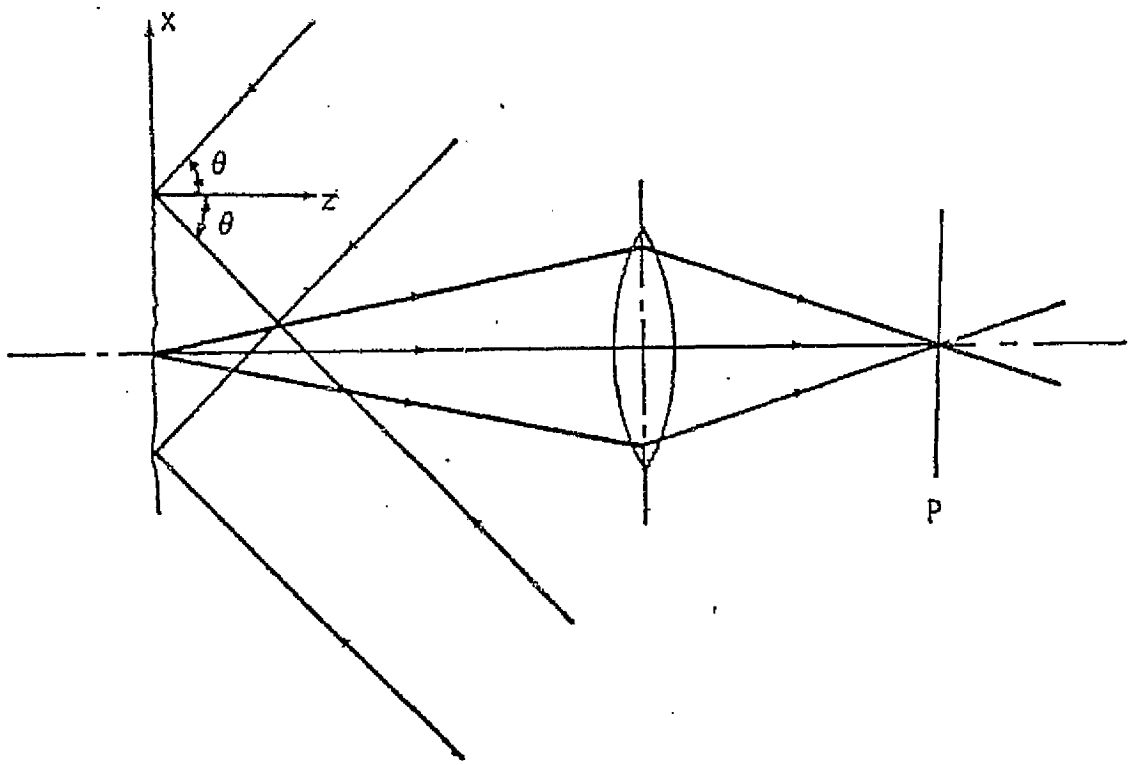

Figure 2. Illumination Conditions for In-plane Measurement - Dual Beam

this technique is the path length difference between the two illuminating beams has to be less than the coherence length of the light used to generate correlation fringes.

Duffy [7] presented two methods for measuring in-plane surface displacements. In the first method, this displacement was determined by photographing a coherently illuminated object through two laterally displaced apertures. The displacement is displayed as a pattern of Moire' fringes over the image of the surface. Thus there is no need for scanning of the beam on a point by point basis. As the surface is illuminated by only a single laser beam, the implementation problems associated with the dual-beam technique (mechanical stability and equal path lengths between the various optical components) are minimized. In the second method, the object is illuminated using a single laser beam and photographed via a double exposure before and after displacement. The Fourier transform of the doubly exposed transparency was obtained optically by illuminating the photographic plate with a converging spherical wave. The main advantage of this procedure is that the whole-field displacement can be analyzed and by appropriate position of a set of apertures in the transform plane any component of the displacement normal to the line of sight can be detected and with variable sensitivity. This thesis presents the mathematical analysis which describes the formation of fringes for both the whole field and point-by-point method of data reduction.

In addition, research has recently been conducted into the use of laser speckle interferometry [8, 9, 10, 11] for vibrational analysis. In this thesis, the time-average theory using the Fourier transform

is developed to present the application of this technique to measurement of in-plane displacement induced by the vibration of an object.

II. DOUBLE EXPOSURE SPECKLE INTERFEROMETRY

2.1 Basic Phenomena

When using a coherent laser light for illumination, a uniformly diffuse surface has a speckle or grainy appearance due to random interference within the resolution of the eye (or photographic system). Additionally, any point in front of this surface will receive contributions from all points on the surface which have similar amplitude but random phases. Thus the amplitude and phase of the radiation field in front of the object vary in a random manner from point to point with the average intensity being the same as if the light were incoherent. This phenomenon is known as the speckle effect and has been investigated by several authors [12]. When an imaging system is used, the size of the speckle in the image plane is inversely proportional to the aperture because intensity variations cannot be produced inside distances less than the Airy disk diameter [13]. The speckle appearance of an illuminated object and the effect of aperture on speckle size is illustrated in Figure 3.

The speckle effect provides a sensitive method for measuring displacements and strains on the surface of an object. The correlation between the relative phases of speckle patterns of a coherently illuminated object, at two different times, is the basic principle of the Leendertz technique [6]. With this technique, a double exposure specklegram (photo-negative) is made of the illuminated surface before

ORIGINAL PAGE IS
OF POOR QUALITY

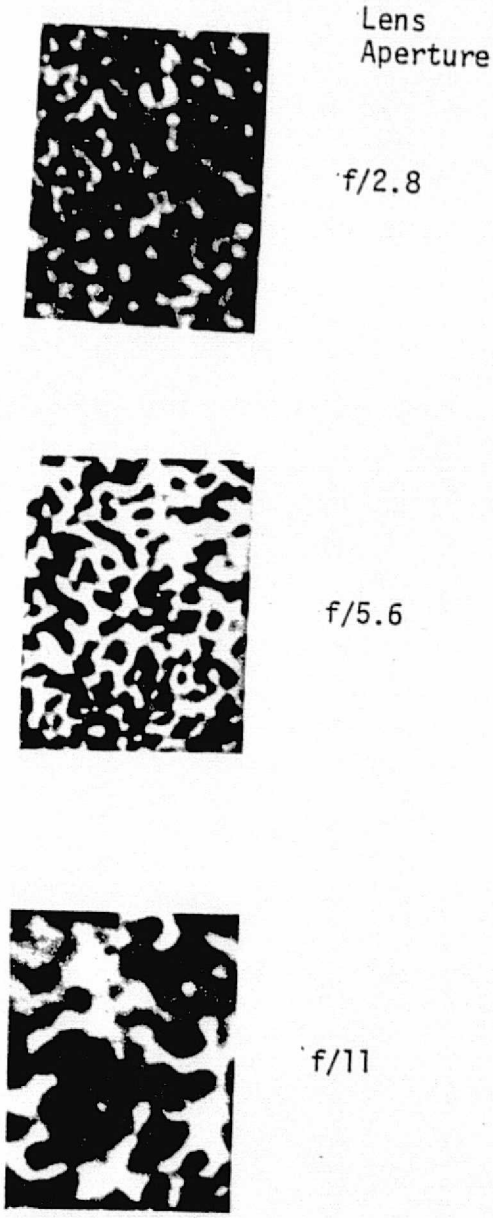

Figure 3. Effect of Aperture Opening on Speckle Size (Enlarged 150X)

and after deformation. Thus, each bright "speckle point" is recorded on the specklegram as two dark points: one in the undisplaced position and the other in the displaced position. Finally, only knowledge of the photographic magnification factor is required to determine the local in-plane displacement once the length and direction of the line segment between two speckle points are known.

In this report, the major emphasis is placed upon the "whole-field" interpretation of Young's fringes and comparison of the results to the "point by point" interpretation. The theory presented here extends works conducted by Burch and Tokarski [5] and Duffy [7] in the interpretation and data collection of the fringes.

One method for determing displacements from the specklegram, as presented by Kinariwala [14], is to direct a narrow collimated laser beam through the specklegram. Diffraction will modify the emerging light rays into a cone. This "diffraction halo" is the result of diffraction from the random distribution of small speckles. Since the speckles are recorded in pairs (displaced and undisplaced), a parallel fringe pattern (Young's fringes) also occur in the "diffraction halo", (Figure 4). From these fringes, displacement at a point can be determined. Thus, the entire in-plane displacement field can be determined by mapping the surface on a point-by-point basis. The number of points analyzed is dependent upon the type of analysis conducted. To decrease the uncertainty in the displacement field, more points would have to be analyzed.

In the second method of data interpretation, a converging spherical wave of coherent light is passed through the specklegram resulting in

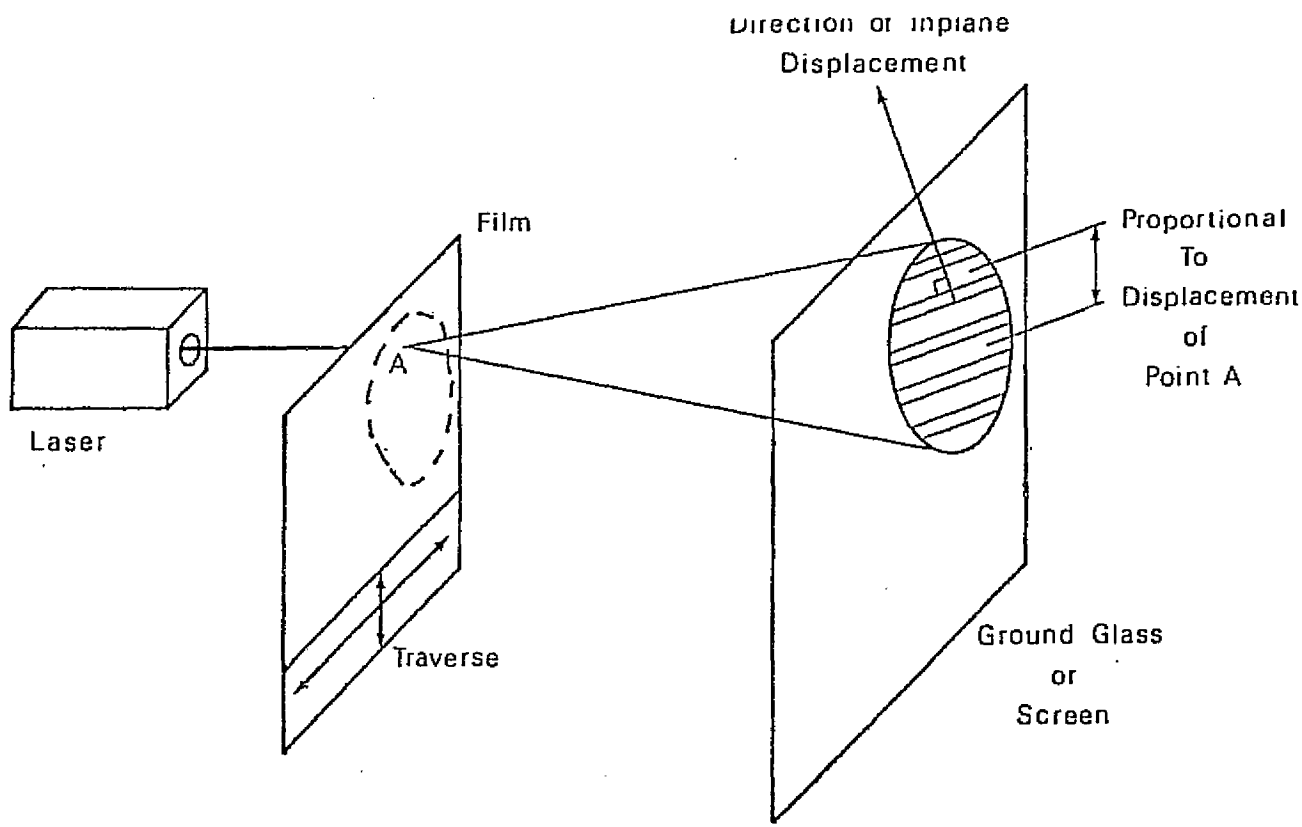

Figure 4. Arrangement for Analysis of the Specklegram - Point-by-Point Interpretation

the specklegram being imaged in the transform plane as shown in Figure 5. Using this "whole field" technique, the displacement field of the entire surface in any direction can be determined with a single photograph. The sensitivity of the displacement magnitude is dependent upon the amount of offset of the aperture, p, in the transformed plane; while the displacement component orientation depends upon the angle between the focal point in the transform plane and the aperture. For example, with a zero angle between the two, only horizontal in-plane motion would be measured. While with a 90° angle, only vertical in-plane motion would be measured.

2.2 Theory of Speckle Interferometry - Double Exposure - Single Beam Analysis

Consider the arrangement shown in Figure 6. An object is illuminated by a single laser beam (monochromatic and coherent). The location of the light source is shown as S which illuminates a point P on the surface of the object. In this analysis, the "double-exposure" technique for obtaining the specklegram is used, meaning that initially an exposure of the undeformed surface is taken, then the surface is deformed and another exposure is taken on the photographic plate. In this development, the intensity distribution on the photographic plate is investigated and, using the results of this analysis, the in-plane displacement of the exposed surface is determined.

From the first exposure, the complex light amplitude can be expressed as

$$\overline{E}\,(x_1,x_2) = \overline{A}\,(x_1,x_2)\,\exp\,[i\Theta\,(x_1,x_2)] \qquad (2.1)$$

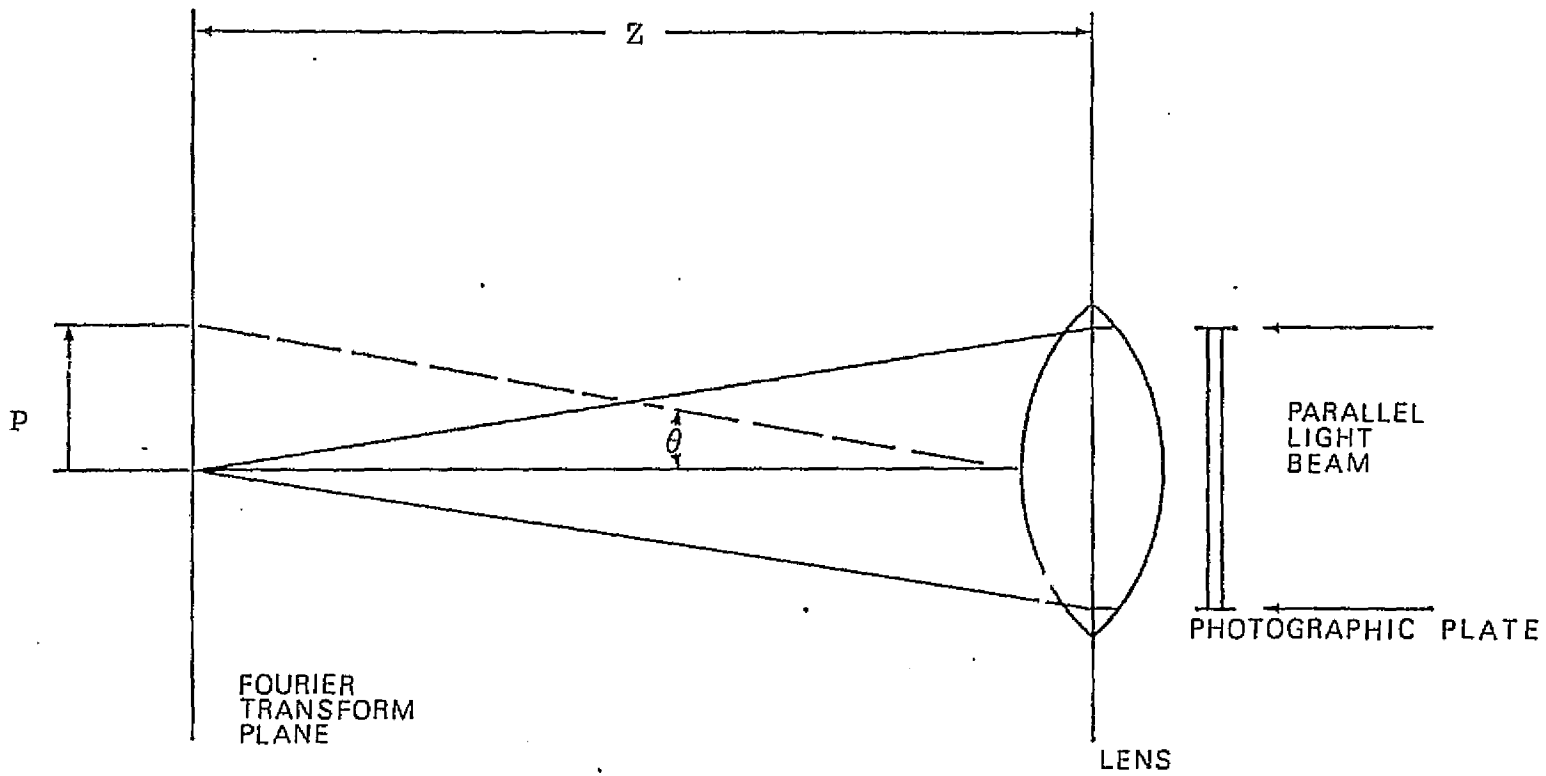

Figure 5. Arrangement for Transform Analysis of the Specklegram

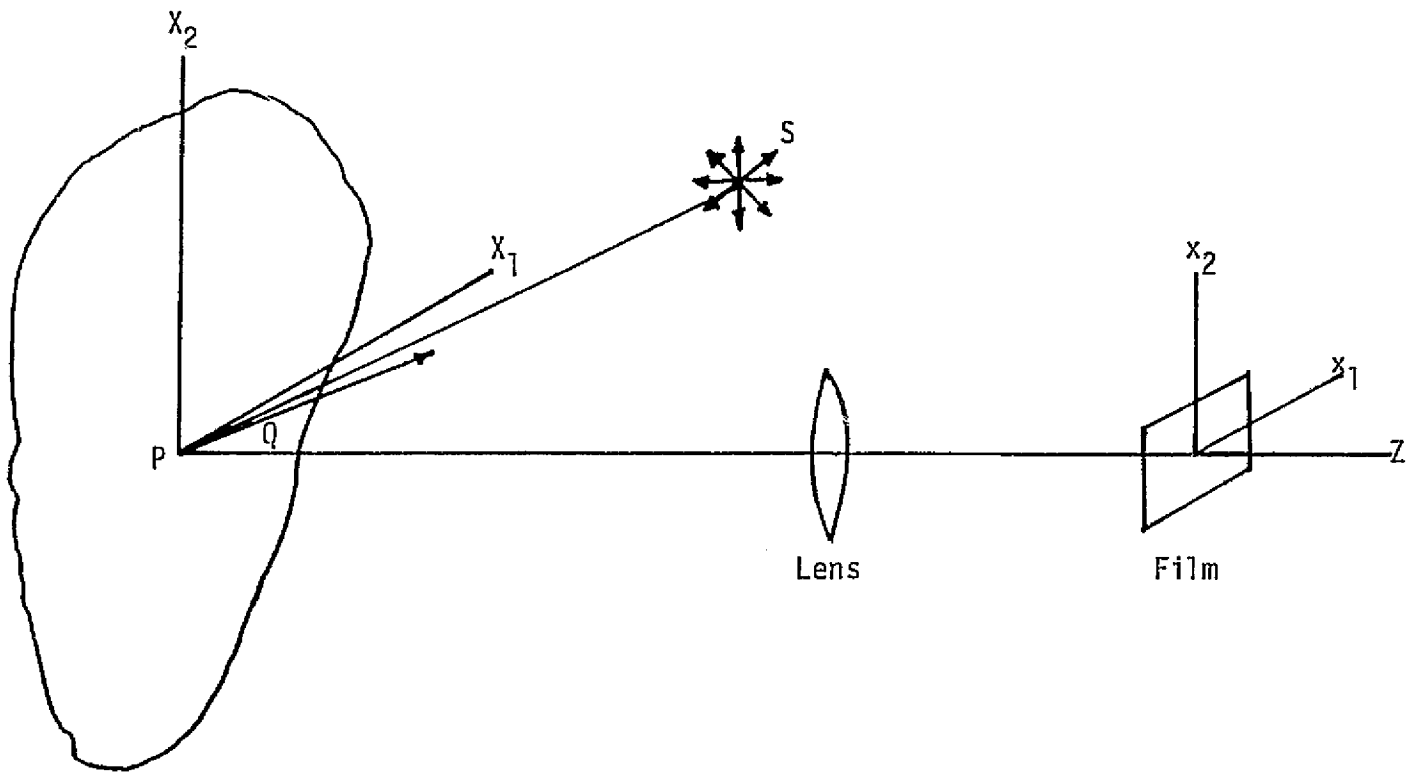

Figure 6. Arrangement for Single Beam Analysis

where

(x_1, x_2) - Film plane coordinates

$\theta(x_1, x_2)$ - Relative phase at each location on the film

$\overline{A}(x_1, x_2)$ - Amplitude factor

The intensity of the first exposure is given by

$$I_1 = \overline{E}_1 \overline{E}_1^* \tag{2.2}$$

where E_1^* is the complex conjugate of E_1

$$I_1 = \overline{A}(x_1, x_2) \exp[i\theta(x_1, x_2)] \overline{A}(x_1, x_2) \exp[-i\theta(x_1, x_2)] \tag{2.3}$$

$$I_1 = A^2(x_1, x_2) \tag{2.4}$$

For the second exporure, each point on the body is displaced to a new position; therefore, the exposure is

$$E_2(x_1', x_2') = \overline{A}(x_1', x_2') \exp[i\theta(x_1', x_2')] \tag{2.5}$$

and the intensity is

$$I_2 = A^2(x_1', x_2') \tag{2.6}$$

Thus, the total intensity on the photographic plate is the total of I_1 and I_2.

$$I_T = I_1 + I_2 \tag{2.7}$$

$$I_T = A^2(x_1, x_2) + A^2(x_1', x_2') \tag{2.8}$$

What is needed is to relate this intensity distribution to the displacement of the surface. In the first exposure, the point P is at coordinate (x_1, x_2). For the second exposure, the point P is displaced to point Q and is imaged on the film plane at coordinate (x_1', x_2'). The displacement vector on the surface of the object, represented by $\overline{PQ}$, is

$$\overline{PQ} = u_1\overline{e}_1 + u_2\overline{e}_2 \tag{2.9}$$

and the displacement vector in the film plane is

$$[\overline{PQ}]_{\text{Film Plane}} = u_{1f}\bar{e}_1 + u_{2f}\bar{e}_2 \tag{2.10}$$

and the displacement in the film plane in relation to the object is

$$u_{1f} = Mu_1 \tag{2.11-1}$$

$$u_{2f} = Mu_2 \tag{2.11-2}$$

where M is the film magnification factor, usually less than 1. Therefore, it follows that the film plane coordinates for the second exposure is given by

$$x_1' = x_1 + u_{1f} \tag{2.12-1}$$

$$x_2' = x_2 + u_{2f} \tag{2.12-2}$$

With these two relations, the total intensity given in Equation (2.8) can be rewritten as

$$I_T = A^2\ (x_1,\ x_2) + A^2\ (x_1 + u_{1f},\ x_2 + u_{2f}) \tag{2.13}$$

If the exposure $E(x_1,\ x_2)$ at each point of the plate represents small fluctuations which are mostly confined to the toe and the bottom portion of the H and D curve, the amplitude transmission $g(x_1,\ x_2)$ of the photographic plate is approximately a linear function of the exposure i.e.

$$g(x_1,\ x_2) = a + b\ I_T \tag{2.14}$$

where a and b are constants of the photographic film. With the result in eq (2.13) this can be written as

$$g(x_1,\ x_2) = a + b\ [A^2\ (x_1,\ x_2) + A^2\ (x_1 + u_{1f},\ x_2 + u_{2f})] \tag{2.15}$$

This expression gives the relationship between transmissivity and intensity in terms of the displacements in the film plane. The next step in the analysis is to relate the displacement in the film plane to some measurable quantities. In this development, the "whole field" interpretation of the fringes was used in the determination of displacement.

2.3 Optical Fourier Fringe Interpretation

The whole field fringes are obtained by taking optically the Fourier transform of the amplitude transmission function $g(x_1, x_2)$ of the specklegram [5]. To simplify the notation, the x_2 coordinate will be suppressed in the following development, i.e.

$$g(x) = a + b\,[A^2\,(x) + A^2\,(x + u_f)] \tag{2.16}$$

This optical transform is accomplished by illuminating the specklegram with a converging spherical wave as shown in Figure 5. Neglecting aberrations, the light amplitude $G(w)$ in the transform plane is proportional to the Fourier transform of $g(x)$ times a quadratic phase factor [5] as given by the following equation

$$G(w) = \exp\left(\frac{izw^2}{2k}\right) \int g(x)\,\exp\,(-iwx)\,dx \tag{2.17-1}$$

where

$$w = \frac{kp}{z} = k\,\tan\,\theta \tag{2.17-2}$$

where p is the coordinate of the iris in the transform plane and $k = 2\pi/\lambda$, where λ is the wave length of the converging beam and θ is defined in Figure 5. The direction of the laser beam and the common axis of the lenses L_1 and L_2 are assumed perpendicular to the

transform plane and to the plane of the specklegram. Equation (2.17-1) follows from the Kirchoff diffraction formula which was derived by Burch and Tokarski [5]. Eq (2.16) can be rewritten as

$$G(w) = \exp\left[\frac{izw^2}{2k}\right] \int \{a + b\,[A(x) + A(x + u_f)]\} \exp(-iwx)dx \tag{2.18}$$

$$G(w) = a \exp\left[\frac{izw^2}{2k}\right] \int \exp(-iwx)dx + b \exp\left[\frac{izw^2}{2k}\right] \int [A^2(x) + A^2(x + u_f)] \exp(-iwx)dx \tag{2.19}$$

The first integral in eq (2.19) is the delta function, $\delta(w)$; therefore,

$$G(w) = a \exp\left[\frac{izw^2}{2k}\right] \delta(w) + b \exp\left[\frac{izw^2}{2k}\right] \int [A^2(x) + A^2(x + u_f)] \exp(-iwx)dx \tag{2.20}$$

Equation (2.20) can be written in the following form with the application of the shift theorem.

$$G(w) = a \exp\left[\frac{izw^2}{2k}\right] \delta(w) + b \exp\left[\frac{izw^2}{2k}\right] [1 + \exp(-iwu_f)] \int A^2(x) \exp(-iwx)dx \tag{2.21}$$

The last integral is the definition of the Fourier Transform of $A^2(x)$ and is represented as $F[A^2]$ which leads to

$$G(w) = a \exp\left[\frac{izw^2}{2k}\right] \delta(w) + b \exp\left[\frac{izw^2}{2k}\right] F[A^2] [1 + \exp(-iwu_f)] \tag{2.22}$$

The delta function represents the (idealized) point focus of the illuminating beam. It contributes to the diffracted amplitude only at the point w=0; in practice, it is a small area around the point. Outside this small area, the delta function is zero and G(w) is given by

$$G(w) = b \exp\left[\frac{izw^2}{2k}\right] F[A^2] [1 + \exp(-iwu_f)] \tag{2.23}$$

The next step in the development is to determine the intensity function in the transformed plane which is

$$I_F = G(w)\ G^*(w) \tag{2.24}$$

where $G^*(w)$ is the complex conjugate of $G(w)$

$$I_F = \left(b \exp \left[\frac{izw^2}{2k} \right] F\,[A^2]\,[1 + \exp(-iwu_f)] \right)$$

$$\left(b \exp \left[\frac{-izw^2}{2k} \right] F\,[A^2]\,[1 + \exp(iwu_f)] \right) \tag{2.25}$$

$$I_F = b^2\ F\,[A^2]^{\,2}\ [2 + \exp(-iwu_f) + \exp(iwu_f)] \tag{2.26}$$

Using the trigometric identity

$$\cos(wu_f) = \frac{\exp(iwu_f) + \exp(-iwu_f)}{2} \tag{2.27}$$

the final expression for the intensity is

$$I_F = 2b^2\ F[A^2]\ (1 + \cos wu_f) \tag{2.28}$$

A fringe will be defined when the intensity, I_F, is equal to zero. Since b and $F\,[A^2]$ are both nonzero, fringes will occur when

$$[1 + \cos wu_f] = 0 \tag{2.29}$$

or

$$\cos wu_f = -1 \tag{2.30}$$

which means

$$wu_f = (2n - 1)\pi \qquad n = 1, 2, 3, \ldots, \infty \tag{2.31}$$

With the use of eq (2.17-2), eq (2.31) can be put in the following form

$$\frac{2\pi p u_f}{\lambda z} = (2n - 1)\ \pi \tag{2.32}$$

or

$$u_f = \left(n - \frac{1}{2}\right)\ \frac{\lambda z}{p} \tag{2.33}$$

Eq (2.33) expresses the in-plane displacement in the film plane in terms

of quantities which can be measured in the transform plane. Finally, the displacement of the deformed surface is given by

$$u = \frac{u_f}{m} \tag{2.34}$$

$$u = (n - \frac{1}{2}) \left(\frac{\lambda z}{mp} \right) \tag{2.35}$$

Information at location p is selected by placing an aperture to pass only the light in the immediate neighborhood of p as shown in Figure 7. Cloud [12] reported that an aperture opening of approximately one-tenth the amount by which the aperture is displaced from the optical axis gives the best results. This light is then imaged on film. Thus p being fixed, the image fringe information is proportional to u_f as shown in eq (2.33). The direction of the measured displacement is determined by the relation of p with the u- and v- axis as shown in Figure 7. In order to measure the horizontal displacement, the aperture is moved along the u-axis and to determine the vertical displacement, the iris is moved along the v-axis with movement always starting from the focal point in the transformed plane. Thus, in-plane displacement in any direction can be determined by appropriate selection of the aperture coordinates. Eq (2.33) illustrates that the sensitivity of the displacement determination is based on the distance of the aperture from the focal point, p. An increase in p causes an increase in the sensitivity of the measurement; however, due to the resolution limit of the film and the relative width of the fringes, the sensitivity of this technique is limited, dependent upon the amount of total displacement.

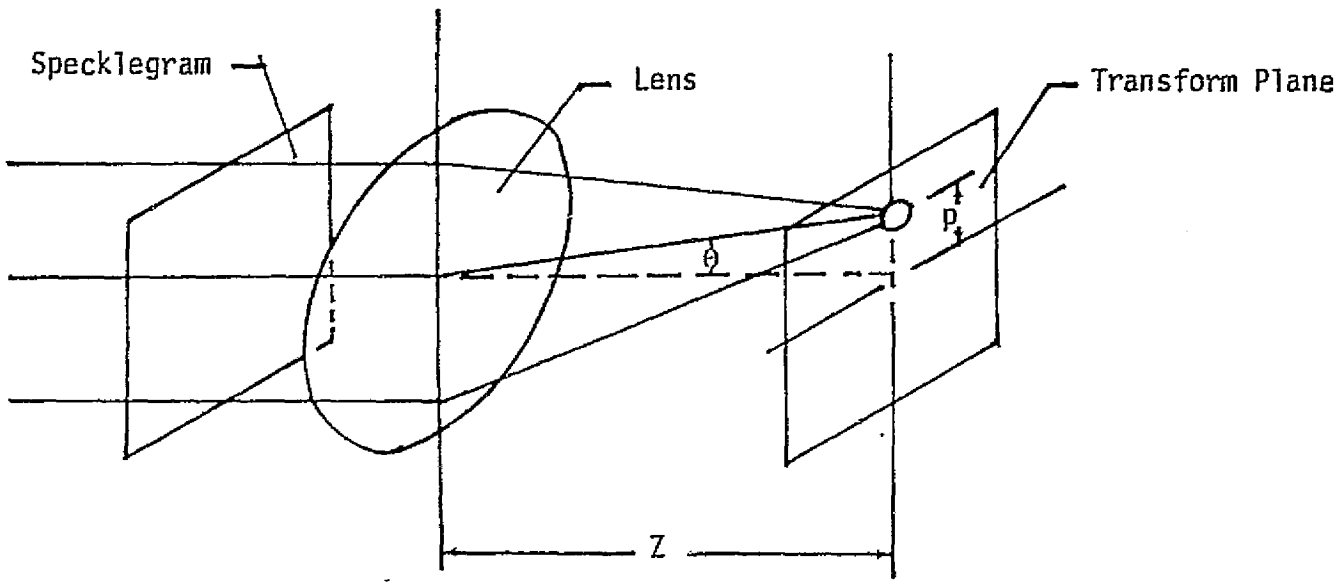

Figure 7. Arrangement for Fringe Interpretation - Whole Field Technique

2.4 Point-by-Point Data Interpretation

The point-by-point data interpretation can also be determined from eq (2.33). Figure 8 is a schematic of the point-by-point data analyzer. A narrow beam of coherent light is passed through a region of the film and fringes occur in the observation plane. To correctly interprete these fringes, a reexamination of eq (2.33) is needed. In the development of the transformed light amplitude (eq 2.17-1), integration over the entire film plane was conducted. For the point-by-point analysis, this intensity relation is zero except in the narrow region of the film through which the light passes. The in-plane film displacement is given by eq (2.33)

$$u_f = (n - \frac{1}{2}) \frac{\lambda z}{p}$$

For this case, the in-plane displacement is constant with p being the variable. From the worked conducted by Kinariwala [14], the expression for the in-plane film displacement for n = 1

$$u_f = \frac{\lambda z}{X} \tag{2.36}$$

where

λ - wavelength length of light source

z - distance from film plane to observation plane

X - distance between fringes

For the case of n = 1, eq (2.33)

$$u_f = \frac{\lambda z}{2p} \tag{2.37}$$

An examination of the last two equations, shows the displacement determined from eq (2.36) to be twice eq (2.37). However, this difference arises in the measurement of X and p. The distance X is measured between the fringes while p is measure from the center of

the halo to the nearest fringe. Figure 8 presents these two measurements. Thus, for the case of $n = 1$,

$$X = 2p \tag{2.38}$$

and the two equations are equivalent.

2.5 Experimental Verifications

Results of experimental verifications of the development in section 2.3 are reported in this section. Two examples are considered and for each case theoretical and point-by-point results are presented for comparison to the whole field results. An account of experimental procedures of recording and collection of data is also presented.

Experimental Equipment

The experimental set up for recording a specklegram is shown in Figure 9 and schematically in Figure 10. An air-supported table was used to isolate the optical elements from surroundings and to provide a vibration free support system.

A Spectra-Physics model 125A He-Ne cw laser operating at 80 mw plane polarized output was used as the light source. The light was spatially filtered using a Spectra-Physics spatial filter 332. Light reflected from the object was imaged onto Kodak High Speed Holographic Film 131-02 using a Wollensok 15 inch f/5.6 lens. The emulsion was supported on a 4 in. x 5 in. glass plate to prevent reduction of the imaged picture.

In the point-by-point fringe interpretation, a set up similar to the one shown in Figure 8 was used. The light source was a Spectra-Physics Stabilite™ Model 120 He-Ne cw laser. The diffraction halo with fringes was photographed with a 35mm Nikon camera using Kodak

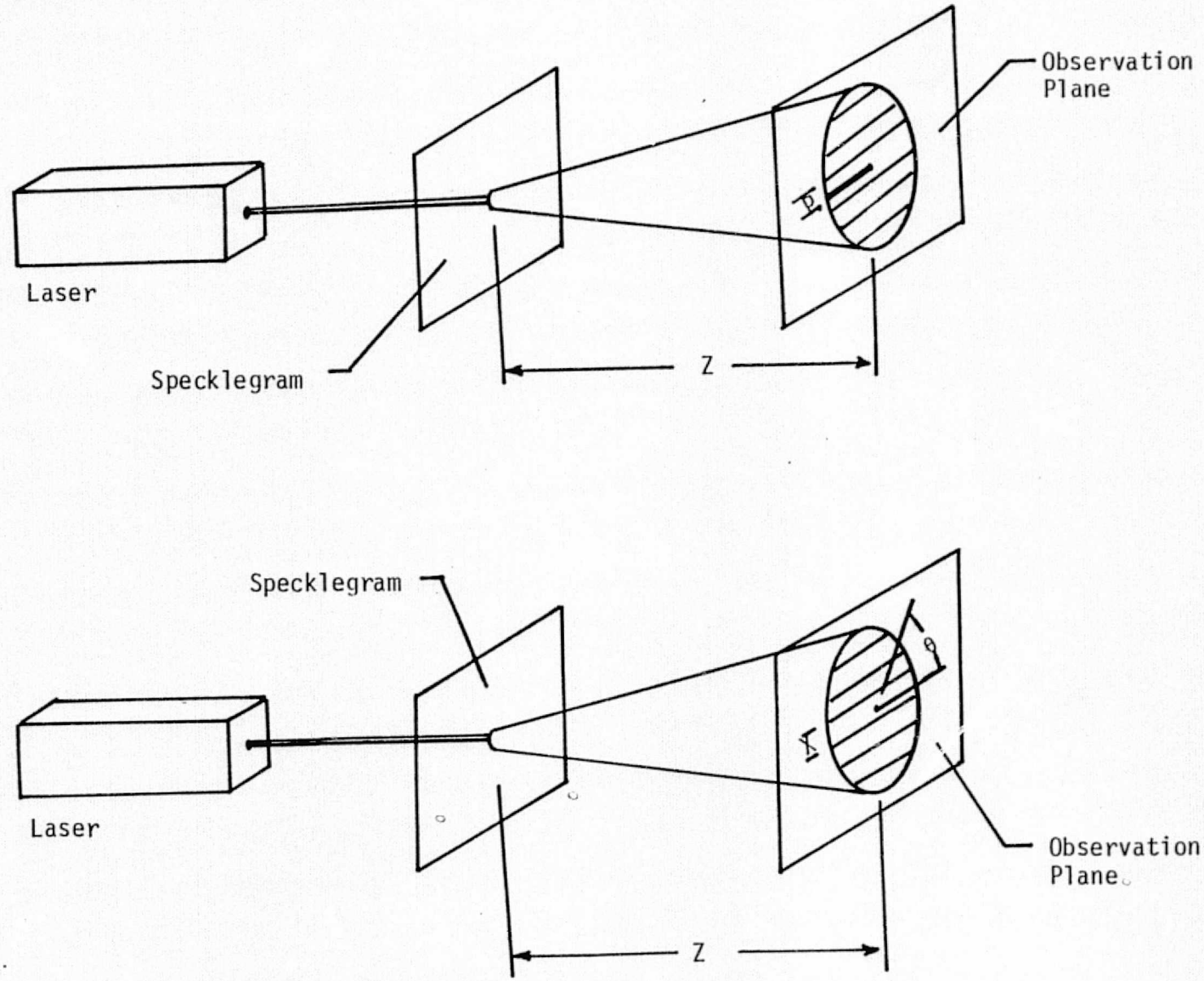

Figure 8. Technique for Determining P, Z, X and θ

ORIGINAL PAGE IS
OF POOR QUALITY

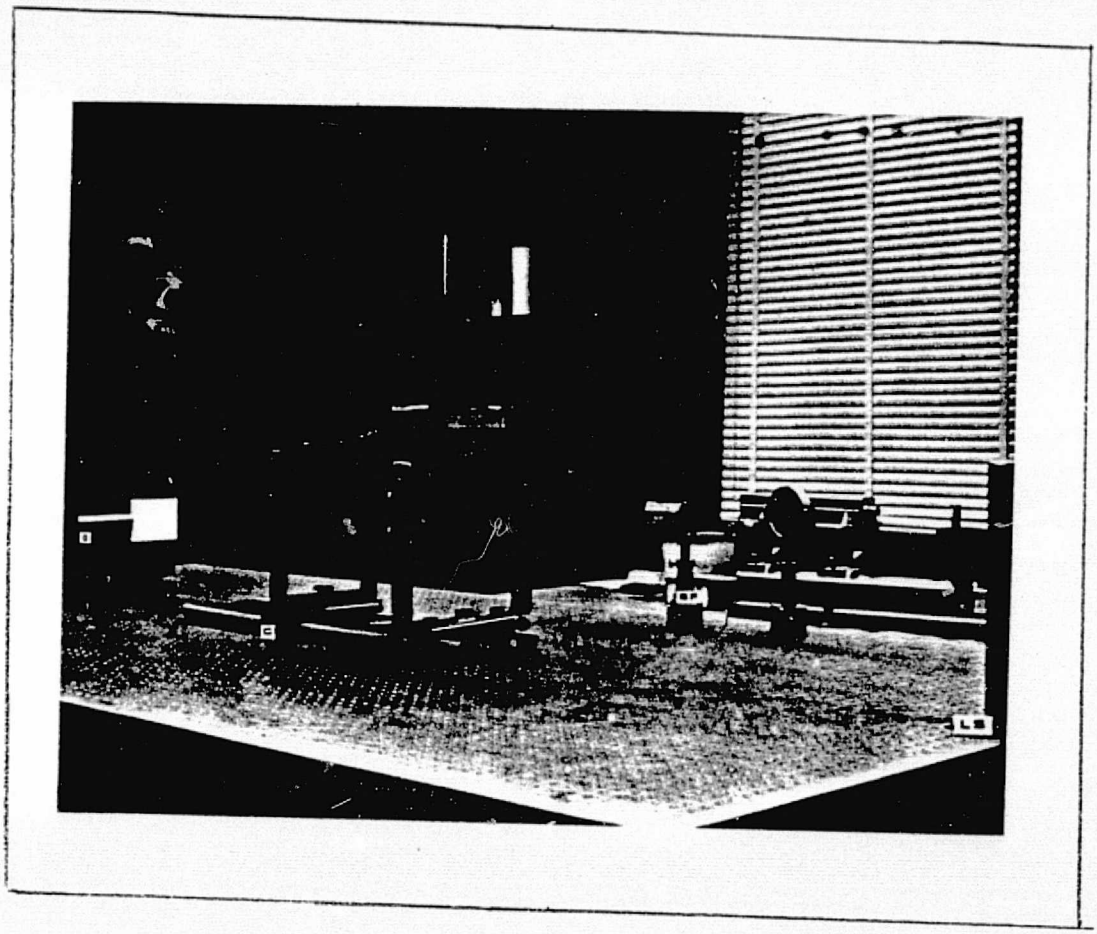

LS - Light Source

SF - Spatial Filter

O - Object

C - Camera

Figure 9. Experimental Set up for Taking a Specklegram

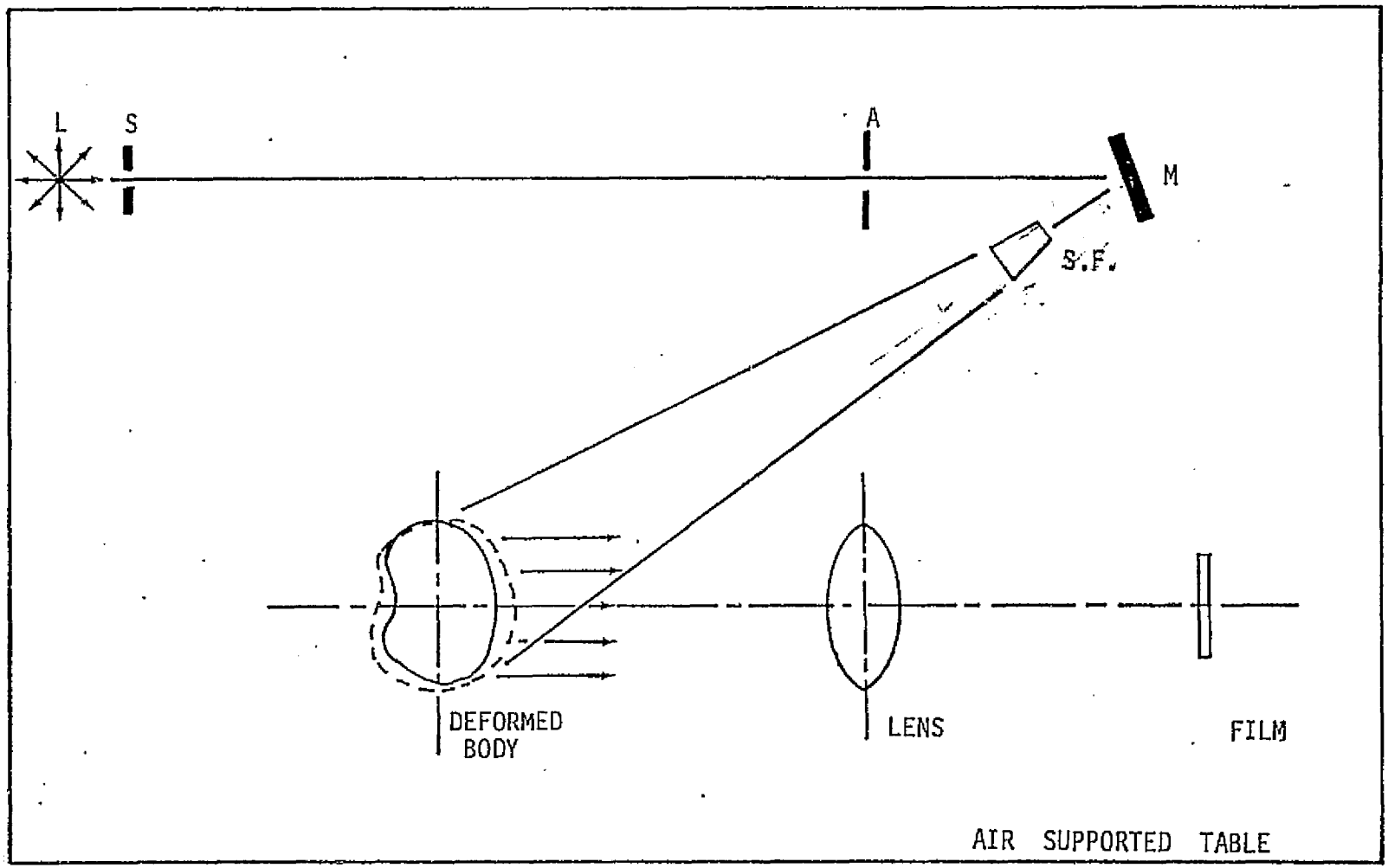

Figure 10. Schematic of Experimental Setup for Recording Speckiegram

ORIGINAL PAGE IS
OF POOR QUALITY

ORIGINAL PAGE IS
OF POOR QUALITY

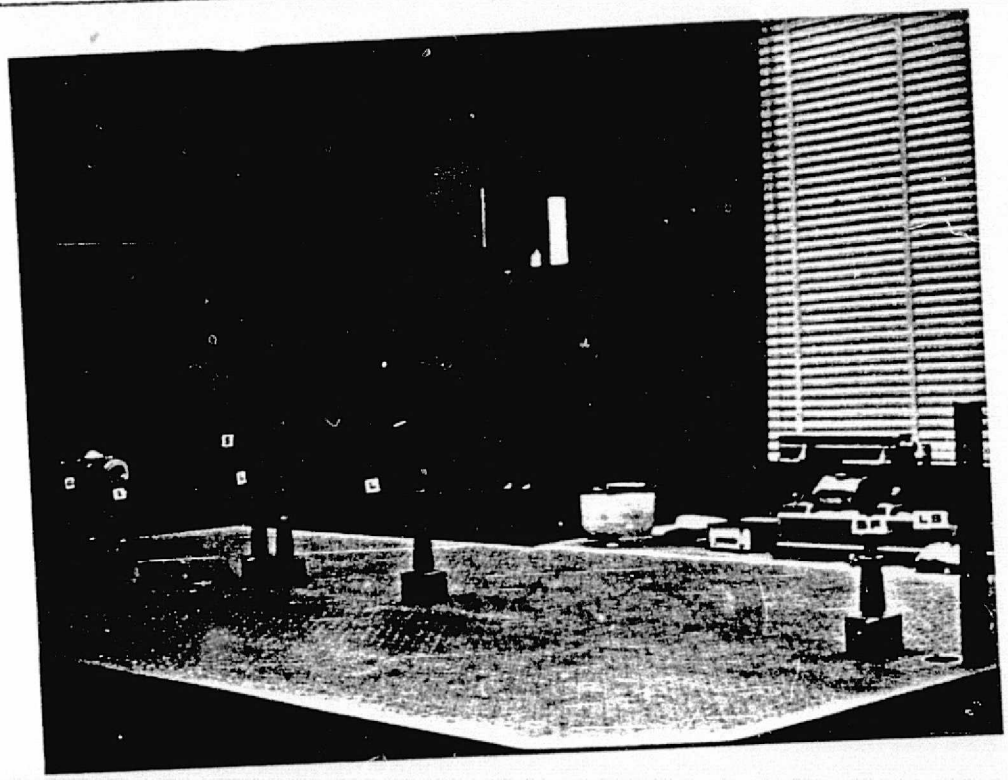

C - Camera

A - Aperture

S - Specklegram

L - Lens

SF - Spatial Filter

LS - Light Source

Figure 11. Whole-Field Fringe Analyzer

Panatomic-X film. For the whole-field fringe interpretation, the set up shown in Figure 11 was used. The Spectra-Physics Model 125A was the light source. The two lenses were spherical lenses with a focal length of 26.5 inches. The fringes were photographed using a 35mm Nikon camera with Kodak Panatomic-X film.

In the first example, only the vertical displacements were determined for comparison to the theoretical results. For the second example, horizontal displacements were determined.

Example 1 - Cantilever Beam

The first experimental example chosen to verify the theoretical results was the bending of a rectangular cantilever beam with an end load, as shown in Figure 12. The beam had the end fixed at $z_1 = 0$ and the end $z_1 = 1$ had a single force P directed along the positive x-axis producing a known deflection, δ , at $z_1 = 1$.

The z_1-axis was taken along the center line of the beam and the x- and y-axes were orthogonal axes intersecting at the centroid of the fixed end. The vertical (u) displacement component as given by Sokolnikoff [15] is listed below

$$u = \frac{P}{EI} \left[\frac{\nu}{2} (1-z_1) (x^2 y^2) - \frac{z_1^3}{6} + \frac{l z_1^2}{2} \right] \tag{2.39}$$

The load P is governed by the deflection of the free end. Suppose the load P is applied at $z_1 = 1$ such that $u(0,0,1) = \delta$ where δ is the known deflection. From eq (2.39)

$$P = \frac{3EI\delta}{l^3} \tag{2.40}$$

$$u = \frac{3\delta}{l^3} \left[\frac{\nu}{2} (1-z_1) (x^2 - y^2) - \frac{z_1^3}{6} - \frac{l z_1^2}{2} \right] \tag{2.41}$$

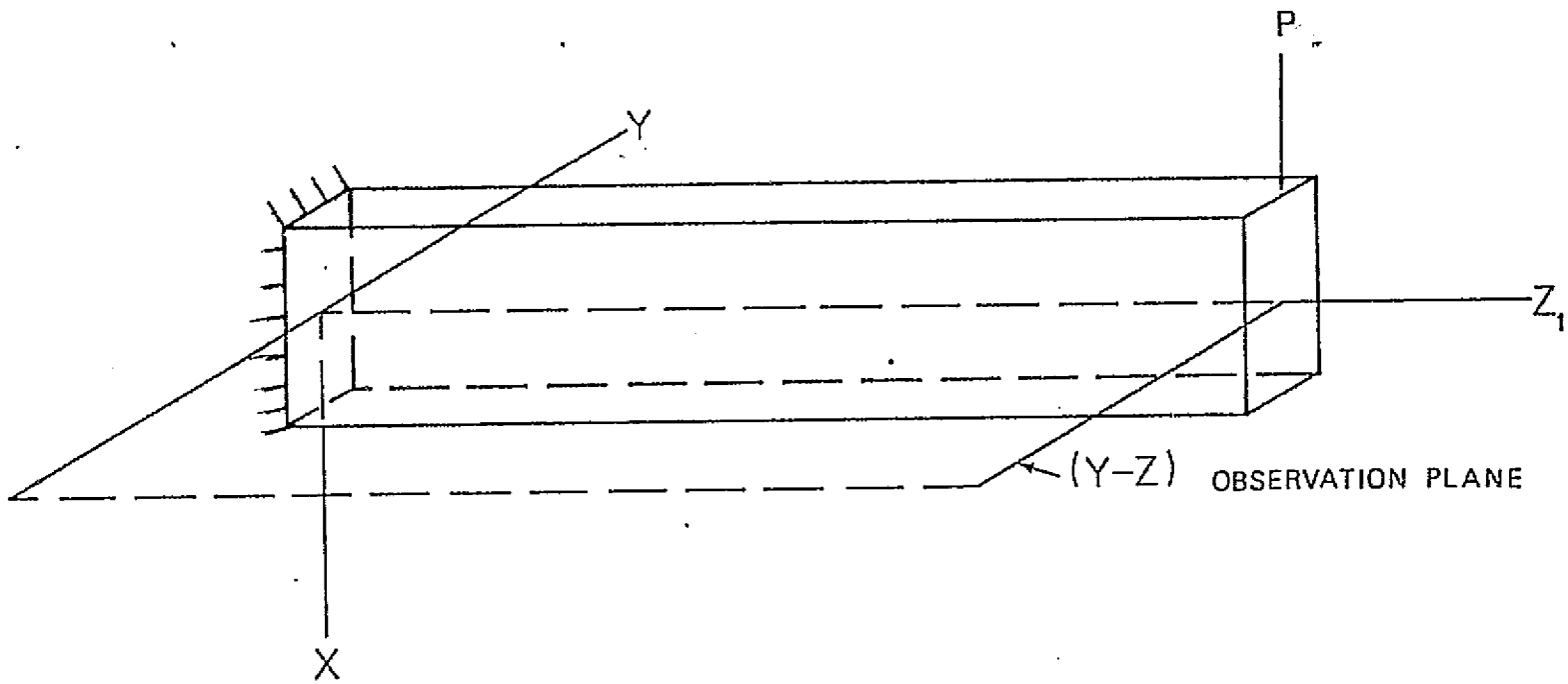

Figure 12. Example 1 - Cantilever Beam

Material used for the beam was plexiglass and the physical properties of the beam are

l = 6.00 inches

b = 0.125 inches

c = .255 inches

ν = .37

E = 456000 psi

δ_1 = .003 inches

δ_2 = .006 inches

Fixed end conditions for the beam were obtained by bonding one end of the plexiglass to an aluminum block as shown in Figure 13. The end load was applied with a micrometer screw and the deflection was recorded with a dial indicator (Figure 14). Deflections of .003 inches and .006 inches were investigated.

Discussion and Results of Cantilever Beam Experiment

Figure 15 presents the experimental set up. The coordinates relative to the cantilever beam are given in Figure 12. Theoretical results for δ = .003 inches and δ = .006 inches are tabulated in Table 3 and Table 4, respectively. Also, a plot of deflection versus distance along the beam for the two loading conditions are shown in Figure 16 and 17.

As discussed in section 2.4, using the point-by-point data reduction method, the in-plane displacement in the principal plane is given by

$$u_f = \frac{\lambda z}{2p} \tag{2.42}$$

Figure 18 shows the diffraction halo and fringes at various locations

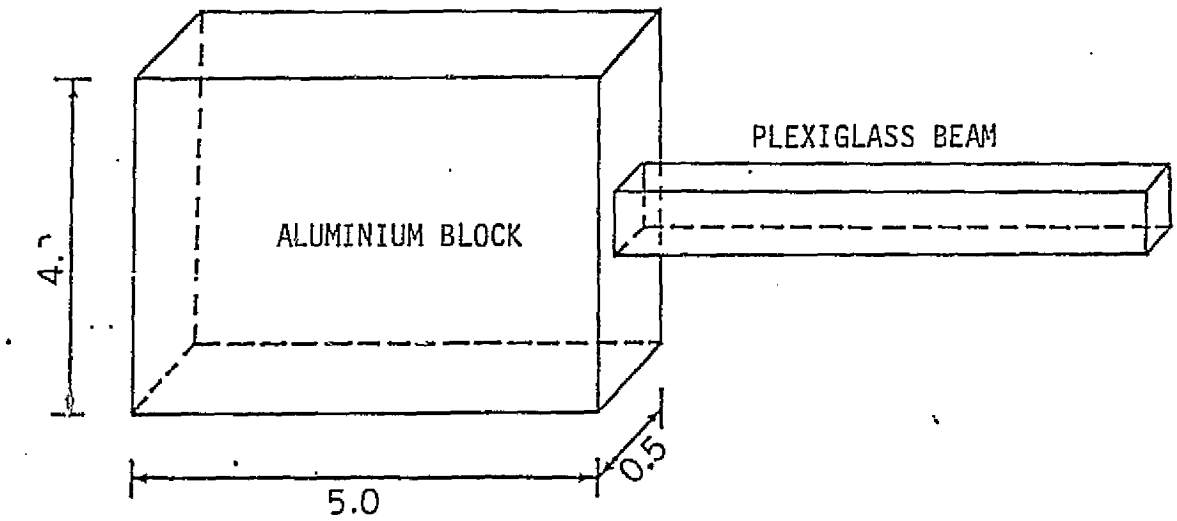

Figure 13. Fixed end Condition for Cantilever Beam

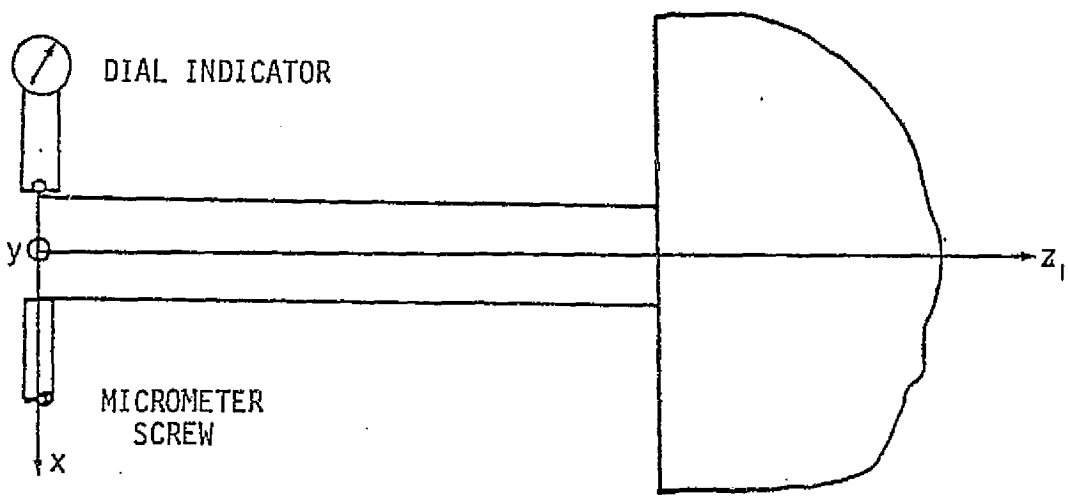

Figure 14. Method of Load Application and Measurement of δ

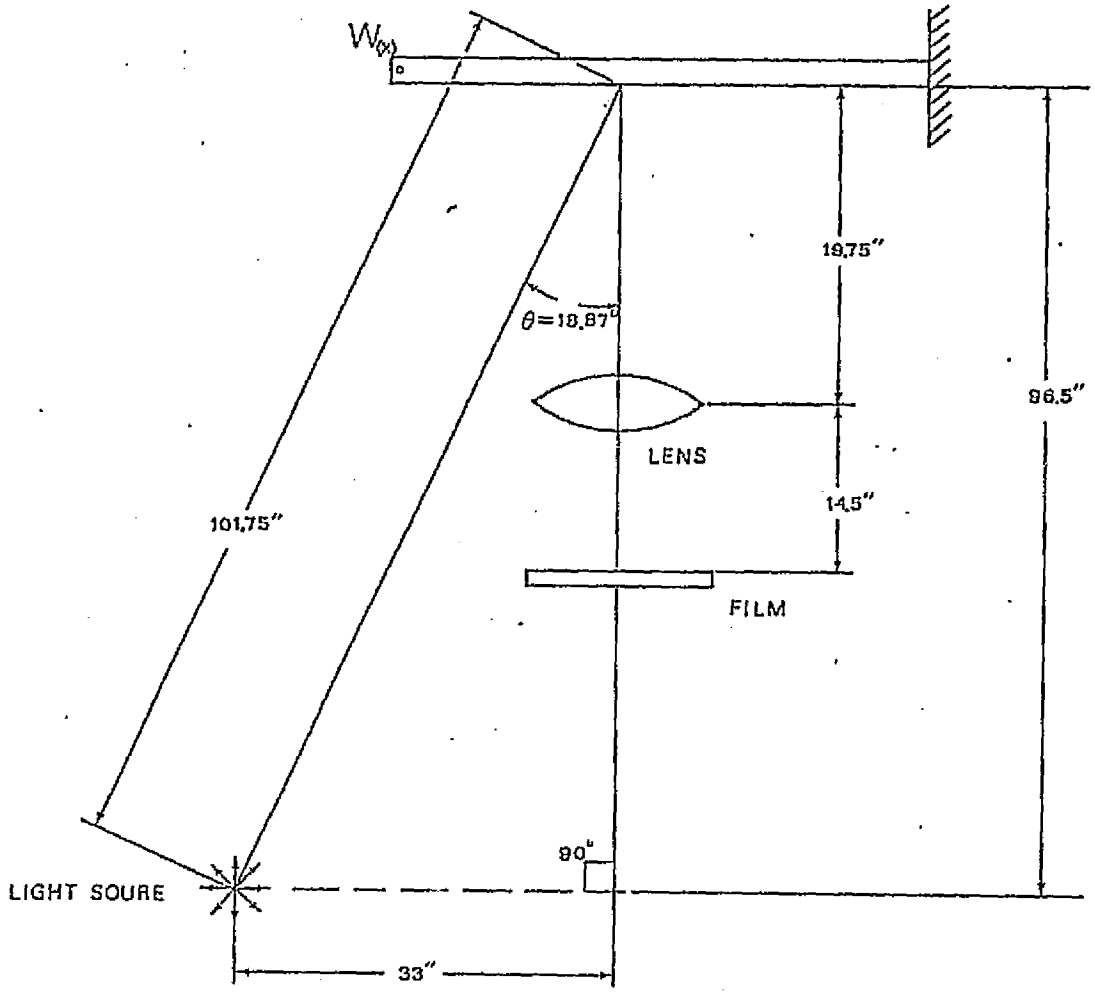

Figure 15. Schematic of Experimental Set up for Example 1

along the beam for δ = .003 inches. The in-plane vertical displacement is given by

$$u = u_f \sin \theta \tag{2.43}$$

where θ is measured as shown in Figure 3. The data taken for the two loading conditions are tabulated in Table 1. For comparison purposes, the experimentally determined displacements are plotted on Figure 16 for δ = .003 in. and Figure 17 for δ = .006 in.

For the whole-field fringe interpretation, the in-plane displacement in the film plane was shown to be equal to

$$u_f = (n - \frac{1}{2}) \frac{\lambda z}{p} \tag{2.33}$$

and the actual displacement is

$$u = (n - \frac{1}{2}) \frac{\lambda z}{mp} \tag{2.35}$$

Figure 19 is a photograph of the fringes in the transformed plane for δ = .006 inches. For these two photographs,

p = .98 inches

z = 33 inches

λ = 20.22 microinches

The data for both load conditions is tabulated in Table 2. Again, for comparison, the experimental results are plotted on Figure 16 for δ = .003 in. and on Figure 17 for δ = .006 in.

As seen from the results presented in Figures 16 and 17, excellent results were obtained for both techniques. The maximum difference in the point-by-point interpretation was ∿5%. For the whole-field interpretation, the maximum error was also ∿5%.

TABLE 1

EXAMPLE 1 - CANTILEVER BEAM - POINT-BY-POINT INTERPRETATION FOR VERTICAL DISPLACEMENT

δ = .003 inches				δ = .006 inches			
z (in)	p (in)	θ (deg)	u (in)	z (in)	p (in)	θ (deg)	u (in)
0	.148	- 3.0	2.88×10^{-3}	0	-	-	-
.3	.148	- 3.0	2.88	.3	.375	- 3.0	5.27×10^{-3}
.6	.148	- 3.0	2.88	.6	.400	- 3.0	4.94
.9	.177	- 3.0	2.40	.9	.450	- 3.5	4.40
1.2	.197	- 4.0	2.15	1.2	.475	- 3.5	4.16
1.5	.216	- 4.0	1.95	1.5	.500	- 3.5	3.96
1.8	.241	- 4.0	1.75	1.8	.625	- 4.5	3.44
2.1	.276	- 4.0	1.54	2.1	.675	- 4.5	2.93
2.4	.315	- 6.5	1.34	2.4	.800	- 7.0	2.48
2.7	.364	- 6.5	1.16	2.7	.925	- 7.0	2.14
3.0	.433	- 6.5	.98	3.0	1.025	- 7.0	1.92
3.3	.521	-10.5	.80	3.3	1.200	- 7.0	1.64
3.6	.630	-14.0	.65	3.6	1.425	-7.5	1.28
3.9	.748	-15.0	.51	3.9	1.765	-12.5	1.00
4.2	1.164	-18.0	.39	4.2	2.325	-12.5	.76

TABLE 2

EXAMPLE 1 - CANTILEVER BEAM - WHOLE FIELD INTERPRETATION

FOR VERTICAL DISPLACEMENT

δ = .003 inches

n	z (inch)	u (inch)
1	3.86	$.487 \times 10^{-3}$
2	2.13	1.461
3	.77	2.436

δ = .006 inches

n	z (inch)	u (inch)
1	4.63	$.487 \times 10^{-3}$
2	3.36	1.461
3	2.45	2.436
4	1.72	3.410
5	1.09	4.386
6	.36	5.360

TABLE 3

EXAMPLE 1 - CANTILEVER BEAM - THEORETICAL RESULTS

FOR VERTICAL DISPLACEMENT

δ = .003 inches	
z (inch)	u (inch)
0	3.000×10^{-3}
.3	2.775
.6	2.552
.9	2.330
1.2	2.112
1.5	1.900
1.8	1.691
2.1	1.489
2.4	1.296
2.7	1.118
3.0	.938
3.3	.775
3.6	.624
3.9	.487
4.2	.365
4.5	.258

δ = .006 inches	
z (inch)	u (inch)
0	6.000×10^{-3}
.3	5.550
.6	5.104
.9	4.660
1.2	4.224
1.5	3.800
1.8	3.382
2.1	2.978
2.4	2.592
2.7	2.236
3.0	1.876
3.3	1.550
3.6	1.248
3.9	.974
4.2	.730
4.5	.516

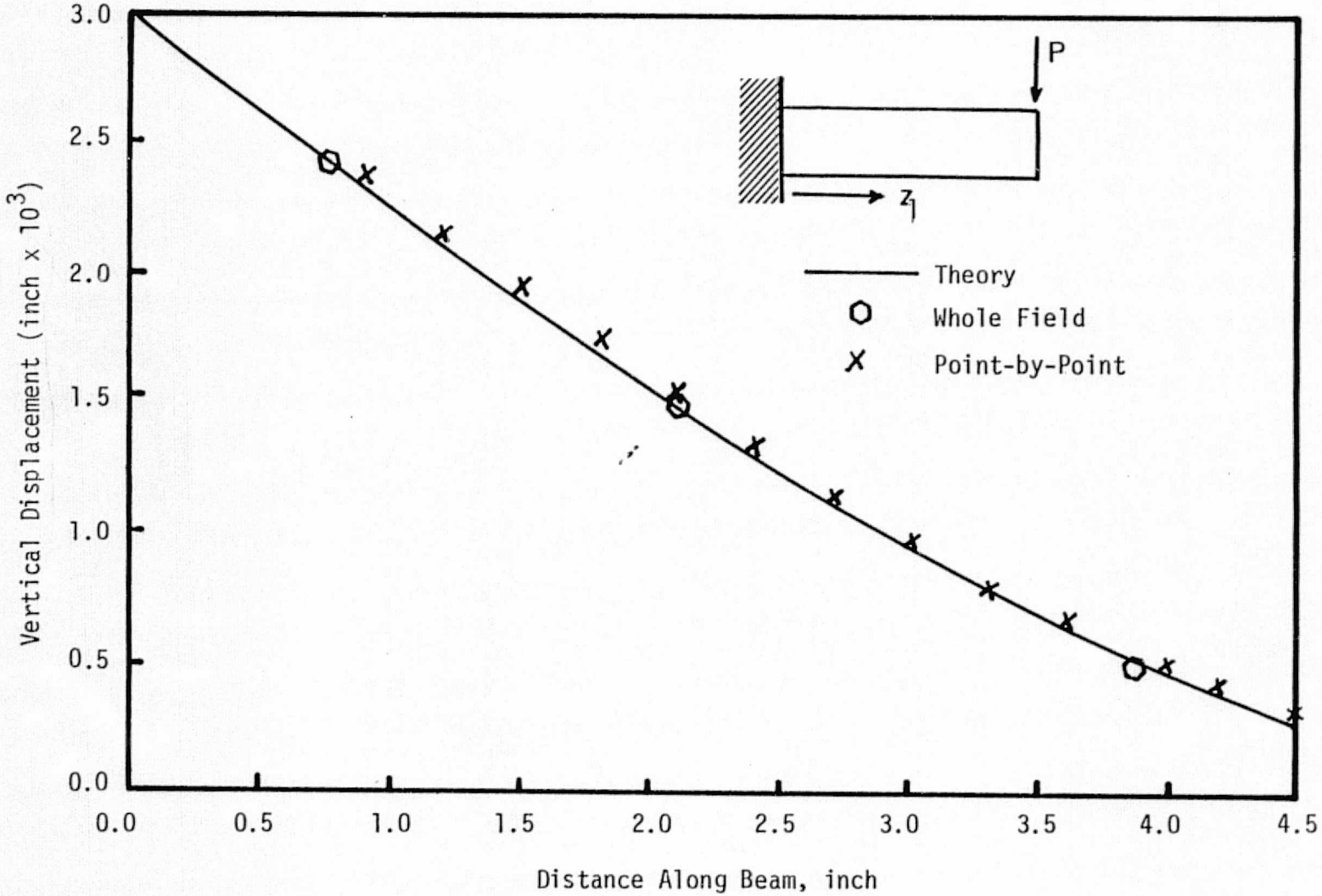

Figure 16. Vertical Displacement for Example 1 as Determined from Theory, Point-by-Point and Whole Field, δ = .003 inches

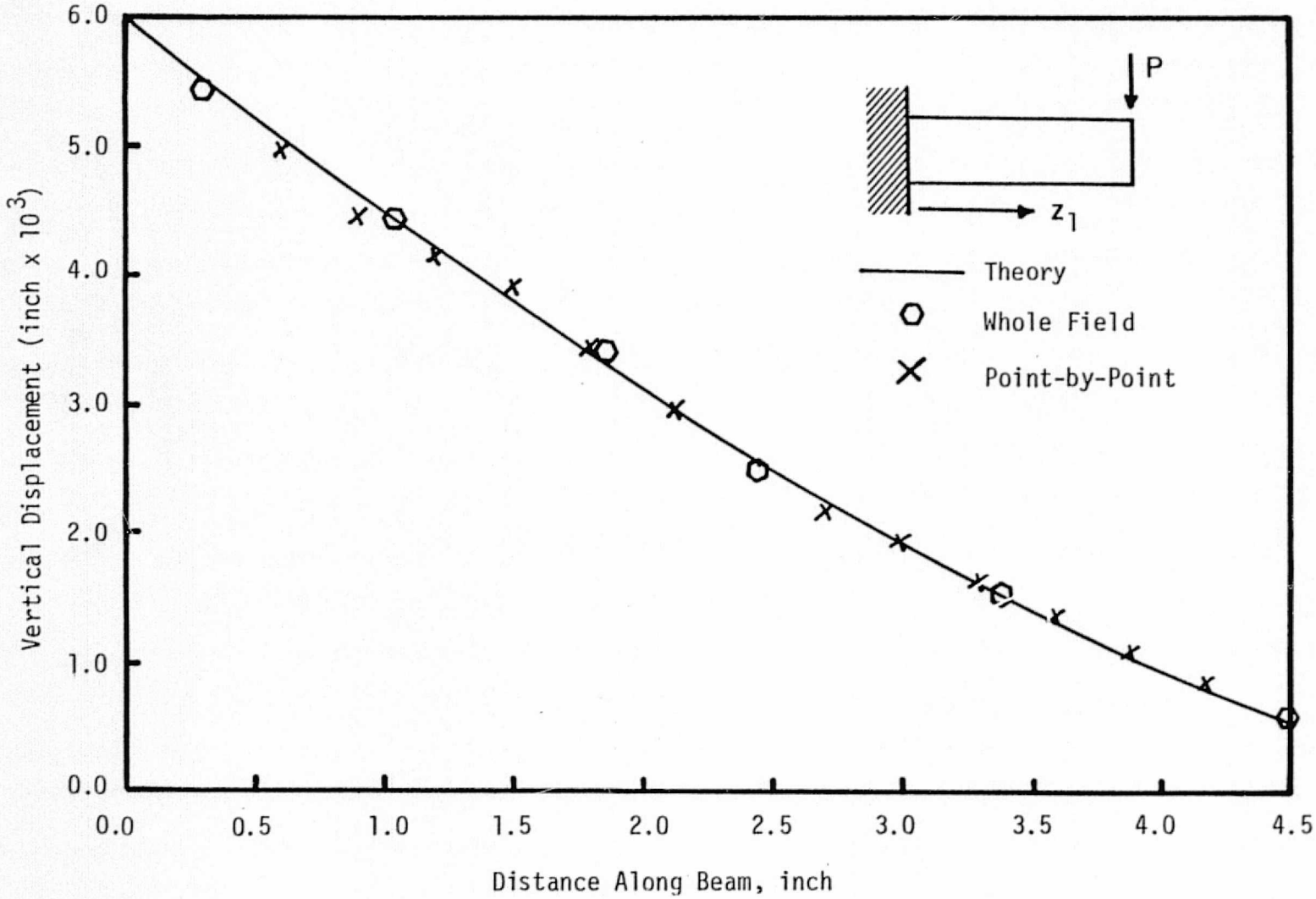

Figure 17. Vertical Displacement for Example 1 as Determined from Theory, Point-by-Point and Whole Field, δ = .006 inches

ORIGINAL PAGE IS
OF POOR QUALITY

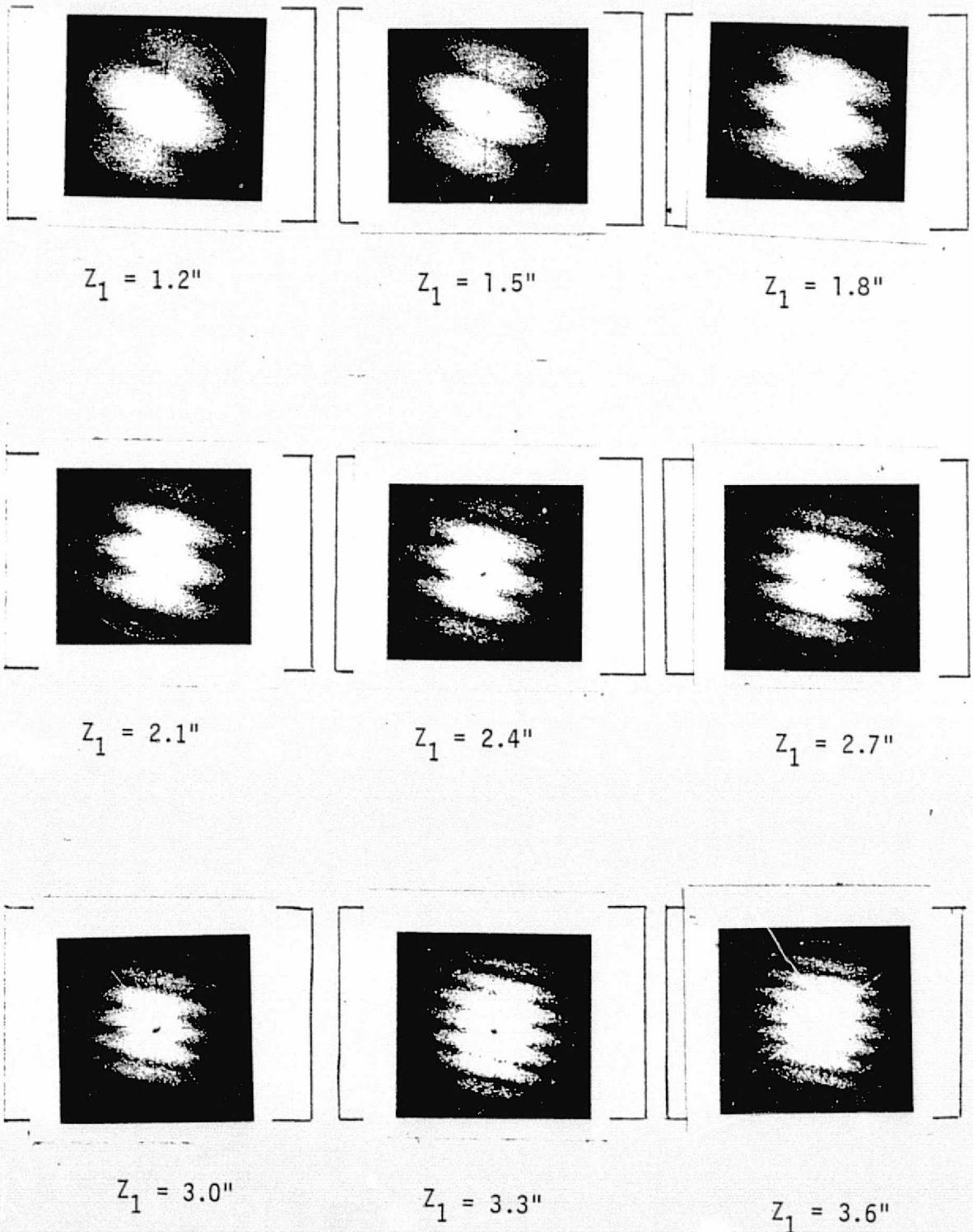

Figure 18. Diffraction Halo and Fringes for Cantilever Beam, δ = .003 inches

ORIGINAL PAGE IS
OF POOR QUALITY

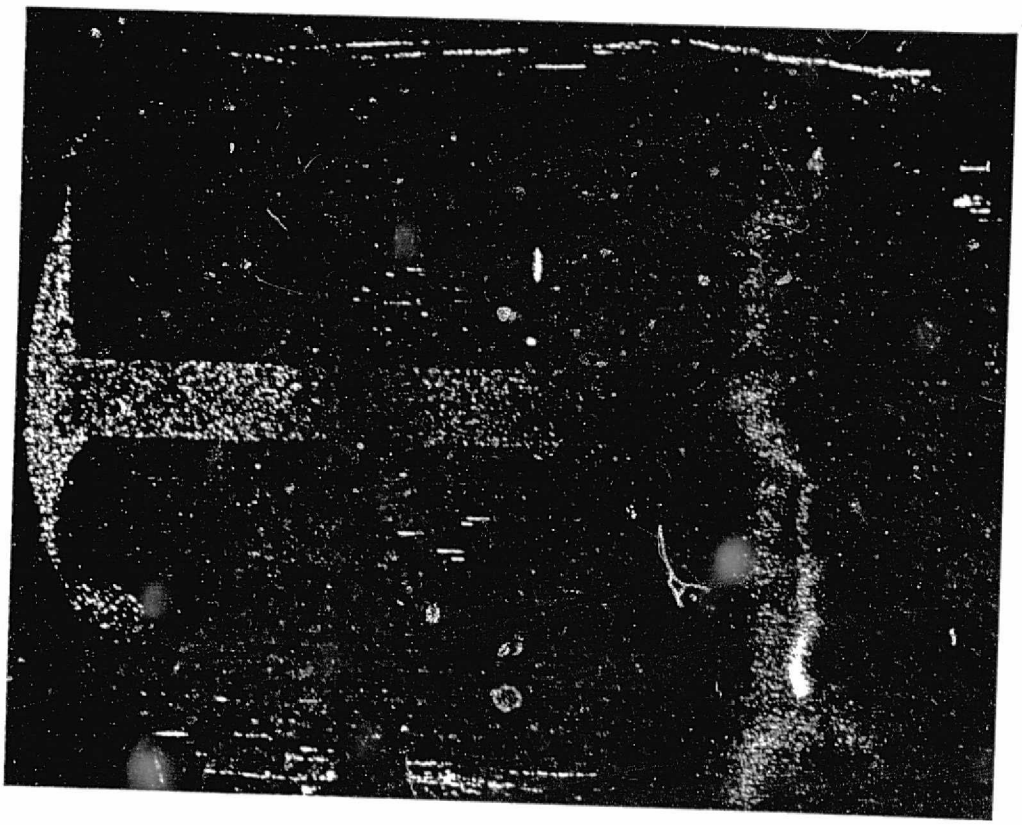

Figure 19. Fringes from Whole Field Interpretation for Cantilever Beam, δ = .003 inches

ORIGINAL PAGE IS
OF POOR QUALITY

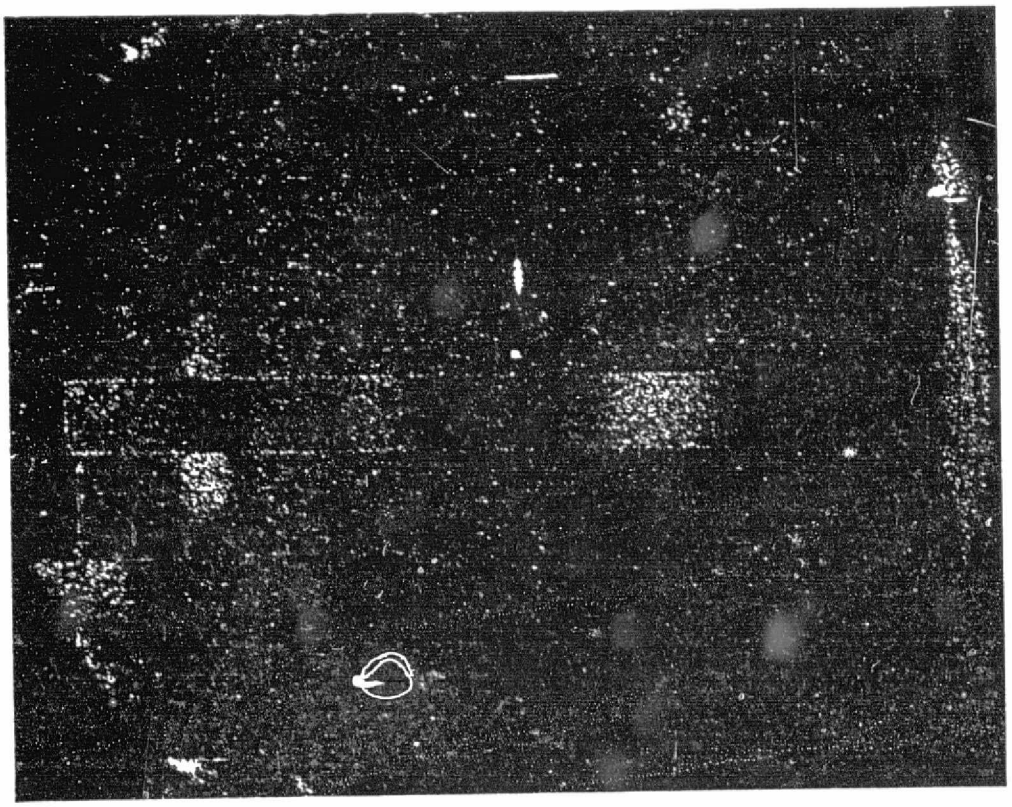

Figure 20. Fringes from Whole Field Interpretation for Cantilever Beam, δ = .006 inches

Example 2 - Pressure Vessel

The second experimental example chosen to verify the results of Section 2.3 was an internally loaded thin walled cylindrical pressure vessel. The coordinate system for this example is shown in Figure 21. The y-axis was chosen at the axis of symmetry. With the x- and z-axes intersecting at the center of the base of the cylinder. The z-axes on the model and on the film were parallel.

The radial strain for a capped end thin wall pressure vessel is

$$\varepsilon_r = \frac{\Delta R}{R} = \frac{1}{E}(\sigma_\theta - \nu\sigma_z) \tag{2.42}$$

where

$$\sigma_\theta = \frac{\Delta PR}{t} \tag{2.43-1}$$

$$\sigma_z = \frac{\Delta PR}{2t} \tag{2.43-2}$$

Therefore, the radial displacement is

$$\Delta R = \frac{\Delta PR^2}{2tE}(2 - \nu) \tag{2.44}$$

The horizontal displacement, u, is

$$u = \Delta R \sin\theta \tag{2.45}$$

However,

$$\sin\theta = \frac{x}{R} \tag{2.46}$$

Thus, the theoretical horizontal displacement is

$$u = \frac{\Delta PRx}{2tE}(2-\nu) \tag{2.47}$$

For this example

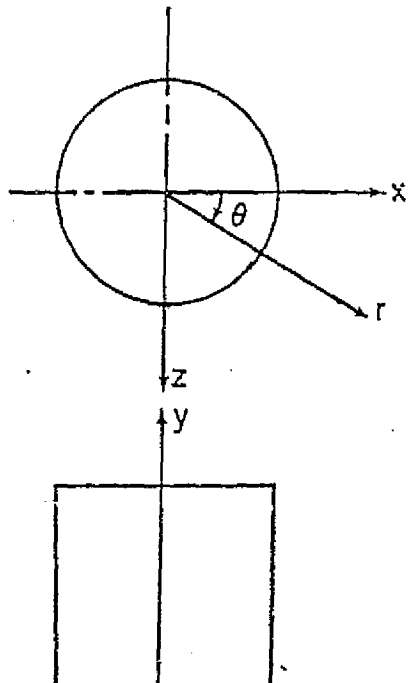

$x = r\cos\theta$
$z = r\sin\theta$
$y = y$

Figure 21. Example 2 - Pressure Vessel

$\Delta P = 400$ psi

$R = 2.54$ inches

$t = .09$ inches

$E = 10 \times 10^6$ psi

$\nu = .33$

A tabulation of theoretical horizontal displacement for various x's is presented in Table 6.

The capped end conditions for the pressure vessel are obtained by welding aluminum plugs at both ends. The physical dimensions for the pressure vessel are shown in Figure 22.

The same procedure was followed as in the first example. The results for the point-by-point interpretation are tabulated for example 2 in Table 4. Results for the whole field interpretation presented in Table 5. A photograph of the whole field fringes is shown in Figure 23.

To verify the speckle theory, a comparison of the experimental results to the theoretical results is presented in Figure 24. Excellent agreement is obtained near the center of the cylinder; however, once removed from the center area, a small difference between the theory and experimental results occurs. For the whole field interpretation, relationship between x and the horizontal displacement is a straight line as would be expected; however, the slope of the curve is less than the theoretical. For the point-by-point results, initially the relationship between x and the displacement component is linear; however, at larger values of x, this linearity disappears. Probable cause for this difference is in the focusing of the cylindrical body onto the film

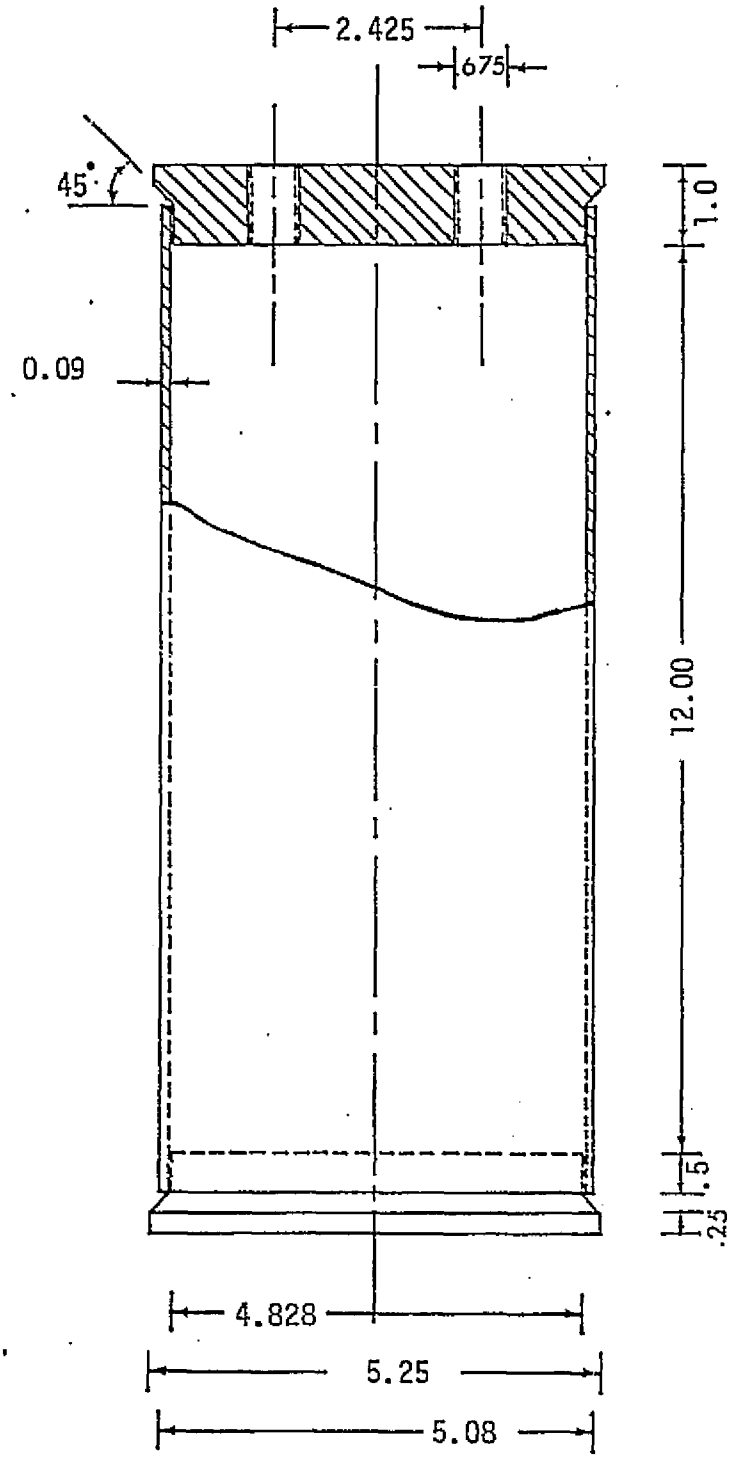

Figure 22. Dimensions for Pressure Vessel

plate. If the center of the cylinder is used for the point of focus, the outer edges (as x increases) will be slightly out of focus dependent upon the radius of the cylinder. Recent work has been conducted into this problem of misfocusing and has shown that this can lead to a difference in fringe spacing.

TABLE 4

EXAMPLE 2 - PRESSURE VESSEL - POINT-BY-POINT INTERPRETATION FOR HORIZONTAL DISPLACEMENT

x (inch)	p (inch)	θ (deg)	u (inch)
0	.25	0.0	
.2	.24	7.5	1.93×10^{-4}
.4	.23	15.0	3.91
.6	.22	21.0	5.92
.8	.21	28.0	7.94
1.0	.20	31.0	8.92
1.2	.19	36.0	10.44

TABLE 5

EXAMPLE 2 - PRESSURE VESSEL - WHOLE-FIELD INTERPRETATION FOR HORIZONTAL DISPLACEMENT

x (inch)	n	u (inch)
.17	1	1.619×10^{-4}
.52	2	4.858
.88	3	8.096
1.25	4	11.330
1.66	5	14.570

TABLE 6

EXAMPLE 2 - PRESSURE VESSEL - THEORETICAL RESULTS

FOR HORIZONTAL DISPLACEMENT

x (inch)	u (inch)
0	0.00
.2	1.88×10^{-4}
.4	3.77
.6	5.65
.8	7.54
1.0	9.43
1.2	11.31
1.4	13.21
1.6	15.14
1.8	17.02

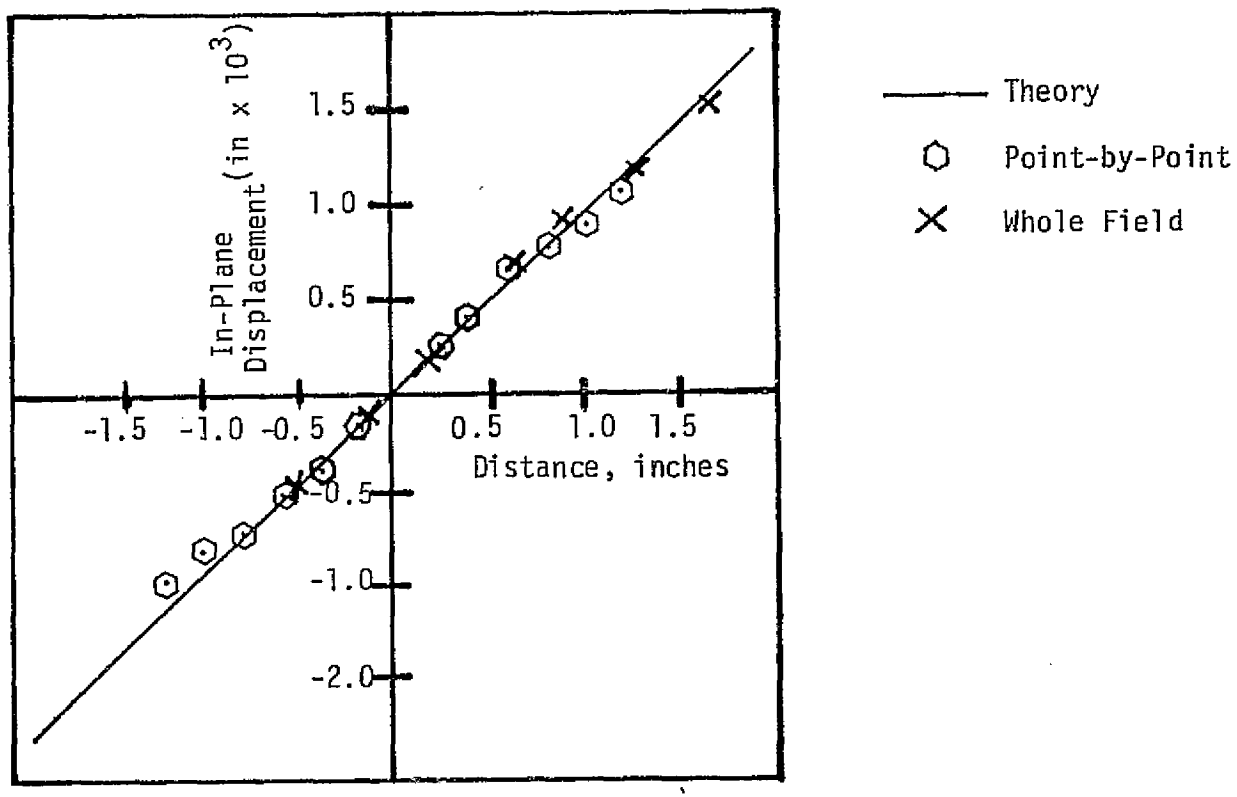

Figure 24. Horizontal Displacement for Example 2 as Determined from Theory, Point-by-Point and Whole Field, ΔP = 400 psi

ORIGINAL PAGE IS
OF POOR QUALITY

Figure 24. Fringes from Whole Field Interpretation for Pressure Vessel, ΔP = 400 psi

III. TIME AVERAGE SPECKLE INTERFEROMETRY

3.1 Basic Phenomena

As presented in Section II, in-plane displacement resulting from a static load can be determined using double exposure speckle interferometry. In this section, the speckle theory is extended to include the time averaging technique for use in determining in-plane displacement due to harmonic vibration of an object. The time averaging technique has previously been sucessfully used in holography [16]. In recent years, time averaging in conjunction with speckle interferometry has been investigated. Tiziani [10] showed the intensity expression in the transformed plane to be a function of the zero order Bessel function for a time average recording of a harmonically oscillating object or image. The work conducted in this section of the report extends the work conducted by Tiziani [10] by determining the relationship between the transformed intensity function and the in-plane displacement of the oscillating object.

The analytical work closely parallels the development of the double exposure technique presented in Section II. The major difference is in the determination of the intensity expression. For the double exposure technique, the intensity is determined for each exposure and summed. For the time averaging technique, integration is performed over the total time to arrive at the intensity expression.

3.2 Theory of Speckle Interferometry - Time Averaging - Single Beam Analysis

The arrangement presented in Figure 6 is also used in the time averaging. An object is illuminated by a single laser beam with the location of the light source shown as S which illuminates a point P on the surface of the object. In time averaging, a single exposure is taken of the vibrating surface with an exposure time at least equal to the time for one complete cycle of the vibration.

For the condition of the time dependent loading, the complex light amplitude can be expressed as

$$\overline{E}\,(x_1, x_2) = \overline{A}\,(x_1 + x_1', x_2 + x_2') \exp i[\theta(x_1, x_2) + \Delta\theta] \tag{3.1}$$

where

x_1, x_2 - Film plane coordinates

x_1', x_2' - Function of the amplitude of vibration, frequency, time and location

θ - Phase angle of the beam

$\Delta\theta$ - The relative change in the phase angle due to the vibration

For the time averaging, the film exposure over a time interval t is

$$tI_T = \int_0^t \overline{E}(x_1, x_2)\ \overline{E}^*\,(x_1, x_2)\ dt \tag{3.2}$$

where $\overline{E}^*\,(x_1, x_2)$ is the complex conjugate of $\overline{E}\,(x_1, x_2)$. Again, to simplify the notation the x_2-coordinate will be suppressed for convenience, i.e.

$$tI_T = \int_0^t \overline{E}(x)\ \overline{E}^*(x)\ dt \tag{3.3}$$

Therefore,

$$tI_T = \int_0^t A \quad (x + x')\ dt \qquad 93.4)$$

A physical interpretation of x' is needed before this development proceeds. At t = 0, the point P is at coordinate (X_1, X_2) on the object. For t > 0, the point is displaced to a new location P which is dependent upon the amplitude of vibration, the frequency and the time. Thus, the line segment $\overline{PQ}$ can be written as

$$\overline{PQ} = u\ (X_1, X_2)\ \sin \omega t \qquad (3.5)$$

where u represents the maximum displacement of the surface at (X_1, X_2) and on the film plane

$$[\overline{PQ}]_{\text{Film Plane}} = u_f\ (x_1, x_2)\ \sin \omega t \qquad (3.6)$$

and

$$u = \frac{u_f}{M} \qquad (3.7)$$

where M is a magnification factor. Thus

$$tI_t = \int_0^t A^2\ (x + u_f \sin \omega t)\ dt \qquad (3.8)$$

As present in Section 2.3, the amplitude transmission g(x) can be approximated by a linear function of intensity, i.e.

$$g(x) = a + b\ I_T \qquad (3.9)$$

where a and b are constants of the film. Thus,

$$g(x) = a + \frac{b}{t} \int_0^t A^2\ (x + u_f \sin \omega t)\ dt \qquad (3.10)$$

Eq (3.10) is a relationship between transmissivity and intensity in terms of the displacement in the film plane.

3.3 Optical Fourier Fringe Interpretation

The whole field fringes are obtained by taking optically the Fourier transform of the amplitude transmission function $g(x_1, x_2)$ as discussed in Section 2.3. The light amplitude function $G(w)$ in the transformed plane is [5]

$$G(w) = \exp\left(\frac{izw^2}{2k}\right) \int g(x) \exp(-iwx)\, dx \tag{3.11}$$

as presented in Section 2.3.

For the time averaging,

$$G(w) = \exp\left(\frac{izw^2}{2k}\right) \int\int_0^t a + \frac{b}{t} [\quad A^2 (x + u_f \sin \omega t)\, dt$$

$$\exp(-iwx)\, dx \tag{3.12}$$

or

$$G(w) = \exp\left(\frac{izw^2}{2k}\right) \int a \exp(-iwx)\, dx + b \frac{\exp}{t} \left(\frac{izw^2}{2k}\right)$$

$$\int\int_0^t A^2 (x + u_f \sin \omega t) \exp(-iwx)\, dt\, dx \tag{3.13}$$

Now

$$\delta(w) = \int \exp(-iwx)\, dx \tag{3.14}$$

Thus

$$G(w) = a\delta(w) \exp\left(\frac{izw^2}{2k}\right) + \frac{b}{t} \exp\left(\frac{izw^2}{2k}\right)$$

$$\int\int_0^t A^2 (x + u_f \sin \omega t) \exp(-iwx)\, dt\, dx \tag{3.15}$$

Since t and x are independent, and $A^2 (x + u_f \sin \omega t)$ and $\exp(-iwx)$ are continuous functions, and u_f is a function of x only, the second part of eq (3.15) can be written as

$$\frac{b}{t} \exp\left(\frac{izw^2}{2k}\right) \int_0^t \int A^2 (x + u_f \sin \omega t) \exp(-iwx)\, dx\, dt \tag{3.16}$$

From eq (2.21), the first integration is the Fourier transform of $A^2\ (x + u_f \sin \omega t)$. Thus,

$$G(w) = a\delta(w)\ \exp\ (\frac{izw^2}{2k}) + \frac{b}{t}\ \exp\ (\frac{izw^2}{2k})$$

$$\int_o^t F\ [A^2\ (x_1 + u_f\ \sin \omega t)]\ dt \tag{3.17}$$

Employing the shift theorem, eq (3.17) can be rewritten as

$$G(w) = a\delta(w)\ \exp\ (\frac{izw^2}{2k}) + \frac{bF[A^2(x)]}{t}\ \exp\ (\frac{izw^2}{2k})$$

$$\int_o^t \exp\ (iu_f w \sin \omega t)\ dt \tag{3.18}$$

As discussed in Section 2.3, the delta function's contribution occurs only at $w = 0$. For any value of w other than zero, eq (3.18) is

$$G(w) = \frac{bF[A^2(x)]}{t}\ \exp\ (\frac{izw^2}{2k})\int_o^t \exp\ (iu_f w \sin\omega t)\ dt \tag{3.19}$$

From Bessel function analysis

$$2\pi J_o(x) = \int_o^{2\pi} \exp\ (ix\cos\theta)\ d\theta = \int_o^{2\pi} \exp\ (ix\ \sin\theta\ )\ d\theta \tag{3.20}$$

where $J_o(x)$ is the zero order Bessel function. For evaluation of eq (3.19), the integration will be for one cycle, that is t will be the time required for one cycle, thus if many cycles occur the time will be some multiple of t. Rearranging eq (3.19), and multiplying and dividing by ω gives

$$G(w) = \frac{b}{t\omega}\ \exp\ [\frac{izw^2}{2k}]\ F\ [A^2(x)]\int_o^t \exp\ (iu_f w\ \sin\ \omega t)\ \omega dt \tag{3.21}$$

Comparing eq (3.21) with eq (3.20)

$$\theta = \omega t$$

$$d\theta = \omega dt$$

$$x = u_f w$$

$$t = 2\pi/\omega$$

Consequently, eq (3.21) becomes

$$G(w) = \frac{b}{t\omega} \exp\left[\frac{izw^2}{2k}\right] F\left[A^2\right] J_o\left(u_f w\right) \tag{3.22}$$

The intensity function in the transformed plane is

$$I_F = G(w)\ G^*(w) \tag{3.23}$$

Therefore,

$$I_F = \frac{b^2}{t^2\omega^2} F\left[A^2\right]^2 J_o^2\left(u_f w\right) \tag{3.24}$$

Fringes are defined in the transformed plane when $I_F = 0$. Since all the terms except $J_o(u_f w)$ are always non-zero, fringes occur when

$$J_o\left(u_f w\right) = 0 \tag{3.25}$$

From eq (2.17)

$$w = \frac{2\pi p}{\lambda z}$$

Thus

$$J_o\left(\frac{2\pi p u_f}{\lambda z}\right) = 0 \tag{3.26}$$

Since all the terms inside the bracket except u_f can be measured or are known, the in-plane displacement for a harmonically oscillating object can be determined. Table 7 is a tabulation of the zero values for $J_o(x)$.

3.4 Point-by-Point Interpretation

Similarly to the discussion in Section 2.4, the point-by-point interpretation can be determined from eq (3.26). For the point-by-point interpretation, the in-plane displacement is constant at each location with the distance p being variable. For the case of n = 1, eq (3.26) yields

TABLE 7

ZERO VALUES FOR $J_o(x)$

$J_o(x)$ Equals Zero when

$x_{01} = 2.40$

$x_{02} = 5.52$

$x_{03} = 8.65$

$x_{04} = 11.79$

$x_{05} = 14.93$

$x_{06} = 18.07$

$x_{07} = 21.21$

$x_{08} = 24.34$

$x_{09} = 27.49$

$x_{10} = 30.63$

$x_{11} = 33.78$

$x_{12} = 36.92$

$x_{13} = 40.06$

$x_{14} = 43.20$

$$\frac{2\pi p u_f}{\lambda z} = 2.40 \tag{3.27}$$

or

$$u_f = \frac{.382\lambda z}{p} \tag{3.28}$$

and

$$u_f = \frac{.382\lambda z}{Mp} \tag{3.29}$$

Comparison of eq (3.28) to eq (2.37), shows the only difference between the time averaging and double exposure point-by-point interpretation is a difference in the constant.

3.5 Numerical Example - Vibrating Cantilever Beam

The numerical example chosen is a vibrating cantilever beam. The beam is made of aluminum and the dimensions of the beam are presented in Figure 25. For this example, the first two modes of vibration were analyzed.

The solution for the amplitude $W(z_1)$, as presented by Nowacki [18] for free transverse vibration of a cantilever beam with the end fixed at $z = 0$ and an initial tip deflection of δ at $z = l$ is for each mode of vibration

$$W_r(z_1) = C\,[U(\lambda_r z_1) - \frac{S(\beta_r)}{T(\beta_r)} V(\lambda_r z_1)] \qquad r = 1,2 \tag{3.30}$$

where C is dependent upon the initial conditions and

$$U(\lambda_r z_1) = \frac{\cosh \lambda_r z_1 - \cos \lambda_r z_1}{2}$$

$$V(\lambda_r z_1) = \frac{\sinh \lambda_r z_1 - \sin \lambda_r z_1}{2}$$

$$S(\beta_r) = \frac{\cosh \beta_r + \cos \beta_r}{2}$$

$$T(\beta_r) = \frac{\sinh \beta_r + \sin \beta_r}{2}$$

$$\lambda_r^4 = \frac{\omega_r^2}{c^2}$$

$$\beta_1 = 1.875$$

$$\beta_2 = 4.694$$

ω_r - natural frequency

If the initial condition is such that only the first mode is activated, then at $z = 1$

$$W_1(1) = \delta = C\,[U(\beta_1) - \frac{S(\beta_1)}{T(\beta_1)} V(\beta_1)] \tag{3.31}$$

Therefore, for this case

$$\frac{W_1(z_1)}{\delta} = \frac{C\,[U(\lambda_1 z_1) - \frac{S(\beta_1)}{T(\beta_1)} V(\lambda_1 z_1)]}{C\,[U(\beta_1) - \frac{S(\beta_1)}{T(\beta_1)} V(\beta_1)]} \tag{3.32}$$

Similarly, if the initial condition is such that only the second mode is activated then

$$\frac{W_2(z_1)}{\delta} = \frac{[U(\lambda_2 z_1) - \frac{S(\beta_2)}{T(\beta_2)} V(\lambda_2 z_1)]}{[U(\beta_2) - \frac{S(\beta_2)}{T(\beta_2)} V(\beta_2)]} \tag{3.33}$$

Therefore, for each case, the ratio of the amplitude to the initial

tip deflection as a function of distance along the beam, z_1, can be determined and is tabulated in Table 8.

The amplitude of vibration is just the in-plane displacement, u, defined in Section 3.2, i.e.

For the first mode of vibration

$$u = \frac{[U(\lambda_1 z_1) - \frac{S(\beta_1)}{T(\beta_1)} V(\lambda_1 z_1)]}{[U(\beta_1) - \frac{S(\beta_1)}{T(\beta_1)} V(\beta_1)]} \tag{3.34}$$

The in-plane displacement in the film plane is

$$u_f = Mu \tag{3.35}$$

where M is a magnification factor.

Then for the first mode of vibration, the in-plane displacement in the film plane is

$$u_f = M \frac{[U(\lambda_1 z_1) - \frac{S(\beta_1)}{T(\beta_1)} V(\lambda_1 z_1)]}{[U(\beta_1) - \frac{S(\beta_1)}{T(\beta_1)} V(\beta_1)]} \tag{3.36}$$

For the second mode

$$u_f = M \frac{[U(\lambda_2 z_1) - \frac{S(\beta_2)}{T(\beta_2)} V(\lambda_2 z_1)]}{[U(\beta_2) - \frac{S(\beta_2)}{T(\beta_2)} V(\beta_2)]} \tag{3.37}$$

Whole Field Interpretation

For the whole field interpretation, let

$p = .3$ inches

$z = 26.5$ inches

TABLE 8

RATIO OF AMPLITUDE/TIP DEFLECTION

FIRST MODE		SECOND MODE	
z_1 (inch)	u/δ	z_1 (inch)	u/δ
0	0	0	0
.3	.0042	.3	-.0254
.6	.0165	.6	-.0926
.9	.0363	.9	-.1888
1.2	.0630	1.2	-.3011
1.5	.0961	1.5	-.4173
1.8	.1349	1.8	-.5262
2.1	.1789	2.1	-.6178
2.4	.2275	2.4	-.6836
2.7	.2803	2.7	-.7171
3.0	.3366	3.0	-.7137
3.3	.3960	3.3	-.6713
3.6	.4580	3.6	-.5896
3.9	.5221	3.9	-.4703
4.2	.5880	4.2	-.3171
4.5	.6551	4.5	-.1351
4.8	.7232	4.8	.0700
5.1	.7919	5.1	.2916
5.4	.8611	5.4	.5237
5.7	.9305	5.7	.7611
6.0	1.0000	6.0	1.0000

λ = 24.9 microinches

M = 1.0

δ = .006 inches

l = 6.0 inches

With these, eq (3.26) becomes

$$J_o(2856\ u_f) = 0 \tag{3.38}$$

With zero values of $J_o(x)$ presented in Table 7 and eq (3.38), a plot of fringe order as a function of in-plane displacement was determined and presented on Figure 26.

With this information, fringe order as a function of length along the beam for the first two modes of vibration can be determined. For the first mode of vibration, eq (3.36) and Figure 26 along with the fact δ= .006 inches and l = 6.0 inches was used and the results are plotted in Figure 27. For the second mode of vibration, eq (3.37) and Figure 26 was used and the results are plotted in Figure 28. Figure 29 is a picture of the fringes for the first mode as they would appear in the transformed plane. Figure 30 is a picture of the fringes for the second mode of vibration.

Point-by-Point Interpretation

For the point-by-point interpretation, let

λ = 24.9 microinches

z = 40.0 inches

M = 1.0

δ = .006 inches

l = 6.0 inches

Therefore for n = 1, eq (3.28) becomes

$$u_f = \frac{3.8 \times 10^{-4}}{p} \tag{3.39}$$

Thus, fringe spacing as a function of displacement was determined and presented in Figure 31. Plots of fringe spacing as a function of length along the beam for the first and second modes of vibration were also determined and are shown in Figures 32 and 33, respectively.

Equipment for experimental verification of the theory presented in this section was unavailable. Thus, no experimental data is presented for this section.

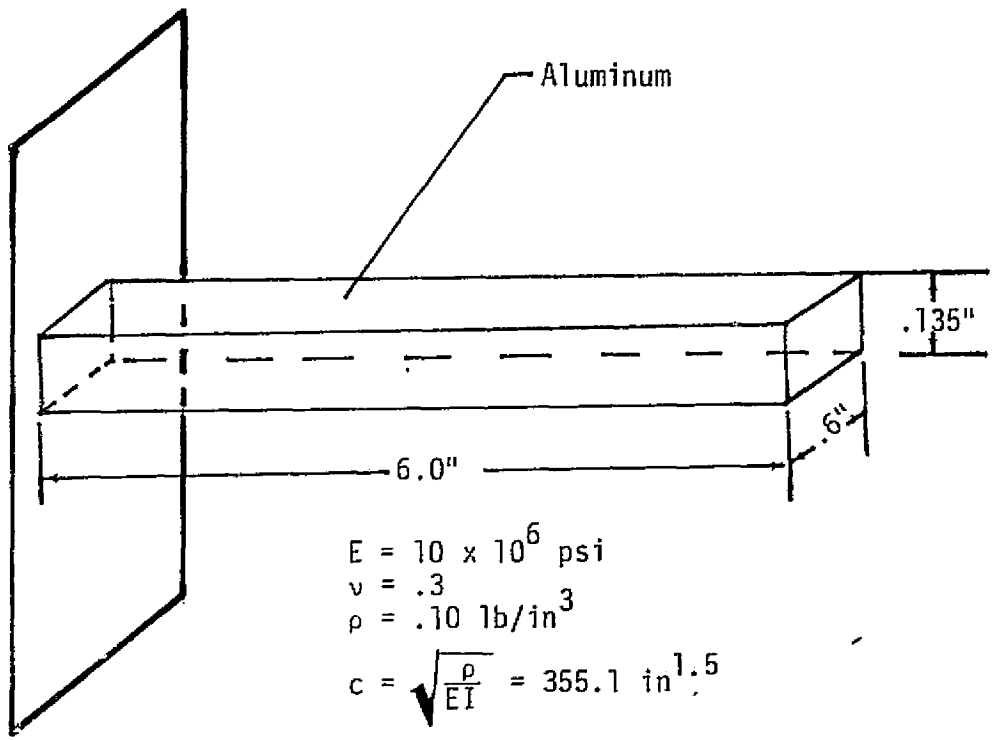

Figure 25. Numerical Example - Vibrating Cantilever Beam

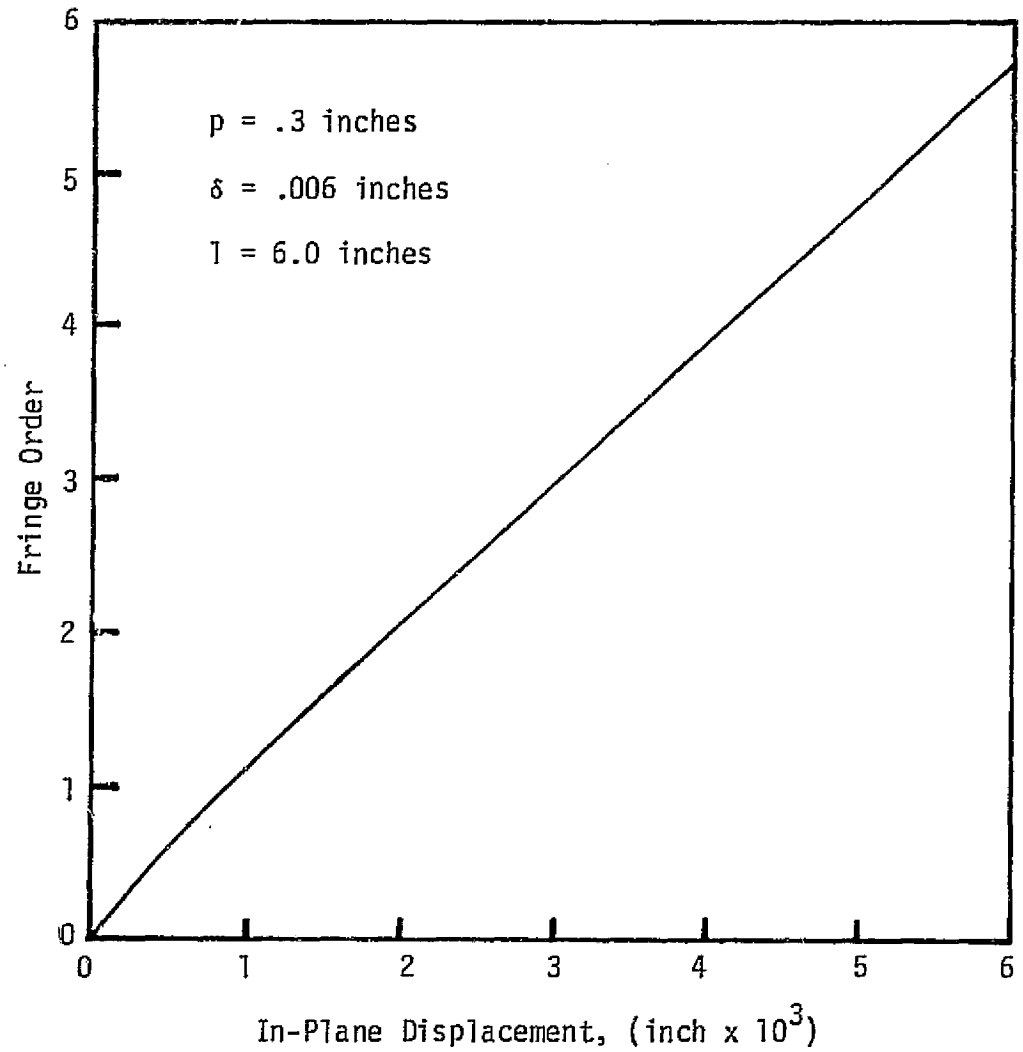

Figure 26. Fringe Order as a Function of In-Plane Displacement

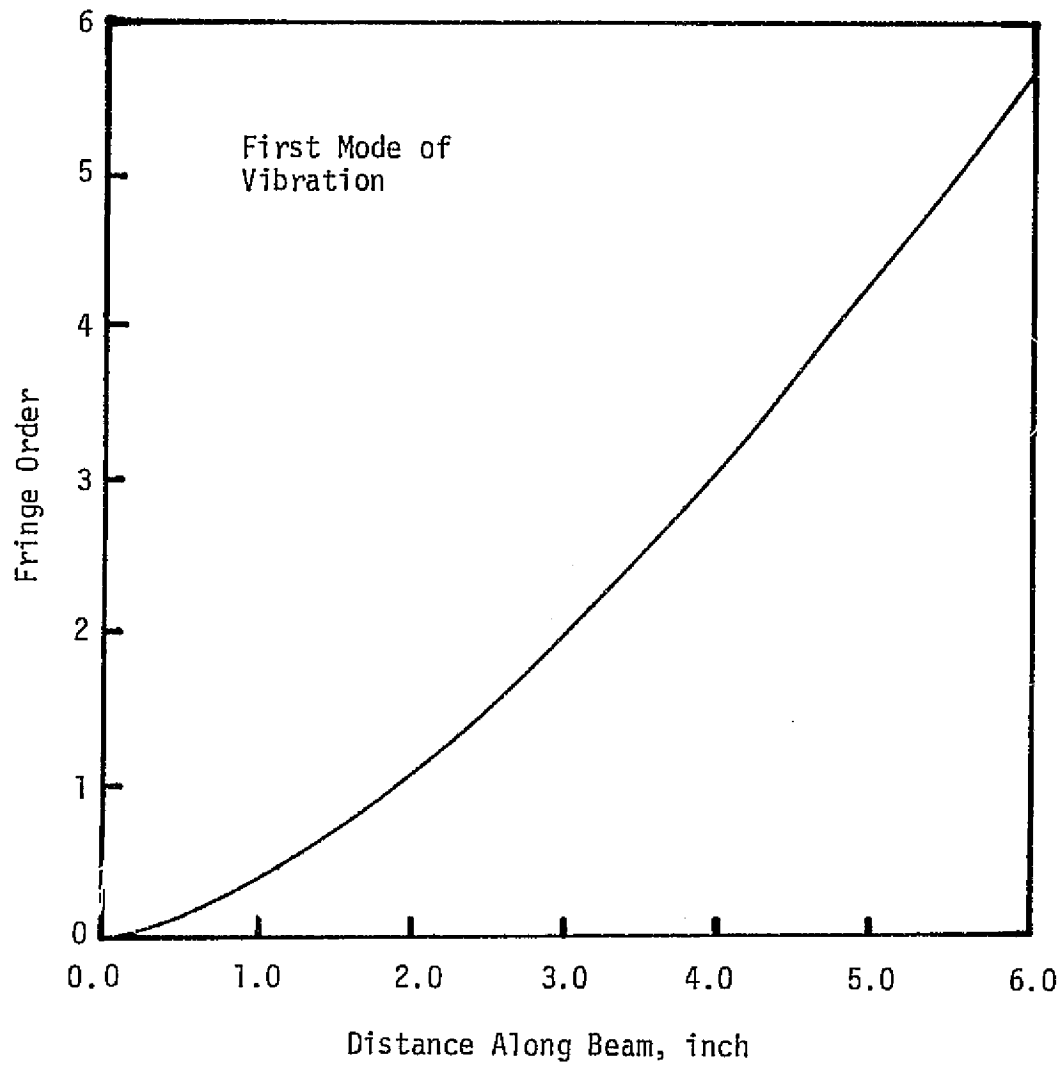

Figure 27. Variation of Fringe Order along the Beam for the First Mode of Vibration

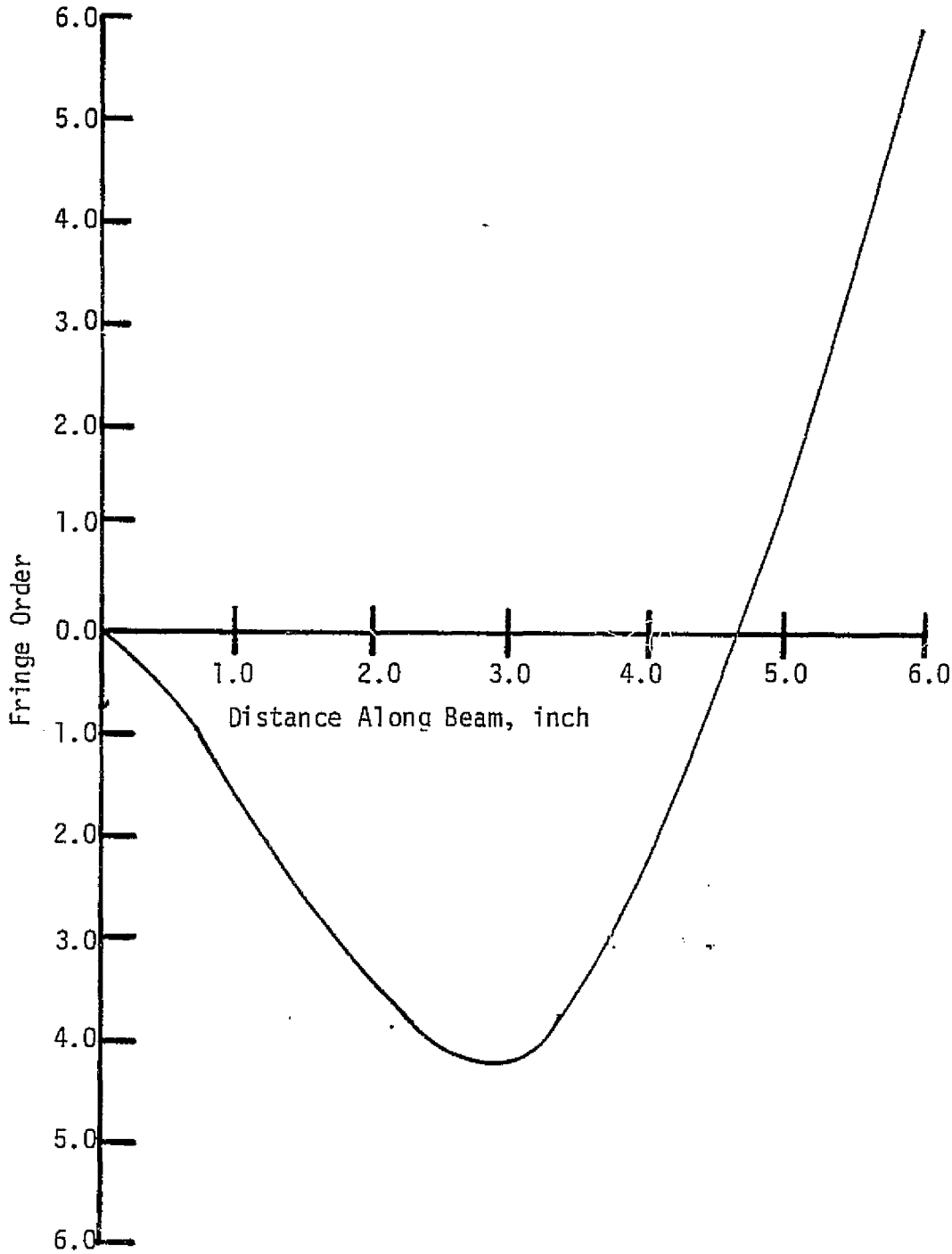

Figure 28. Variation of Fringe Order along the Beam for the Second Mode of Vibration

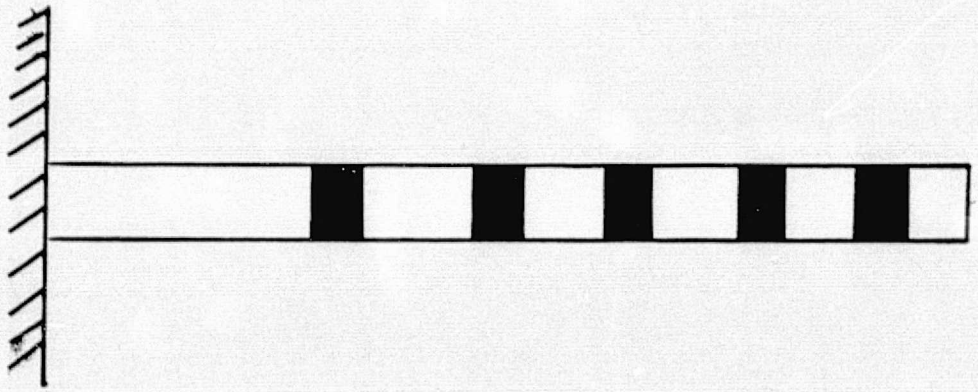

Figure 29. Fringe Location on Cantilever Beam for First Mode of Vibration

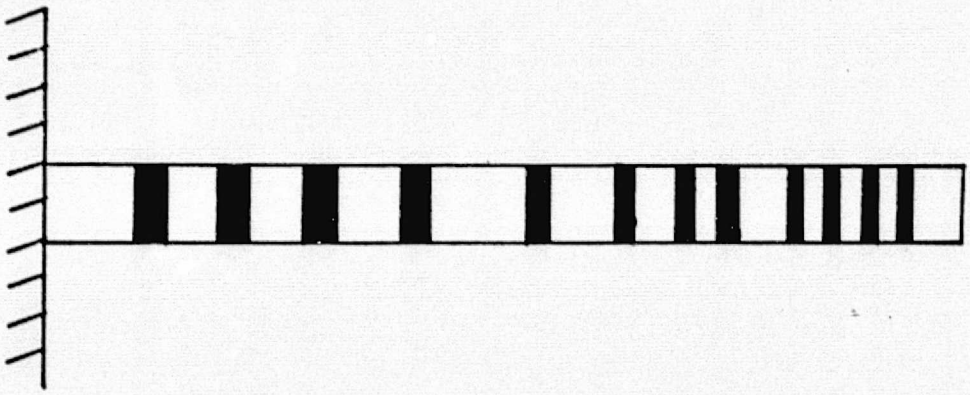

Figure 30. Fringe Location on Cantilever Beam for Second Mode of Vibration

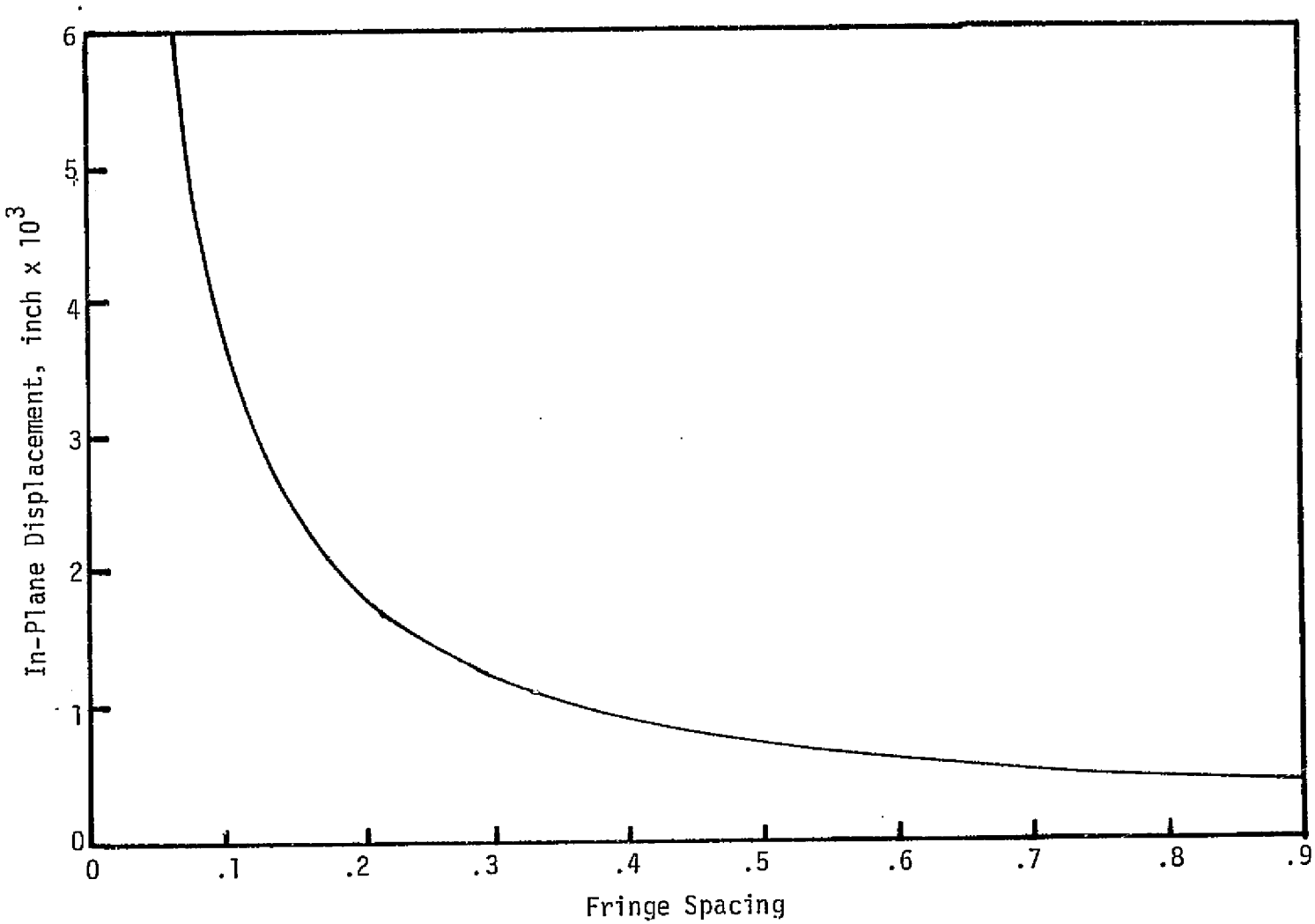

Figure 31. In-Plane Displacement as a Function of Fringe Spacing for the Numerical Example

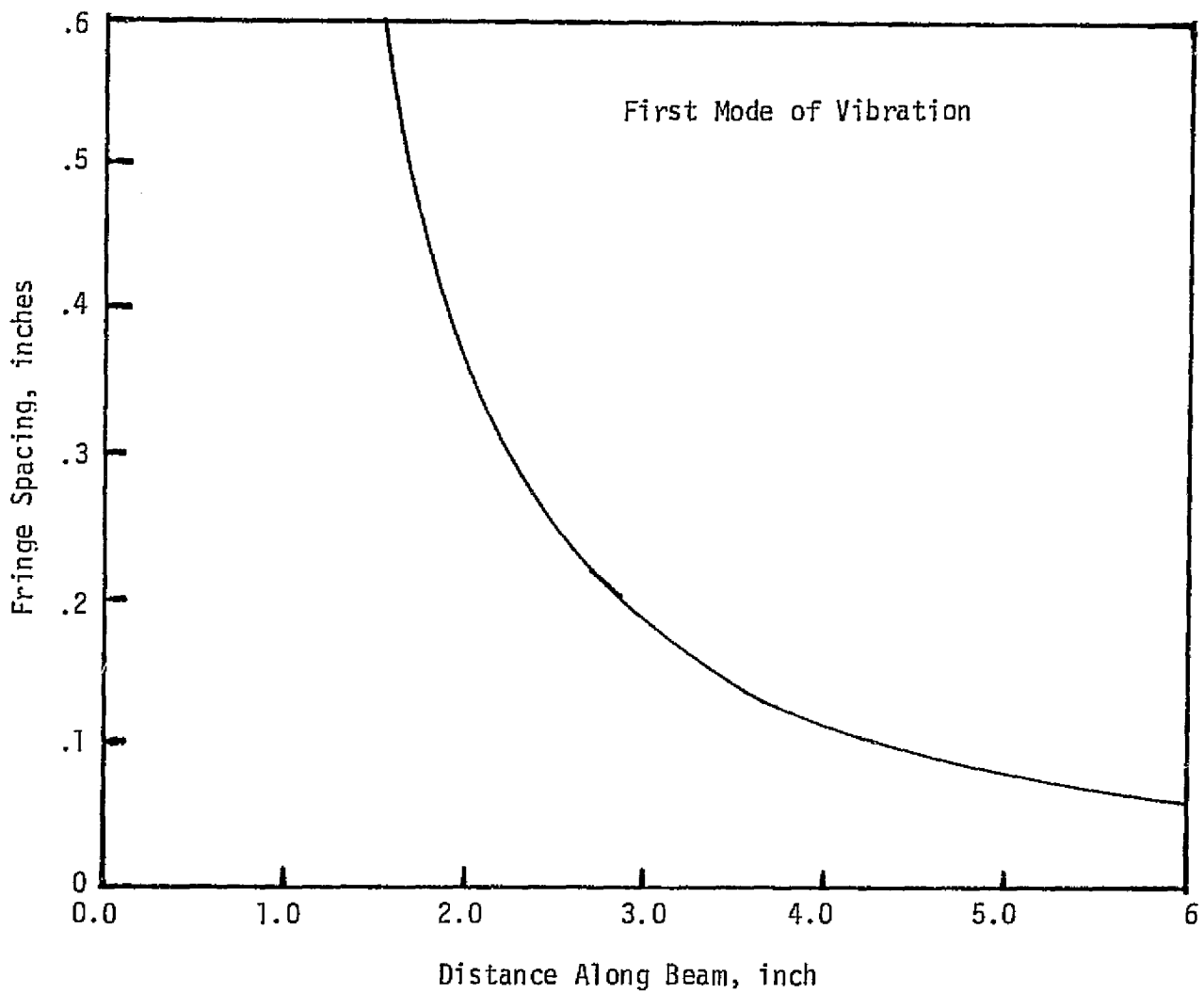

Figure 32. Fringe Spacing Along the Beam for the First Mode of Vibration

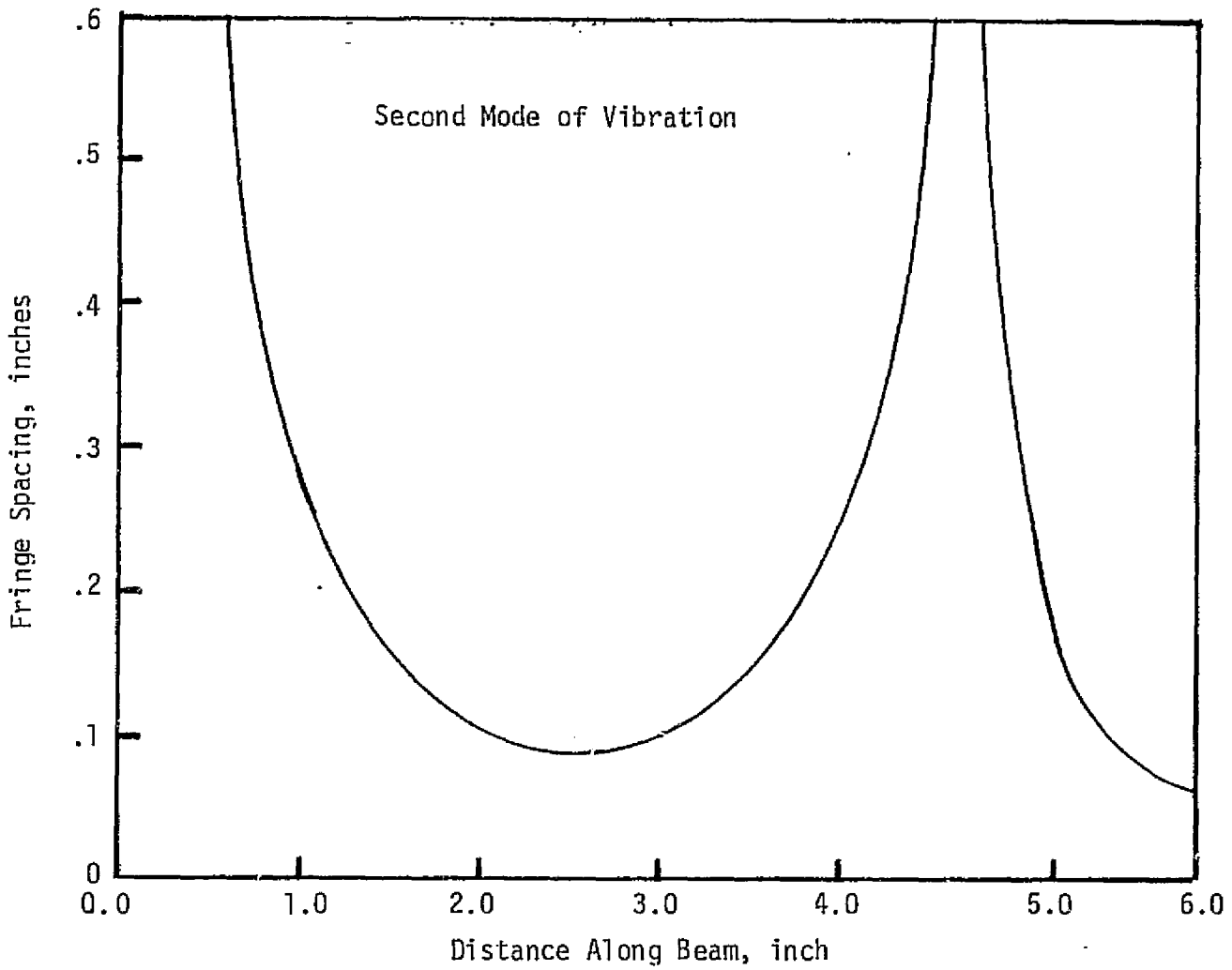

Figure 33. Fringe Spacing Along the Beam for the Second Mode of Vibration

IV. CONCLUSIONS

The theory for the formation of fringes in the transform plane for double exposure and time averaging speckle interferometry was developed. Thus, in-plane displacement resulting from either static or dynamic loading can be determined. For the evaluation of the fringes, the whole field concept was used and the relationship between fringes in the transform plane and displacement was derived. The technique is simple and needs no calibration and no laborious alignment of optical elements for the formation of the fringes.

The sensitivity of the technique is dependent upon the resolving power of the film, the magnification factor and the location of the aperture in the transform plane. In addition, the magnitude of the displacement has to be larger than the speckle size which is dependent upon the aperture opening of the camera lens.

In general, speckle interferometry has the ability to measure in-plane displacement for either the static or dynamic case within an accuracy of $\sim$5% for most of the displacement field.

REFERENCES

1. Brooks, R. E. and Heflinger, L. O., "Moire' Gaging Using Optical Interference Patterns", Applied Optics, V. 8 (5) (1969), pp. 935 - 939.

2. Adams, F. D. and Corwin, R. R., "A Technique for Measuring In-Plane Displacement by Holographic Interferometry", AFFDL-TR-72-5, (February, 1972).

3. Ennos, A. E., "Measurement of In-plane Surface Strain by Hologram Interferometry", Journal of Scientific Instruments (Journal of Physics E), V. 1 (7) (1968), pp. 731 - 734.

4. Groh, G., "Engineering uses of Laser-Produced Speckle Patterns, Symposium on the Engineering uses of Holography", University of Strathclyde, 1968.

5. Burch, J. M. and Tokarski, J. M. J., "Production of Multiple Beam Fringes from Photographic Scatterers", Optica Acta, V 15 (2) (1968), pp. 101 - 111.

6. Leendertz, J. A., "Interferometric Displacement Measurement on Scattering Surfaces Utilizing Speckle Effect", Journal of Scientific Instruments (Journal of Physics E), V 3 (3) (1970).

7. Duffy, D., "Measurement of Surface Displacement Normal to the Line of Sight", Spring, 1973 Meeting of Society for Experimental Stress Analysis, Los Angeles, California.

8. Archbold, E., Burch, J., Ennos, A., Taylor, D., "Visual Observation of Surface Vibration Nodal Pattersn", Nature, 222, 263, (April, 1969).

9. Eliasson, B., Mottier, F., "Determination of the Granular Radiance Distribution of a Diffuser and its use for Vibration Analysis", Journal of the Optical Society of America, 60, (5), 559 (May, 1971).

10. Tiziani, H., "Analysis of Mechanical Oscillations by Speckling", Applied Optics, 11, (12), 2911, (December, 1972).

11. Kopf, U., "Application of Speckling for Measuring the Deflection of Laser Light by Phase Objects", Optics Communications, 5, (5), 347, (August, 1972).

12. Cloud, G., "Quantitative 'Speckle-Moire' Interferometry", 1973 Meeting, Society for Experimental Stress Analysis, Indianapolis, Indiana.

13. Rayleigh, Lord, Scientific Papers of Lord Rayleigh, Dover, New York, New York, V. 1, pp. 491 - 496.

14. Kinariwala, V. R., "Determination of Surface Stresses Using Speckle Interferometry", M. S., Auburn University, March, 1976.

15. Sokolnikoff, I. S., Mathematical Theory of Elasticity, McGraw - Hill, 1956.

16. Hinariwala, V. R., Ranson, W. F., Swinson, W. F., "Stress Analysis of Vibrating Compressor Blades", ME-UC-7405, March, 1976.

17. Nowacki, W., Dynamics of Elastic Systems, John Wiley and Sons, Inc., 1963.

PART II

THE LASER SPECKLE EFFECT
APPLIED TO OPTICAL STRESS ANALYSIS

TABLE OF CONTENTS

LIST OF TABLES viii

LIST OF FIGURES ix

LIST OF SYMBOLS xi

I. INTRODUCTION. 1

Basic Phenomena
Photoelasticity
Holography

II. SHEARING SPECKLE INTERFEROMETRY 17

Static Loading
Time Average

III. SINGLE BEAM SPECKLE INTERFEROMETRY. 33

Static Loading
Time Average

IV. EXPERIMENTAL VERIFICATION 39

Double Exposure Shearing Speckle Interferomentry
Shearing Speckle Interferometry Vibration
Double Exposure Single Beam Speckle Interferometry
Single Beam Speckle Vibration

V. CONCLUSIONS AND RECOMMENDATIONS 59

REFERENCES. 60

LIST OF TABLES

1. Zero Values for $J_0(x)$. 32

2. Solutions for Transendental Equation for Vibrating Cantilever Beam. 45

3. Data Reduction for Vibration Speckle 58

LIST OF FIGURES

1. Optical Arrangement for Cross and Circular Polariscope. 3

2. Cross Polariscope with Model. 4

3. Circular Polariscope with Model 7

4. Optical Arrangement for Holography. 11

5. Reconstruction of Hologram. 14

6. Geometry of Fringe Formation. 15

7. Optical Configuration for Shearing Speckle. 18

8. Optical Configuration for Fourier Transform 21

9. Wedge Effect. 24

10. Lens Geometry 24

11. Shearing Speckle Interferometry 25

12. Specific Optical Arrangement for Vibration Shearing Speckle . . 30

13. Optical Arrangement for Single Beam 34

14. Experimental Arrangement for Double Shearing Speckle Interferometry. 40

15. Shearing Speckle Photograph After Fourier Filtering 42

16. Theoretical Fringe Plot with Experimental Fringes for Double Exposure Shearing Speckle. 43

17. Experimental Arrangement for Vibration Shearing Speckle 47

18. Vibration Shearing Speckle Fringe Drawings. 48

19. Plot of Theoretical Curves and Experimental Fringes for Vibration Shearing Speckle. 49

20. Experimental Configuration for Double Exposure Single Beam Speckle Interferometry. 51

21. Fourier Transformed Image for Double Exposure Single Beam Speckle. 52

22. Graph of Theoretical Curve with Experimental Fringes for Double Exposure Single Beam Speckle 53

23. Experimental Configuration for Single Beam Speckle Vibration . 55

24. Sample of Fringes from Point by Point Data Reduction for Single Beam Speckle. 56

25. Theoretical Curve and Experimental Points for Vibration Single Beam Speckle. 57

LIST OF SYMBOLS

a,b	film constant
A	maximum amplitude
$\vec{E}$, $\vec{E}_R$, $\vec{E}_o$	optic vector
I	intensity
i	$\sqrt{-1}$
g(x)	optical transmission function
G(x)	Fourier transform function
J_o	zero order Bessel function
$l_s, m_s, n_s, l_o, m_o, n_o$	direction cosines
M	magnification factor
m	index of refraction
n	fringe order
p	distance in transform plane
p_1, p_2	points on the object
p,q	principal axes of stress
(x,y,z)	coordinates
u,v,x	displacement components
ωt	phase
ϕ	initial phase
Θ	angle
μ	constant of proportionality
Θ	angle between the fast axis and the vertical

$\Delta\phi$	difference in phase angles
f_σ	stress optic coefficiect
τ_{max}	maximum shear stress
$\Delta\Theta$	change in phase due to deformation
Δ_i	separation on film
α	wedge angle
δ	tip deflection
Δz	shift in z direction
ω	frequency of vibration
λ	wavelength
Φ_i	zeros of the Bessel function
β_r	radian angle for vibration of beam
Θ_{xp}	angle between vertical and fast axis

I. INTRODUCTION

1.1 Basic Phenomena

The relation between the elastic and electromagnetic material properties was studied by Wertheim in 1844.(Annales de Chimie,T. XII pp. 610-624). This interest was continued by Lord Kelvin who in 1856 noticed that the resistance of wires changed as the wires were stretched [1]. This later led to the developement of the electrical-resistance strain gage.

Since World War II strain gages have been used extensively by industry to determine strains in variously loaded members. The major disadvantage is the fact that three gages are required (rossette) to analyze a single point thus requiring many gages for a complete analysis [2].

Recently several optical stress analysis techniques have been developed that give a full field representation of displacement, strain or stress fields which utilize the wave nature of light as the mathematical model [3] .

$$\vec{E} = \bar{A} \cos(\omega t + \phi) \tag{1.1}$$

where

$\vec{E}$ - optic vector $\qquad$ ωt - phase

$\bar{A}$ - maximum amplitude $\qquad$ ϕ - initial phase

From Euler's identity

$$\exp(i\theta) = \cos\theta + i \sin\theta \tag{1.2}$$

$\vec{E}$ becomes

$$\vec{E} = \vec{A} \exp[i(\omega t + \phi)]$$

where it is understood that we are dealing with the real part of the exponential function.

The intensity is

$$I = \mu \vec{E} \cdot \vec{E}^*$$

where $\vec{E}^*$ is the complex conjugate, and μ is a constant.

1.2 Photoelasticity

Photoelasticity uses the property of birefringence in certain materials [4]. When polarized light is incident on certain crystals it can be resolved into two components along the pricipal directions. One component is retarded with respect to the other and is referred to as the slow axis. The other is the fast axis. For a more rigorous discussion see [3], or [5].

There are two basic arrangements for photoelasticity [5], the cross polariscope and the circular polariscope (Figure 1).

In a crossed or standard polariscope, the two elements are a polarizer and an analyzer. Both are polarizing prisms that convert ordinary light into plane polarized light. There is no light output from the analyzer since it is "crossed" relative to the polarizer.

If a birefringent model is placed between the polarizer and analyzer (Figure 2), then loaded, there is light output.

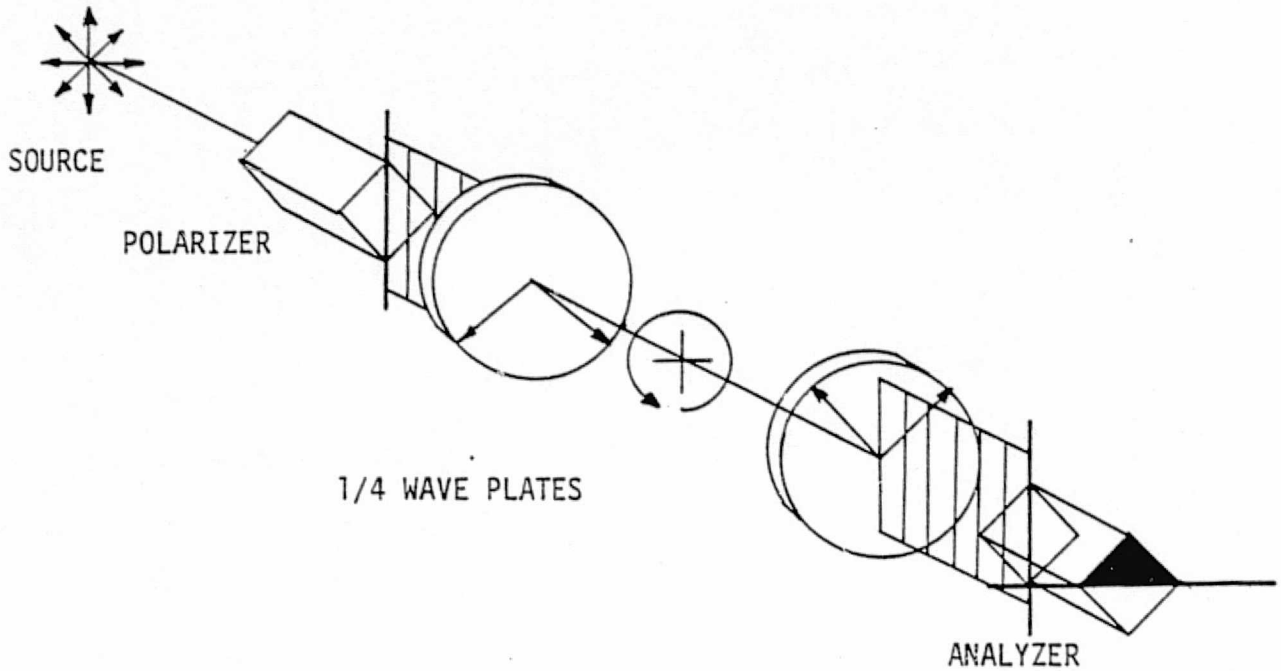

(A) Circular Polaricope

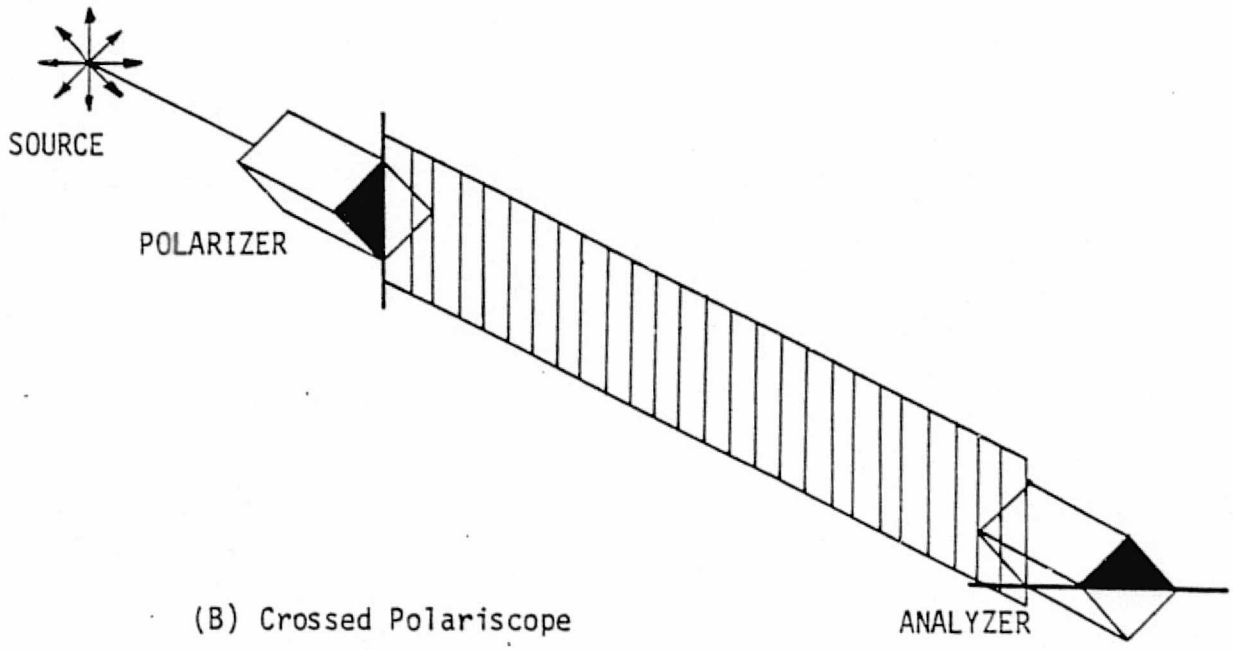

(B) Crossed Polariscope

Figure 1. Optical arrangement for cross and circular polariscope

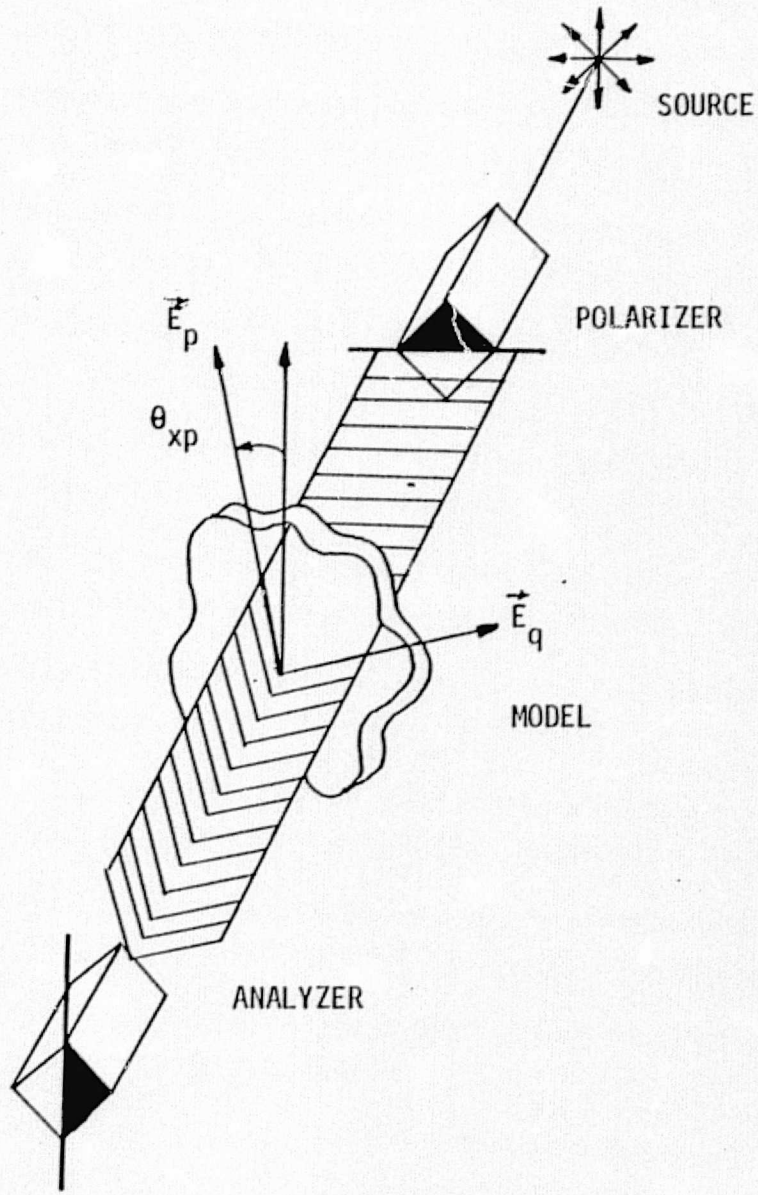

Figure 2. Cross Polariscope with Model

The light from the polarizer can be described by

$$\vec{E} = \vec{A}_o \exp(i\omega t) \tag{1.3}$$

When light enters the model, it is resolved into two components

$$\vec{E}_p = \vec{E} \cos\theta_{xp} = \vec{A}_o \exp(i\omega t) \cos\theta_{xp} \tag{1.4}$$

$$\vec{E}_q = \vec{E} \sin\theta_{xp} = \vec{A}_o \exp(i\omega t) \sin\theta_{xp}$$

When it leaves the model, the light vector becomes

$$\vec{E}_{p'} = \vec{A}_o \exp(i\omega t + \phi_p) \cos \theta_{xp} \tag{1.5}$$

$$\vec{E}_{q'} = \vec{A}_o \exp(i\omega t + \phi\ ) \sin \theta_{xp}$$

and when it leaves the analyzer

$$\vec{E}_r = \vec{E}_{p'} \sin\theta_{xp} + \vec{E}_{q'} \cos\theta_{xp} \tag{1.6}$$

which reduces to

$$\vec{E}_r = \vec{A}_o \exp(i\omega t) \sin 2\theta_{xp} \exp(i\phi_p) - \exp(i\phi_q) \tag{1.7}$$

The intensity becomes

$$I = \mu A_o^2 \sin^2 2\theta_{xp}[1 - \cos\Delta\phi] \tag{1.8}$$

or

$$I = \mu\ A_o^2 \sin^2 2\theta_{xp} \sin^2 \left(\frac{\Delta\phi}{2}\right) \tag{1.9}$$

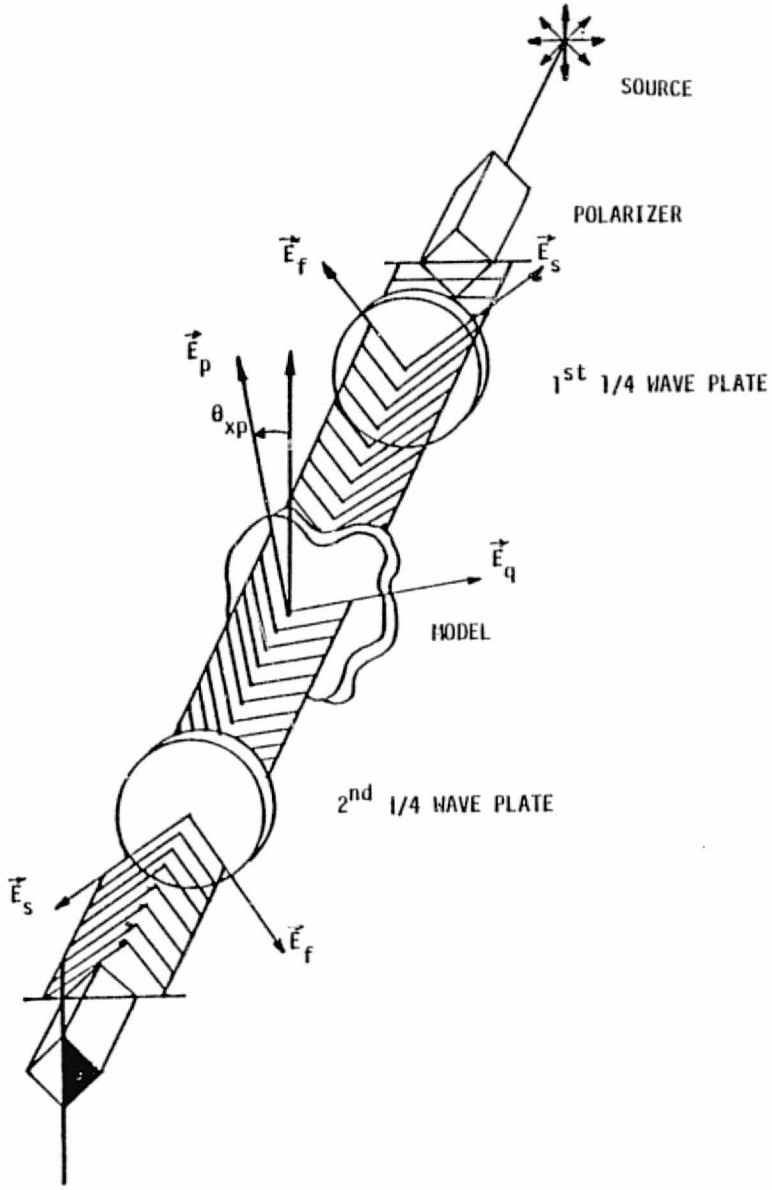

Figure 3. Circular Polariscope with Model

$$\vec{E}_s = \sqrt{2}/2\ \overline{A}_o \exp(i\omega t) \tag{1.13}$$

After leaving the quarter wave plate, the light vectors become

$$\vec{E}_{f'} = \sqrt{2}/2\ \overline{A}_o \exp i(\omega t + \phi_f)$$

$$\vec{E}_{s'} = \sqrt{2}/2\ \overline{A}_o \exp i(\omega t + \phi_s) \tag{1.14}$$

where

$$\phi_f = \pi/2 + \phi_s$$

Upon entering the model, the light is resolved into two light vectors along the principal axes, p and q. They are

$$\vec{E}_p = \vec{E}_{f'}\ (\cos(\pi/4 - \theta_{xp})) + \vec{E}_{s'}\ (\sin(\pi/4 - \theta_{xp}))$$

$$\vec{E}_q = \vec{E}_{f'}\ (\sin(\pi/4 - \theta_{xp})) - \vec{E}_{s'}\ (\cos(\pi/4 - \theta_{xp})) \tag{1.15}$$

and upon leaving the model, these light vectors become

$$\vec{E}_{p'} = i\ \frac{\overline{A}_o\sqrt{2}}{2} \exp i\ (\omega t + \phi s - \pi/4 + \theta_{xp} + \phi_p)$$

$$\vec{E}_{q'} = -\ \frac{\overline{A}_o\sqrt{2}}{2} \exp i\ (\omega t + \phi s - \pi/4 + \theta_{xp} + \phi_q) \tag{1.16}$$

Note that

$$\exp(i\frac{\pi}{2}) = i$$

and that

$$i\exp(i\theta) = i\cos\theta - \sin\theta\ .$$

Upon entering the second quarter wave plate

$$\vec{E}_s = \vec{E}_{p'} \cos(\frac{\pi}{4} - \theta_{xp}) + \vec{E}_{q'} \sin(\frac{\pi}{4} - \theta_{xp})$$

$$\vec{E}_f = \vec{E}_{p'} \sin(\frac{\pi}{4} - \theta_{xp}) - \vec{E}_{q'} \cos(\frac{\pi}{4} - \theta_{xp}) \tag{1.17}$$

and after leaving the second quarter wave plate

$$\vec{E}_{s'} = \frac{A_o\sqrt{2}}{2} \exp i(\omega t + 2\phi_s - \frac{\pi}{4} + \theta_{xp})[i\exp(i\phi_p) \cos(\frac{\pi}{4} - \theta_{xp})$$
$$- \exp(i\phi_q) \sin(\frac{\pi}{4} - \theta_{xp})]$$

$$\vec{E}_{f'} = \frac{A_o\sqrt{2}}{2} \exp i(\omega t + 2\phi_s - \frac{\pi}{4} + \theta_{xp})[-\exp(i\phi_p) \sin(\frac{\pi}{4} - \theta_{xp})$$
$$+ i\exp(i\phi_q)\cos(\frac{\pi}{4} - \theta_{xp})] \tag{1.18}$$

Finally going into the analyzer

$$\vec{E}_r = \vec{E}_{f'} \frac{\sqrt{2}}{2} - \vec{E}_{s'} \frac{2}{2} \tag{1.19}$$

and after leaving the analyzer $\vec{E}_r$ reduces to

$$\vec{E}_r = \frac{A_o}{2} \exp i(\omega t + 2\phi_s + 2\theta_{xp})[\exp(i\phi_p) - \exp(i\phi_q)] \tag{1.20}$$

The intensity becomes

$$I = \mu A_o^2(1 - \cos\Delta\phi)$$

or

$$I = \mu A_o^2 \sin \frac{(\Delta\phi)}{2} \tag{1.21}$$

For a fringe

$$\frac{\Delta\phi}{2} = n_{11}\pi \tag{1.22}$$

and from the stress optic law [5],

$$\Delta\phi = f_\sigma h(p - q)$$

Where

$f\sigma$ is a stress-optic coefficient

h is plate thickness

$(p - q)$ differences in principal stresses.

So

$$p - q = \frac{n_{11}}{h} f\sigma = 2\,\tau max \tag{1.23}$$

Equation 1.23 is the basic equation for photoelasticity. The information above, along with the isoclinic information, gives an accurate description of the shear stress field.

Photoelasticity has many applications in stress analysis, for example it is used as a tool in fracture mechanics[7,8] for analyzing cracks. It can also be used in finding stress concentration factors for various structures and has application for wave propagation[9].

1.3 Holography

Holography takes advantage of the interference of two coherent light waves at a point on a film plane. The same mathematical model can be used as described in 1.1. Figure 4 shows the optical arrangement for holography. There are two beams, an object which illuminates

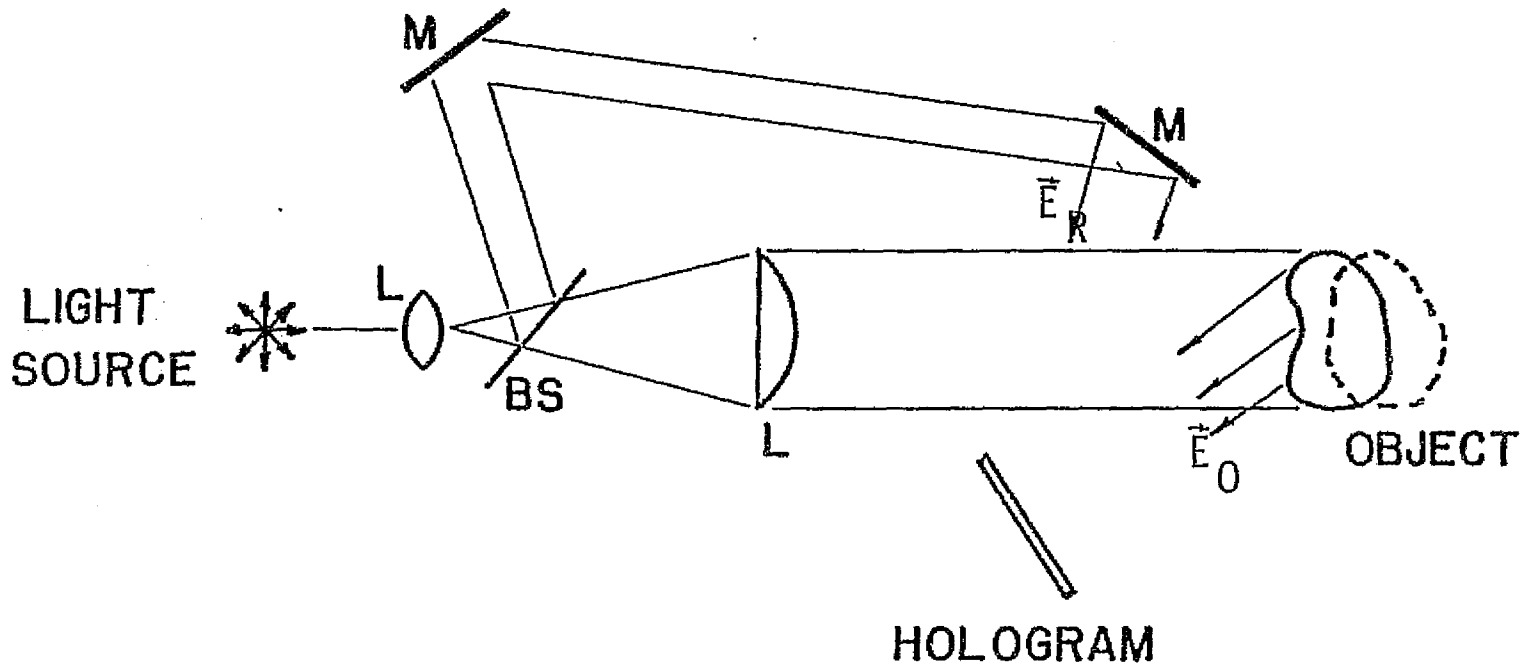

Figure 4. Optical arrangement for holographic interferometry.

the object, and a reference beam which is directed to the film plane. This is the off-axis reference beam method developed by Leith and Upatnieks [10].

Holographic interferometry is a double exposure technique. An exposure is made of the object before deformation, and an exposure is made after deformation. The surface displacement of a point is recorded as a phase variation, and fringes are produced.

With the arrangement shown in Figure 4 [11]

$$\vec{E}_R = \overline{A}_R \exp i(\omega t + \theta_R)$$

$$\vec{E}_o = \overline{A}_o \exp i(\omega t + \theta_o) \tag{1.24}$$

The total light vector for the first exposure is

$$\vec{E}_1 = \vec{E}_R + \vec{E}_o \tag{1.25}$$

$$= \overline{A}_R \exp i(\omega t + \theta_R) + \overline{A}_o \exp i(\omega t + \theta_o) \tag{1.26}$$

For the second exposure after deformation

$$\vec{E}_2 = \overline{A}_R \exp i(\omega t + \theta_R) + \overline{A}_0 \exp i(\omega t + \theta_o + \Delta\theta_o) \tag{1.27}$$

where $\Delta\theta_o$ is the change in the object wave due to deformation of the object by loading.

The intensity at the film for the two exposures is

$$I = \vec{E}_1 \cdot \vec{E}_1^* + \vec{E}_2 \cdot \vec{E}_2^* \tag{1.28}$$

After developing the hologram, the film is then reconstructed (Figure 5), where

$$\vec{E}_{Recon} = I\ \overline{A}_R \exp i(\omega t + \theta_R) \tag{1.29}$$

From this, three distinct terms may be separated: a virtual term, a real image term, and an undiffracted term.

The virtual term is used for analysis, and it reduces to [12].

$$I_{Virtual} = 2\ A_R^2\ A_o^2\ (1 + \cos\Delta\theta) \tag{1.30}$$

As in photoelasticity , the $\Delta\theta$ term can be interpreted physically. Ranson [12] shows (Figure 6) that the $\Delta\theta$ term is related to a geometry change or

$$\Delta\theta = \frac{2\pi}{\lambda}\ [(\vec{p}s + \vec{p}o) \cdot \vec{p}p'] \tag{1.31}$$

where

$\vec{p}s$ is a unit vector from a point on the body to the light source.

$\vec{p}o$ is a unit vector from a point on the body to the film.

$\vec{p}p'$ is the displacement vector.

The final intensity expression becomes

$$I_{Virtual} = 2\ A_R^2\ A_o^2\ [1 + \cos(\frac{2\pi}{\lambda}(\vec{p}s + \vec{p}o) \cdot pp')] \tag{1.32}$$

A fringe occurs when $I = 0$ or when $\cos\Delta\theta = -1$.

With the use of a photopolymer, holography can be used to find natural frequencies in complex vibrating objects [13]. It is very

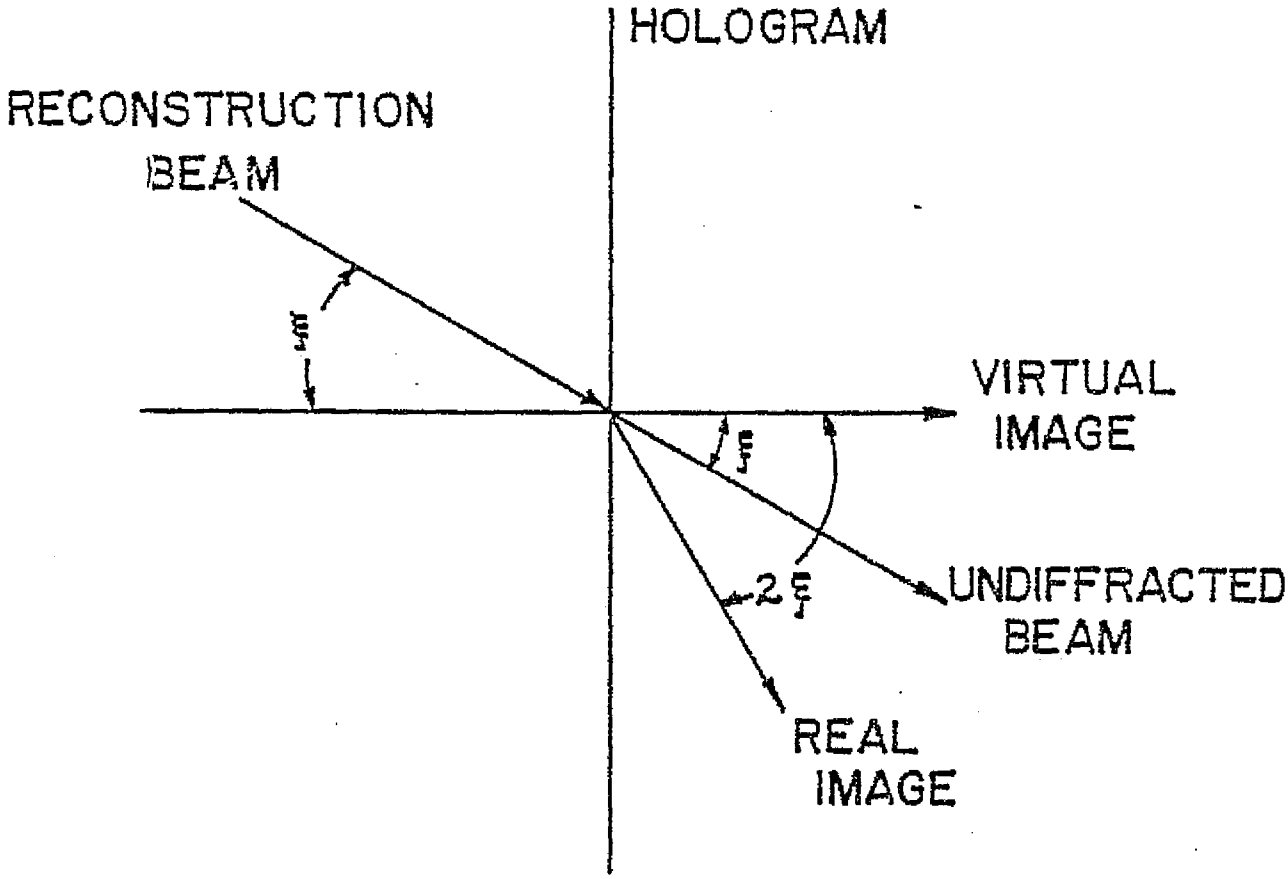

Figure 5. Reconstruction of Hologram

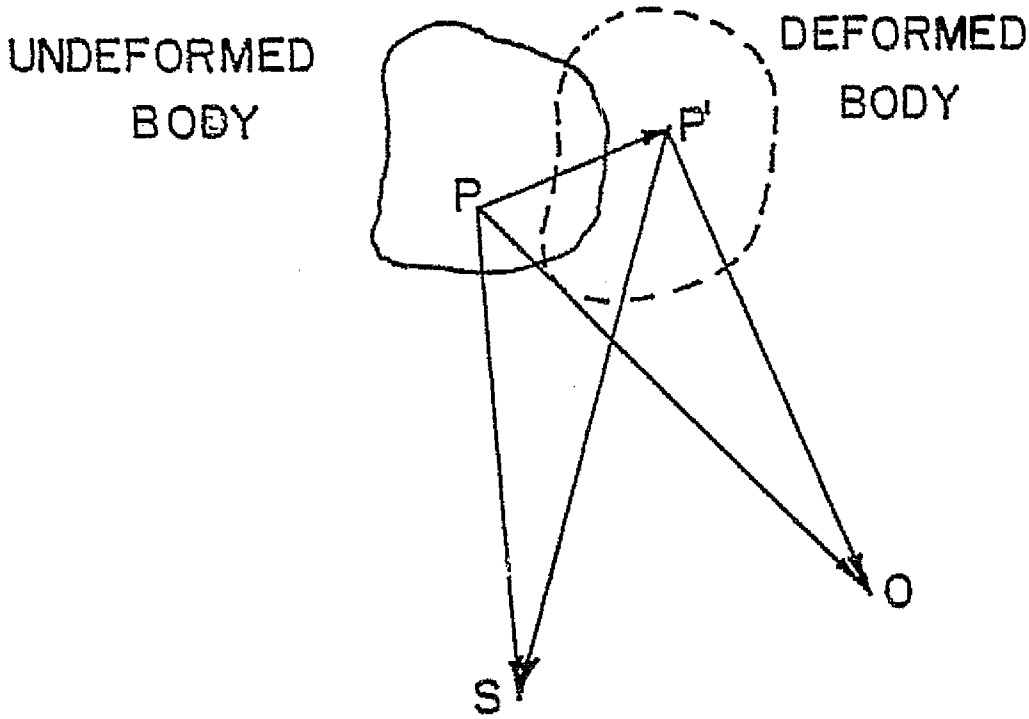

Figure 6. Geometry of Fringe Formation

sensitive to out of plane motion, and can be used in wave propagation studies when a pulsed laser is used [11].

Several optical techniques can be used to determine strains [12]. These are all based on geometry changes in a grid pattern either etched or projected onto the object. The most popular of these is Moire' [15].

Recently the speckle effect has received attention as a possible means of determining displacement components. This thesis will deal with this speckle effect in more detail.

II. SHEARING SPECKLE INTERFROMETRY

2.1 Static Loading Theory

The optical configuration for shearing speckle interferometry is shown in Figure 7. Note the use of the wedge in the system. Because of this wedge, the focused image has superimposed on it a "shifted" image in the direction of the shear. For a shear in the x_1 direction, a point P is imaged at (x_1, x_2) and $(x_1 + \Delta x_1, x_2)$ in the film plane, and a point P_1 is imaged at (x_1, x_2) in the film plane.

In order to obtain fringe data, a double exposure technique is used. A photograph is taken of the body in some reference position. The body is then deformed and another exposure is superimposed on the same film.

Ranson and Swinson [16] have shown that at the point (x_1, x_2), the light amplitude for the first exposure will be given by

$$\vec{E}_{T1} = \vec{E}_p + \vec{E}_{p1}$$

where

$$\vec{E}_p = \bar{A} \exp[i\ \theta_p(x_1,x_2)]$$

$$\vec{E}_{p1} = \bar{A} \exp[i\ \theta_{p1}(x_1,x_2)] \tag{2.1}$$

The total intensity for the first exposure is

$$I_1 = \vec{E}_{T1} \cdot \vec{E}_{T1}^* \tag{2.2}$$

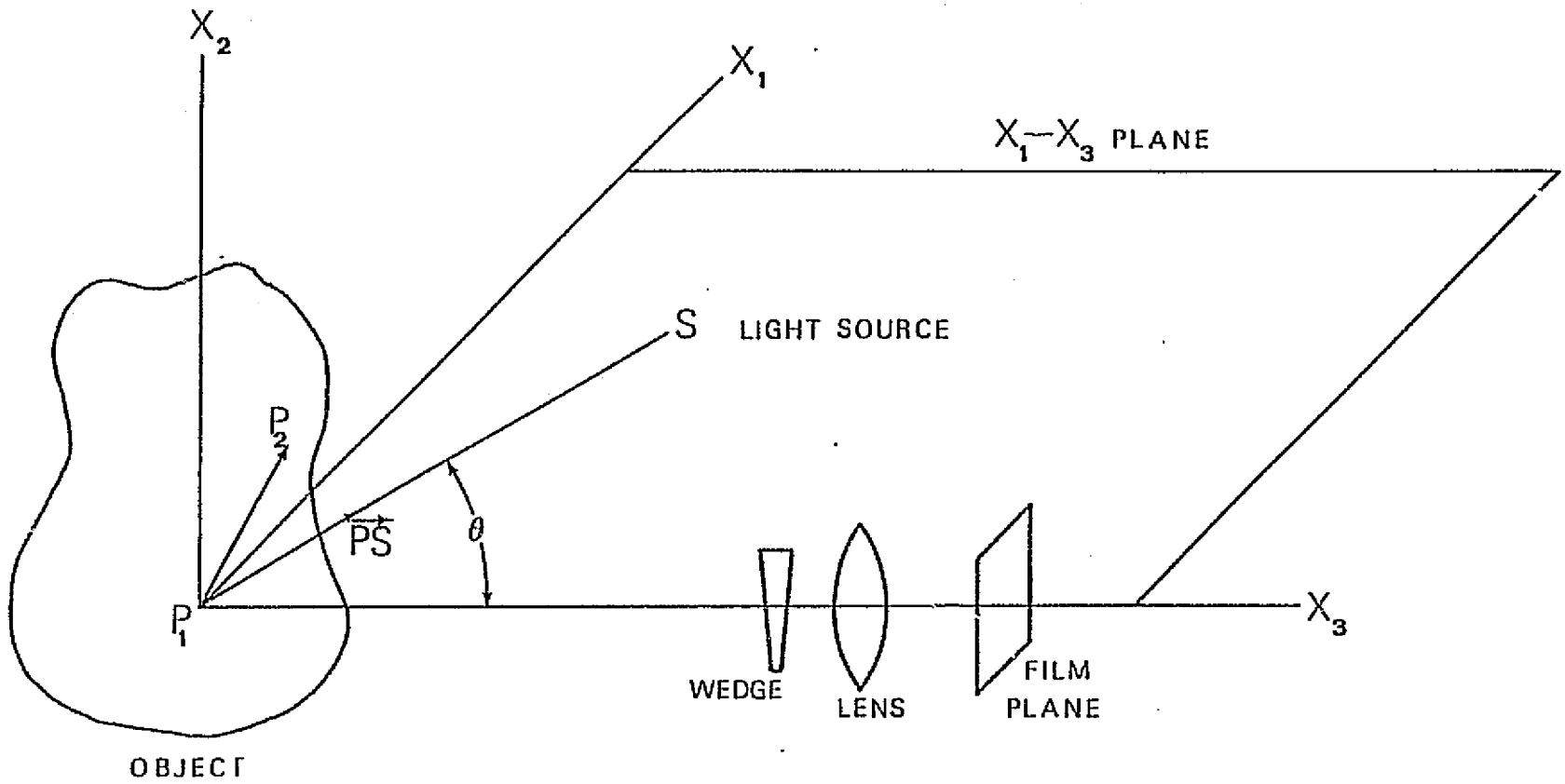

Figure 7. Optical configeration for shearing speckle interferometry.

where E_{T1}^* denotes the complex conjugate

or

$$I_1 = \{\bar{A}\exp[i\ \theta_p(x_1,x_2)] + \bar{A}\exp[i\ \theta_{p1}(x_1,x_2)]\}$$

$$\cdot\ \{\bar{A}\exp[-i\theta_p(x_1,x_2) + \bar{A}\exp[-i\theta_{p1}(x_1,x_2)]\} \tag{2.3}$$

$$= \bar{A}^2 + \bar{A}^2\exp[i\theta_p(x_1,x_2) - i\theta_{p1}(x_1,x_2)] +$$

$$\bar{A}^2\exp[i\theta_{p1}(x_1,x_2) - i\theta_p(x_1,x_2)] + \bar{A}^2 \tag{2.4}$$

$$= 2\bar{A}^2 + 2\bar{A}^2\cos[\theta_p(x_1,x_2) - \theta_{p1}(x_1,x_2)] \tag{2.5}$$

For convenience we define $\Theta = \Theta_p(x_1,x_2) - \Theta_{p1}(x_1,x_2)$

so

$$I_1 = 2\bar{A}^2 + 2\bar{A}^2\cos\theta \tag{2.6}$$

Similarily for the second exposure

$$\vec{E}_{T2} = \vec{E}_{p'} + \vec{E}_{p1'} \tag{2.7}$$

Where

$$\vec{E}_{p'} = \bar{A}\ \mathrm{expi}[\theta_p + \Delta\theta_p].$$

$$\vec{E}_{p1'} = \bar{A}\ \mathrm{expi}[\theta_{p1} + \Delta\theta_{p1}]$$

$\Delta\Theta_p$ is the change in phase due to deformation. The total intensity for the second exposure will be

$$I_2 = \vec{E}_{T2} \cdot \vec{E}_{T2}^{*} \tag{2.9}$$

$$= \bar{A}\ \exp i[\theta_p + \Delta\theta_p] + \bar{A}\ \exp i[\theta_{p1} + \Delta\theta_{p1}] \cdot$$

$$\bar{A}\ \exp(-i[\theta_p + \Delta\theta_p]) + \bar{A}\ \exp(-i[\theta_{p1} + \Delta\theta_{p1}]) \tag{2.10}$$

which reduces to

$$I_2 = 2A^2 + 2A^2 \cos(\theta + \Delta\theta) \tag{2.11}$$

where $\Delta\theta = \Delta\theta_p - \Delta\theta_{p1}$

So the total intensity expression for both exposures is

$$I_T = I_1 + I_2 \tag{2.12}$$

$$= 4\bar{A}^2 + 2\bar{A}^2\cos\theta + 2\bar{A}^2\cos(\theta + \Delta\theta) \tag{2.13}$$

Fringe data is obtained by taking the optical transform of the film as illustrated in Figure 8. For a transparency, the amplitude transmission function is linear for the ranges of interest or [16],

$$g(x) = a + bI_T \tag{2.14}$$

Where $g(x)$ is the transmission function. The Fourier transform of $g(x)$ is

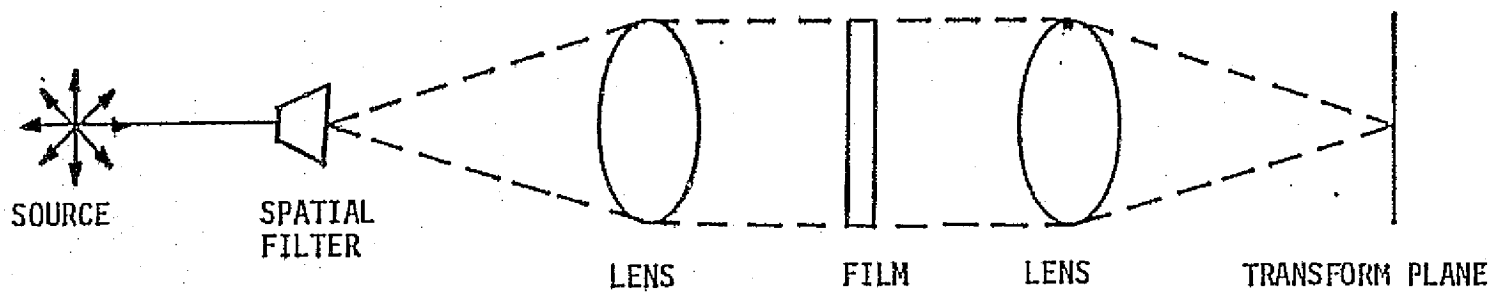

Figure 8. Optical Configuration for a Fourier Transform.

$$G(w) = \exp[-izw\ /2k] \int_{-\infty}^{\infty} g(x)\ \exp(-iwx)dx \tag{2.15}$$

Where G(w) is the Fourier transform function of g(x) which is the light amplitude in the transform plane.

$k = 2\pi/\lambda$ and

$w = \frac{kp}{z}$.

Now define

$$\delta(w) = \int_{-\infty}^{\infty} \exp[-iwx]dx \tag{2.16}$$

$$C(w) = \int_{-\infty}^{\infty} \cos\theta\ \exp[-iwx]dx \tag{2.17}$$

$$S(w) = \int_{-\infty}^{\infty} \sin\theta\ \exp[-iwx]dx \tag{2.18}$$

So

$$G(w) = \exp[\frac{-izw^2}{2k}]\int_{-\infty}^{\infty}\{a + b[4\overline{A}^2 + 2\overline{A}^2\cos\theta + 2\overline{A}^2\cos(\theta + \Delta\theta)]$$

$$\exp[-iwx]\}dx \tag{2.19}$$

$$= \exp[\frac{-izw^2}{2k}]\int_{-\infty}^{\infty}\{a + b[4A^2 + 2A^2\cos\theta(1 + \cos\Delta\theta)$$

$$- 2\overline{A}\ \sin\theta\ \sin\Delta\theta]\} \cdot \exp[-iwx]dx \tag{2.20}$$

$$= \exp[\frac{-izw^2}{2k}][(a + 4b\overline{A}^2)\delta(w) + 2b\overline{A}^2C(w)(1 + \cos\Delta\theta)$$

$$- 2b\overline{A}^2S(w)\sin\Delta\theta \tag{2.21}$$

The displacement information is related to the minimum of $|G(w)|$ or when $(1 + \cos\Delta\theta) = 0$ and $\sin\Delta\theta = 0$ or

$$\Delta\theta = (2n - 1)\pi \quad n = 1,2,3,\ldots$$

As in other optical techniques, this $\Delta\theta$ term can be physically interpreted. Ranson and Swinson [16] have shown that for a wedge, the wedge angle α is related to the deviation angle δ by (Figure 9)

$$\delta = (m - 1)\alpha \tag{2.22}$$

Where m is the index of refraction and the amount of shift or deviation Δi is

$$\Delta i = (m - 1)\alpha s' \tag{2.23}$$

Where s' is the distance from the lens to the focal point (Figure 10).

When an object is illuminated by a single beam (Figure 11), the wedge causes points P and P_1 to be imaged at the same film location. The separation on the film plane is Δi.

Consider now the phase variation of the two points P and P_1. As in holography the displacement vectors are

$$\vec{p}p' = u_i\vec{e}_i$$

$$\vec{p}_1p_1' = u_i\vec{e}_i = u_i(x_i + \Delta x_i)\vec{e}_i \tag{2.24}$$

The phase change is now

$$\Delta\theta_2 = \frac{2\pi}{\lambda}[\vec{p}_1s + \vec{p}_1o] \cdot \vec{p}_1p_1'$$

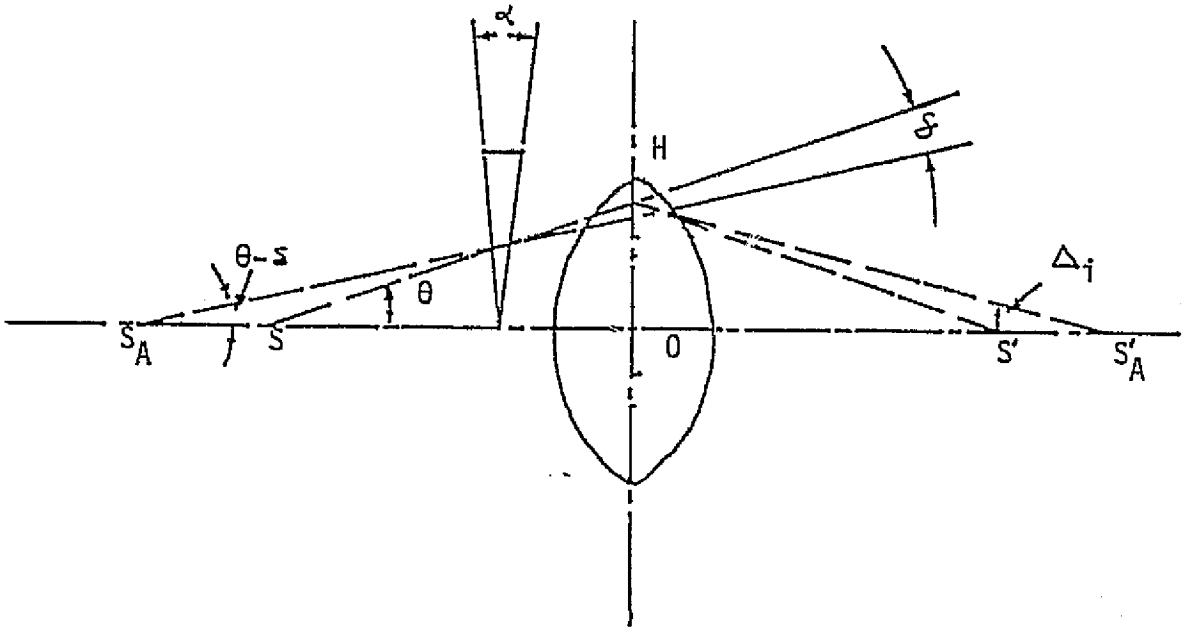

Figure 9. Wedge Effect

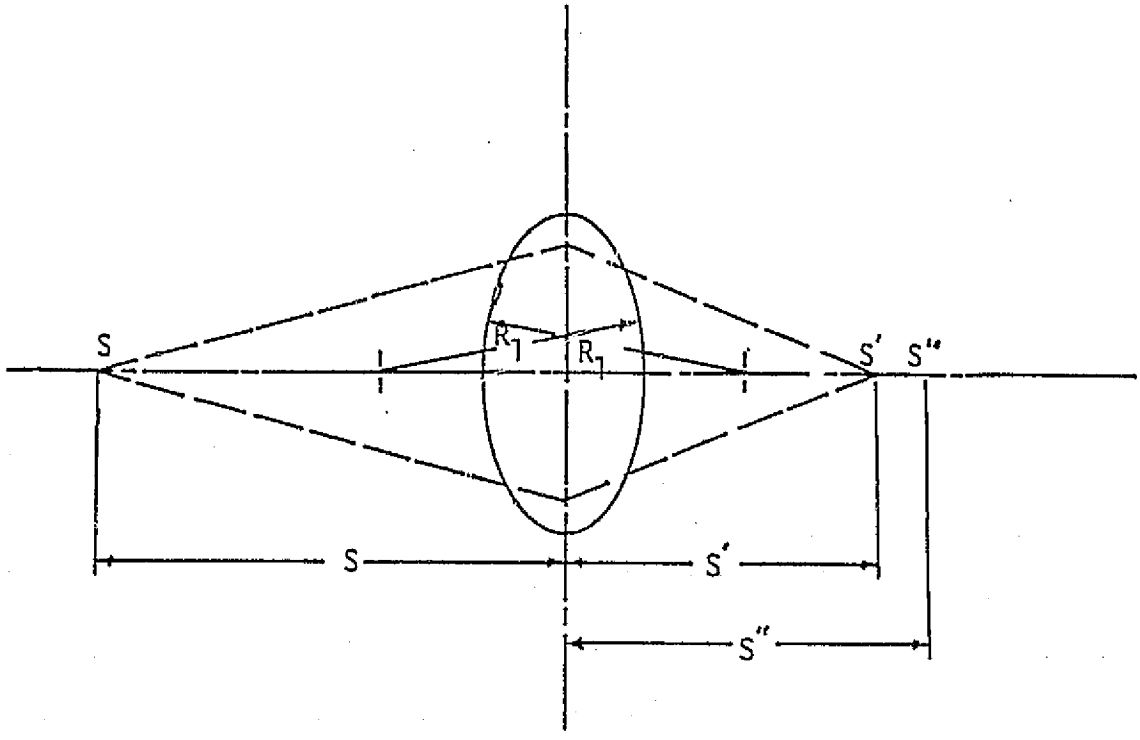

Figure 10. Lens Geometry

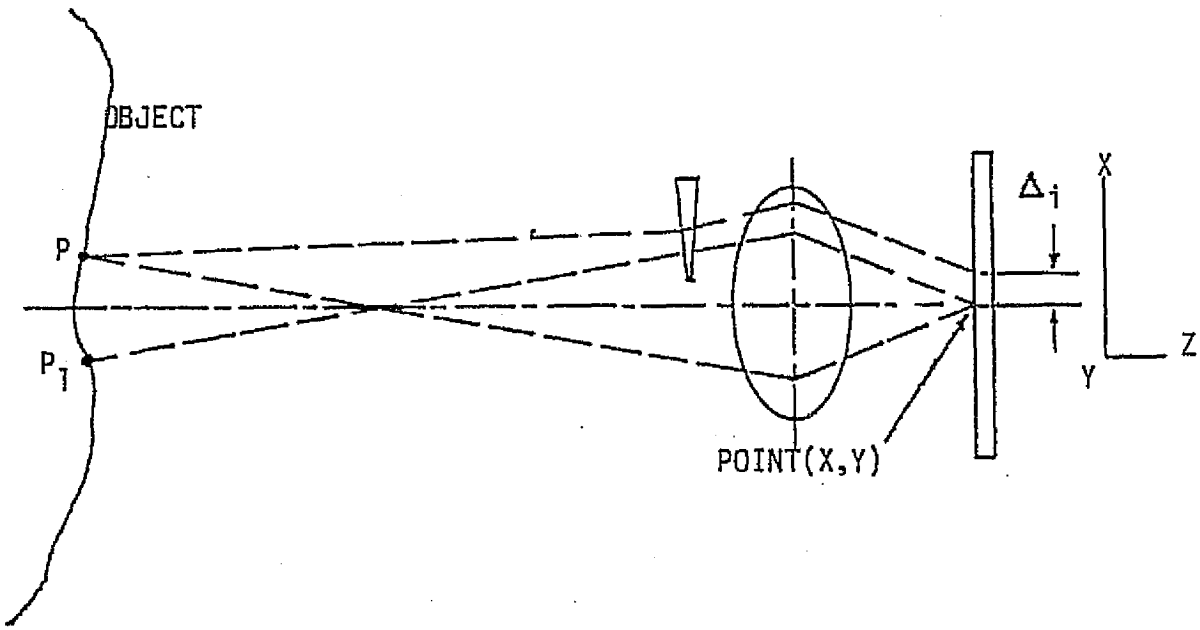

Figure 11. Shearing speckle interferometry.

$$\Delta\theta_1 = \frac{2\pi}{\lambda}[\vec{ps} + \vec{po}] \cdot \vec{pp'} \tag{2.25}$$

or for parallel unit vectors

$$\Delta\theta = \frac{2\pi}{\lambda}[\vec{ps} + \vec{po}] \cdot (\vec{p_1}p_1' - \vec{pp'}) \tag{2.26}$$

and fringes occur when $\Delta\theta = \pi, 3\pi, \ldots (2n - 1)\pi$

so [16]

$$\begin{aligned}(2n - 1)\pi = \frac{2\pi}{\lambda}\,(l_s + l_o)\left(\frac{\partial u}{\partial x}\Delta x + \frac{\partial u}{\partial y}\Delta y + \frac{\partial u}{\partial z}\Delta z\right) + \\ (m_s + m_o)\left(\frac{\partial v}{\partial x}\Delta x + \frac{\partial v}{\partial y}\Delta y + \frac{\partial v}{\partial z}\Delta z\right) + \\ (n_s + n_o)\left(\frac{\partial w}{\partial x}\Delta x + \frac{\partial w}{\partial y}\Delta y + \frac{\partial w}{\partial z}\Delta z\right) +\end{aligned} \tag{2.27}$$

An experimental example of this technique is shown in section 4.1.

2.2 Time Average

Consider again the arrangement of Figure 7 . This time the object is caused to vibrate toward the camera, usually by a frequency generator or oscillator. A film record is made of the object during vibration. During the vibration, the object reaches two positions of zero motion. This effect is in essence the double exposure or the recording at two different configurations. The film record is processed and placed in a Fourier filter system as before.

Again

$$\vec{E}_T = \vec{E}_p + \vec{E}_{p1} \tag{2.28}$$

where

$$\vec{E}_p = \overline{A}((x_1 + x_1'),(x_2 + x_2'))\exp i[\theta_p(x_1,x_2) + \Delta\theta_p]$$

and

$$\vec{E}_{p1} = \overline{A}((x_1 + x_1'),(x_2 + x_2'))\exp i[\theta_{p1}(x_1,x_2) + \Delta\theta_{p1}] \tag{2.29}$$

Note that the amplitude $\overline{A}$ is a function of the frequency of vibration and $\Delta\theta_p$ and $\Delta\theta_{p1}$ are the relative phase changes due to vibration.

The total intensity I is

$$I = \int_0^t (\vec{E}_p + \vec{E}_{p1}) \cdot (\vec{E}_p{}^* + \vec{E}_{p1}{}^*)dt \tag{2.30}$$

$$= \int_0^t \overline{A} \exp i[\theta_p + \Delta\theta_p] + \overline{A} \exp i[\theta_{p1} + \Delta\theta_{p1}] \cdot$$

$$\overline{A}\exp[-i(\theta_p + \Delta\theta_p)] + \overline{A}\exp[-i(\theta_{p1} + \Delta\theta_{p1})] \tag{2.31}$$

$$= \int_0^t 2\overline{A}^2 + \overline{A}^2\exp i[\theta_p + \Delta\theta_p - \theta_{p1} - \Delta\theta_{p1}] +$$

$$\overline{A}^2\exp[-i(\theta_p + \Delta\theta_p - \theta_{p1} - \Delta\theta_{p1})] \tag{2.32}$$

$$= \int_0^t 2\overline{A}^2 + \overline{A}^2\exp[i(\theta + \Delta\theta)] + \overline{A}^2\exp[-i(\theta + \Delta\theta)] \tag{2.33}$$

where

$$\theta = \theta_p - \theta_{p1}$$

$$\Delta\theta = \Delta\theta_p - \Delta\theta_{p1}$$

Recall $g(x) = a + bI$ (2.34)

which becomes

$$g(x) = a + b\int_0^t 2\overline{A}^2 + \overline{A}^2\exp[i(\theta + \Delta\theta)] + \overline{A}^2\exp[-i(\theta + \Delta\theta)]dt \tag{2.35}$$

$$= a + b[2\overline{A}^2 t + \overline{A}^2\exp(i\theta)\int_0^t \exp(i\Delta\theta)dt + \overline{A}^2\exp(-i\theta)\int_0^t \exp -i(\Delta\theta)]dt \tag{2.36}$$

As before

$$G(w) = \exp\left(\frac{izw^2}{2k}\right)\int g(x)\exp(-iwx)dx \tag{2.37}$$

$$= \exp\left(\frac{izw^2}{2k}\right)\int\{a + b[2\overline{A}^2 t + \overline{A}^2\exp(i\theta)\int_0^t \exp(i\Delta\theta)dt$$

$$+ \overline{A}^2\exp(-i\theta)\int_0^t \exp(-i\Delta\theta)dt]\}\exp(-ixw)dx \tag{2.38}$$

$$= \exp\left(\frac{izw^2}{2k}\right)a\,\delta(w) + 2\overline{A}^2 bt\,\delta(w)\exp\left(\frac{izw^2}{2k}\right)$$

$$+ b\exp\left(\frac{izw^2}{2k}\right)[\overline{A}^2\exp(i\theta)\int_0^t \exp(i\Delta\theta)dt$$

$$+ \bar{A} \exp(-i\Theta)\int_0^t \exp(-i\Delta\Theta)dt \exp[-iwx]dx \tag{2.39}$$

As before the $\Delta\Theta$ term can be expressed as

$$\Delta\Theta = \frac{2\pi}{\lambda}(l_s + l_0)\left(\frac{\partial u}{\partial x}\Delta x + \frac{\partial u}{\partial y}\Delta y + \frac{\partial u}{\partial z}\Delta z\right) +$$

$$(m_s + m_0)\left(\frac{\partial w}{\partial x}\Delta x + \frac{\partial w}{\partial y}\Delta y + \frac{\partial w}{\partial z}\Delta z\right) +$$

$$(n_s + n_0)\left(\frac{\partial w}{\partial x}\Delta x + \frac{\partial w}{\partial y}\Delta y + \frac{\partial w}{\partial z}\Delta z\right)$$

Now consider a specific optical arrangement (Figure 12).

$l_0 = 1$ $\qquad$ $l_s = \cos\beta$

$m_0 = 0$ $\qquad$ $m_s = 0$

$n_0 = 0$ $\qquad$ $n_s = \sin\beta$

$\Delta x = \Delta y = 0$

So $\Delta\Theta$ now becomes

$$\Delta\Theta = \frac{2\pi}{\lambda}(1 + \cos\beta)\frac{\partial u}{\partial z} + \sin\beta\frac{\partial w}{\partial z}\Delta z \tag{2.40}$$

Assume $\frac{\partial w}{\partial z}$ is negligible and $u = u_0(z)\sin t$, where u_0 is the maximum amplitude of vibration and ω is the frequency of vibration.

$$\frac{\partial u}{\partial z} = \frac{\partial u_0}{\partial z}\sin\omega t \tag{2.42}$$

For convenience define

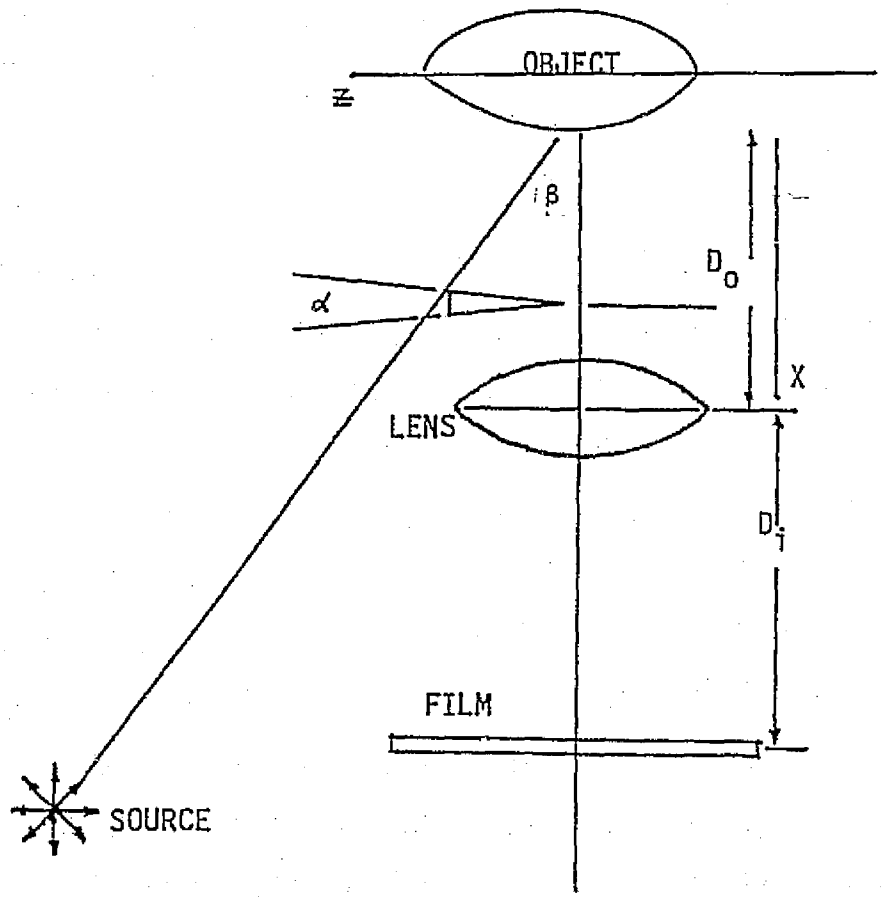

Figure 12. Specific optical arrangement for vibration shearing speckle interferometry.

$$B + \frac{\exp(izw^2)}{2k}\ \delta(w)[a + 2\overline{A}^2\ bt] \tag{2.43}$$

Now substituting Equations 2.40 - 2.43 into equation 2.39

$$G(w) = B + b\exp(\frac{izw^2}{2k})\int[\overline{A}^2\exp(i\Theta)\int_0^t \exp i[\frac{2\pi}{\lambda}(1 + \cos\beta)\Delta z\frac{\partial u_0}{\partial z}\sin\omega t]dt$$

$$+ \overline{A}^2\exp(-i\Theta)\int_0^t\exp(-i[\frac{2\pi}{\lambda}(1 + \cos\beta)\Delta z\frac{\partial u_0}{\partial z}\sin\omega t])dt\ \exp(-iwx)dx \tag{2.44}$$

Recall that

$$2\pi J_0(x) = \int_0^{2\pi}\exp(ix\ \sin\Theta)d\Theta \tag{2.45}$$

if $x = \frac{2\pi}{\lambda}\ (1 + \cos\beta)\frac{\partial u_0}{\partial z}\Delta z$

$\Theta = \omega t$

$d\Theta = \omega dt$

$t_1 = 2\pi/\omega$

then

$$G(w) = B + b\exp(\frac{izw^2}{2k})\int[\overline{A}^2\exp(i\Theta)\ J_0(\frac{2\pi}{\lambda}(1 + \cos\beta)\Delta z\frac{\partial u_0}{\partial z})$$

$$+ \overline{A}^2\exp(i\Theta)\ J_0(\frac{2\pi}{\lambda}(1 + \cos\beta)\Delta z\frac{\partial u}{\partial z})]\ \exp(-iwx)dx \tag{2.46}$$

Relative minimums occur when $J_0(x) = 0$ or when $x = \phi_i$ where ϕ_i values are tabulated in Table 1.

So

$$\frac{2\pi}{\lambda}(1 + \cos\beta)\Delta z\frac{\partial u_0}{\partial z} = \phi_i \tag{2.47}$$

TABLE 1

ZERO VALUES FOR $J_o(x)$

Φ_i

$\Phi_{01} = 2.40$

$\Phi_{02} = 5.52$

$\Phi_{03} = 8.65$

$\Phi_{04} = 11.79$

$\Phi_{05} = 14.93$

$\Phi_{06} = 18.07$

$\Phi_{07} = 21.21$

$\Phi_{08} = 24.34$

$\Phi_{09} = 27.49$

$\Phi_{10} = 30.63$

$\Phi_{11} = 33.78$

$\Phi_{12} = 36.92$

$\Phi_{13} = 40.06$

$\Phi_{14} = 43.20$

III. SINGLE BEAM SPECKLE INTERFEROMETRY

3.1 Static Loading

An object is illuminated by the laser light before deformation, and a photograph is taken with a conventional camera system as illustrated in Figure 13. The object is then deformed, and again another photograph is taken superimposed on the first.

For the first exposure, the light vector can be expressed as

$$\vec{E}_1(x_1,x_2) = \overline{A}(x_1,x_2)\ \exp[i\theta(x_1,x_2)] \tag{3.1}$$

where

(x_1,x_2) - film plane coordinates

$\theta(x_1,x_2)$ - phase at film

$\overline{A}(x_1,x_2)$ - amplitude factor

The intensity expression for the first exposure is

$$I = \vec{E}_1 \cdot \vec{E}_1^* \tag{3.2}$$

Now for the second exposure, again

$$\vec{E}_2(x'_1,x'_2) = \overline{A}(x'_1,x'_2)\ \exp[i\theta(x'_1,x'_2)] \tag{3.3}$$

and a similar expression exists for I_2

Wilson [17] has shown that the total intensity at the film plane is

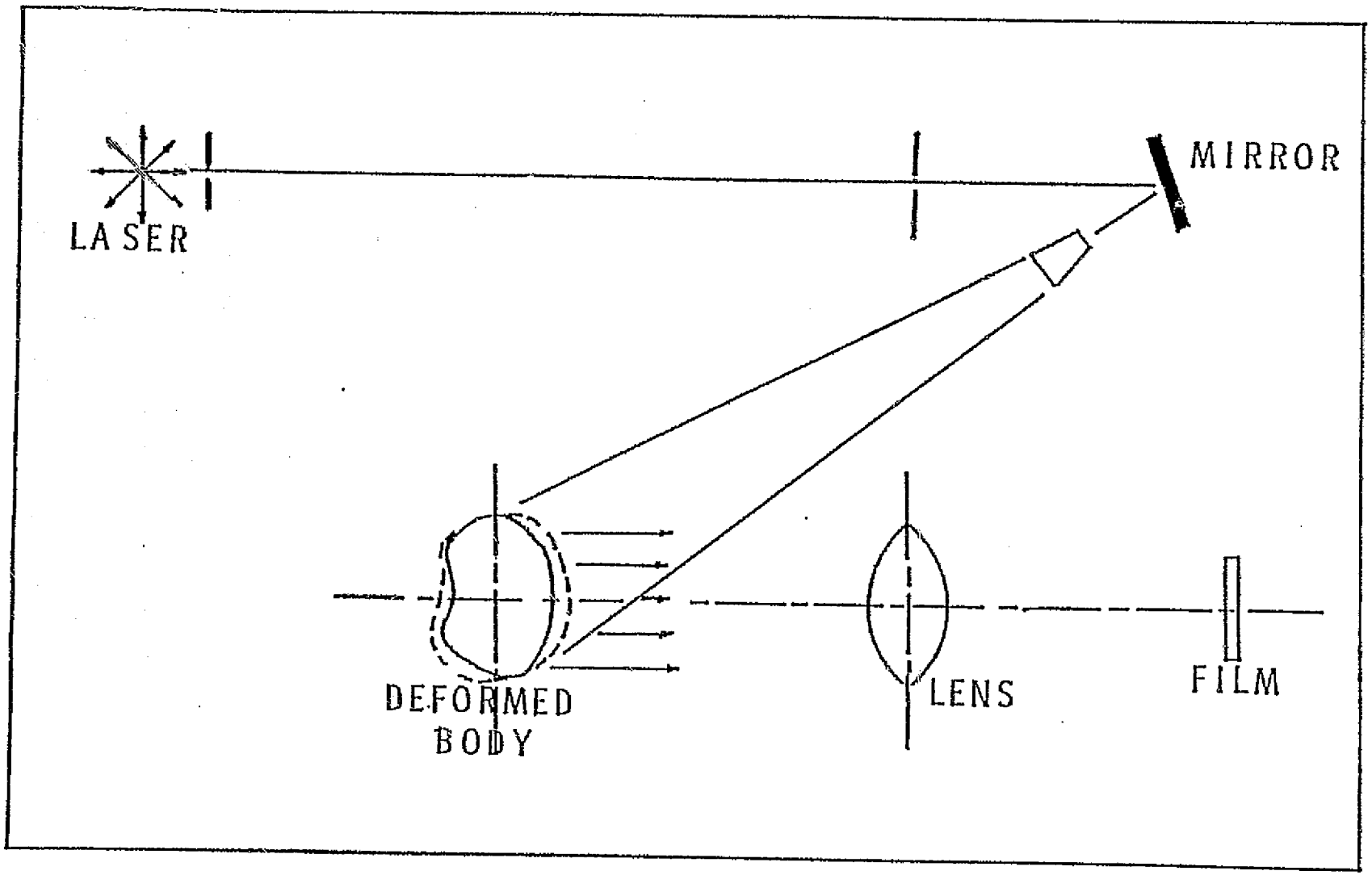

Figure 13. Optical arrangement for single beam speckle interferometry.

$$I_T = A^2(x_1,x_2) + A^2(x'_1,x'_2) \tag{3.4}$$

Wilson further shows the relation between the intensity distribution to the displacement of the surface.

$$I_T = A^2(x_1,x_2) + A^2(x_1 + u_{1f},x_2 + u_{2f}) \tag{3.5}$$

where

$u_{1f} = Mu_1$

$u_{2f} = Mu_2$

M = Magnification factor

u_1,u_2 - displacements in x_1,x_2 directions

The amplitude transmission function $g(x_1,x_2)$ for a photographic film can be approximated as a linear function of intensity for the ranges of interest, or

$$g(x_1,x_2) = a + bI_T \tag{3.6}$$

where a and b are film constants.

So

$$g(x_1,x_2) = a + b[A^2(x_1,x_2) + A^2(x_1 + u_{1f},x_2 + u_{2f})]$$

Again the Fourier transform of the transmission function must be obtained. For convenience the x_2 coordinate will be suppressed or

$$g(x) = a + b[A^2(x) + A^2(x + u_f)] \tag{3.7}$$

Therefore as in equation 2.15

$$G(w) = \exp\left(\frac{izw^2}{2k}\right) \int g(x) \exp(-iwx)dx \tag{3.8}$$

Wilson has shown that G(w) reduces to

$$G(w) = b \exp\left(\frac{izw^2}{2k}\right) F[A^2][1 + \exp(-iwu_f)] \tag{3.9}$$

where

$$F[A^2] = \int A^2(x) \exp(-iwx)dx \tag{3.10}$$

The intensity in the transform plane is expressed by

$$I_F = G(w) \cdot G^*(w) \tag{3.11}$$

So I_F finally reduces to

$$I_F = 2b^2 F[A^2](1 + \cos(wu_f)) \tag{3.12}$$

and fringes are defined when

$$1 + \cos(wu_f) = 0 \tag{3.13}$$

$$\text{or } wu_f = (2n - 1)\pi \tag{3.14}$$

$$\text{or } u_f = \left(n - \frac{1}{2}\right) \frac{\lambda z}{P} \tag{3.15}$$

An experimental example of this technique is shown in section 4.3.

3.2 Time Average

Again, refer to Figure 13 for this arrangement. A frequency oscillator is used to induce vibration, a single beam of laser light is used to illuminate the object, and a camera records the motion.

The light amplitude can be expressed as [17]

$$\vec{E}(x_1,x_2) = \overline{A}(x_1 + x'_1, x_2 + x'_2) \exp[i(\Theta(x_1,x_2) + \Delta\theta] \tag{3.16}$$

where

x_1, x_2 - film constants

x'_1, x'_2 - function of amplitude of vibration, frequency, time, and location

Θ- phase angle

$\Delta\Theta$- change in phase due to vibration

The film exposure time t is

$$tI_T = \int_0^t \vec{E}(x_1,x_2) \cdot \vec{E}^*(x_1,x_2)dt \tag{3.17}$$

Again, suppress the coordinate notation so

$$tI_T = \int_0^t \vec{E}(x) \cdot \vec{E}^*(x)dt = \int_0^t A(x + x')dt \tag{3.18}$$

Physically x' is related to the frequency of vibration and the time or

$$x' = u_f(x_1,x_2) \sin \omega t \tag{3.19}$$

where u_f is the maximum displacement on the film plane.

Recall

$$g(x) = a + bI_T$$

$$= a + \frac{b}{t} \int_0^t A^2(x + u_f \sin\omega t)dt \tag{3.20}$$

This amplitude transmission function is then Fourier transformed or

$$G(w) = \exp(\frac{izw^2}{2k}) \int g(x) \exp(-iwx)dx \tag{3.21}$$

As before, this expression is evaluated and is a function of the Bessel Function as Wilson has shown [17].

$$G(w) = \frac{b}{tw} \exp(\frac{izw^2}{2k}) F[A^2] J_o (u_f w) \tag{3.22}$$

where F is the Fourier Transform function. Zeros occur when

$$J_o (u_f w) = 0$$

or

$$J_o(\frac{2\pi p u_f}{\lambda z}) = 0 \tag{3.23}$$

Refer to Table I for zeros of the Bessel function. An experimental example is shown in section 4.4.

IV. EXPERIMENTAL VERIFICATION

4.1 Double Exposure Shearing Speckle Interferometry

Consider a cantilever beam with a shift in the z direction only (Figure 14). Equation 2.27 reduces to [16].

$$(2n-1)\lambda = 2[(l_s + l_o)\frac{\partial u}{\partial z} + (m_s + m_o)\frac{\partial v}{\partial z} + (n_s + n_o)\frac{\partial w}{\partial z}]\Delta z \tag{4.1}$$

From figure 14

$l_o = 1$ $\qquad$ $l_s = \cos\theta$

$m_o = 0$ $\qquad$ $m_s = 0$

$n_o = 0$ $\qquad$ $n_s = \sin\theta$

so

$$(n-1/2)\lambda = [(1 + \cos\theta)\frac{\partial u}{\partial z} + \sin\theta\frac{\partial w}{\partial z}]\Delta z \tag{4.2}$$

For a cantilever beam with tip deflection δ, then

$$u = \frac{3\delta}{l^3}[\frac{\nu}{2}(l-z)(x^2 - y^2) - \frac{1}{6}z^3 + \frac{1}{2}lz^2] \tag{4.3}$$

$$w = \frac{3\delta}{l^3}[xy^2 - (lz - \frac{z^2}{2})x] \tag{4.4}$$

$$\frac{\partial u}{\partial z} = \frac{3\delta}{l^3}[\frac{-\nu}{2}(x^2 - y^2) - \frac{1}{2}z^2 + lz] \tag{4.5}$$

$$\frac{\partial w}{\partial z} = \frac{3\delta}{l^3}[-lx + zx] \tag{4.6}$$

Along the center of the beam $y=0$ and $x=.125$ in.

Then

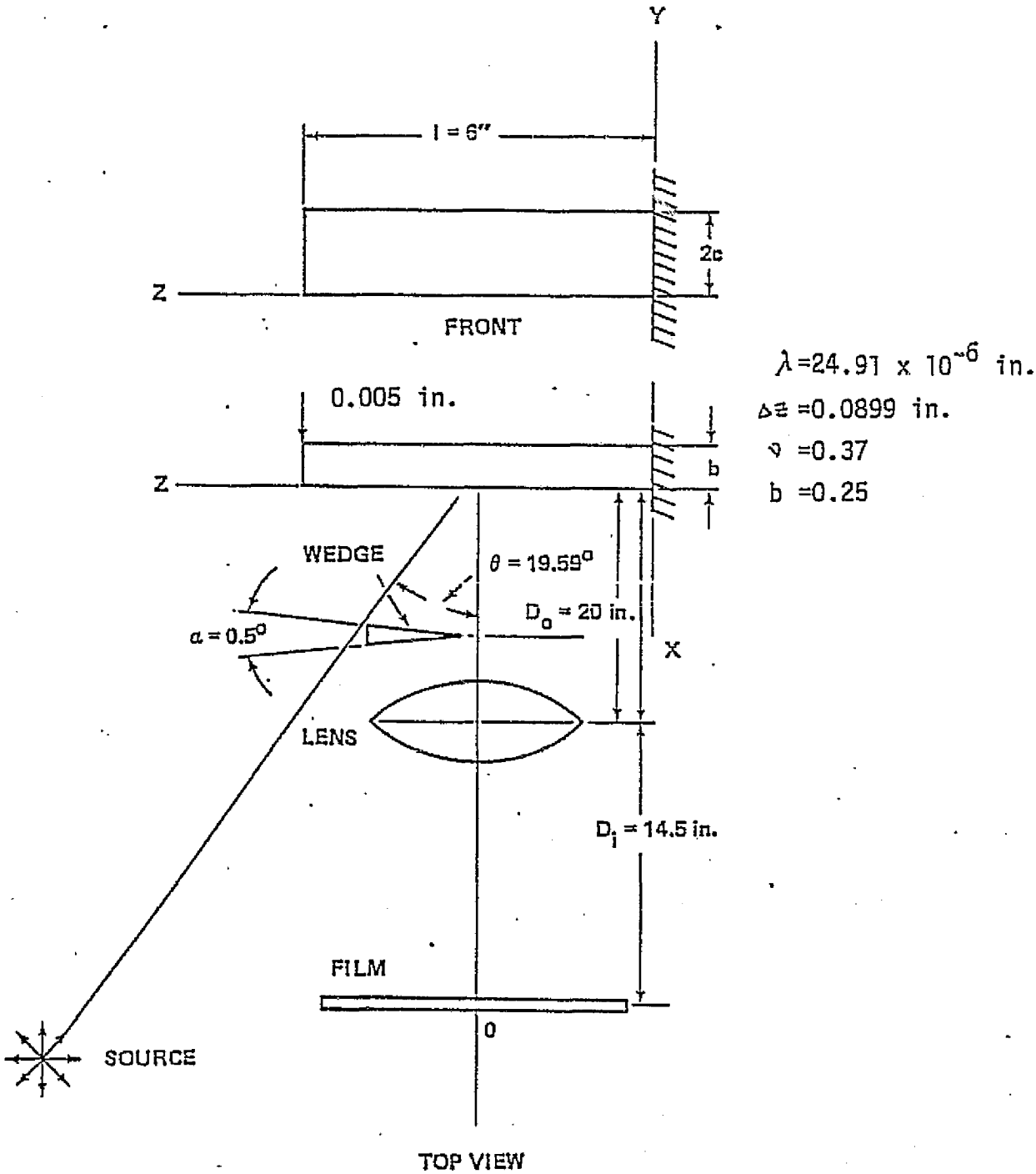

Figure 14. Experimental arrangement for double exposure shearing speckle interferometry.

$$\frac{\partial u}{\partial z} = (-.201 - 34.7z^2 + 416.6z) \times 10^{-6} \tag{4.7}$$

$$\frac{\partial w}{\partial z} = (-52.1 + 8.68z) \times 10^{-6} \tag{4.8}$$

By substituting 4.7 and 4.8, plus the other information, into equation 4.2, a theoretical fringe equation can be obtained as a function of beam length z.

$$(n-\tfrac{1}{2})\lambda = [1.942(-.201 - 34.7z^2 + 416.6z) \times 10^{-6} + 0.335\,(-52.1 + 8.68z) \times 10^{-6}]\,(.0899) \tag{4.9}$$

or

$$n = .436 + 2.93z - .244z^2 \tag{4.10}$$

A shearing speckle photograph was taken and filtered, which is shown in Figure 15.

Using Equation (4.10), a theoretical fringe plot was made and is shown in Figure 16. Using the shearing speckle photograph, the actual fringe order as a function of distance can be found and is plotted on the theoretical curve of Figure 16. The agreement is obvious.

4.2 Shearing Speckle Interferometry Vibration

Again look at Figure 12 and let the object be a cantilever beam with the configeration shown in Figure 17. Nowacki [18] presents a solution for the amplitude of vibration along the beam as

$$W_r(z_1) = C[U(\lambda_r z) - \frac{S(\beta_r)}{T(\beta_r)}\, V(\lambda_r z) \tag{4.11}$$

ORIGINAL PAGE IS
OF POOR QUALITY

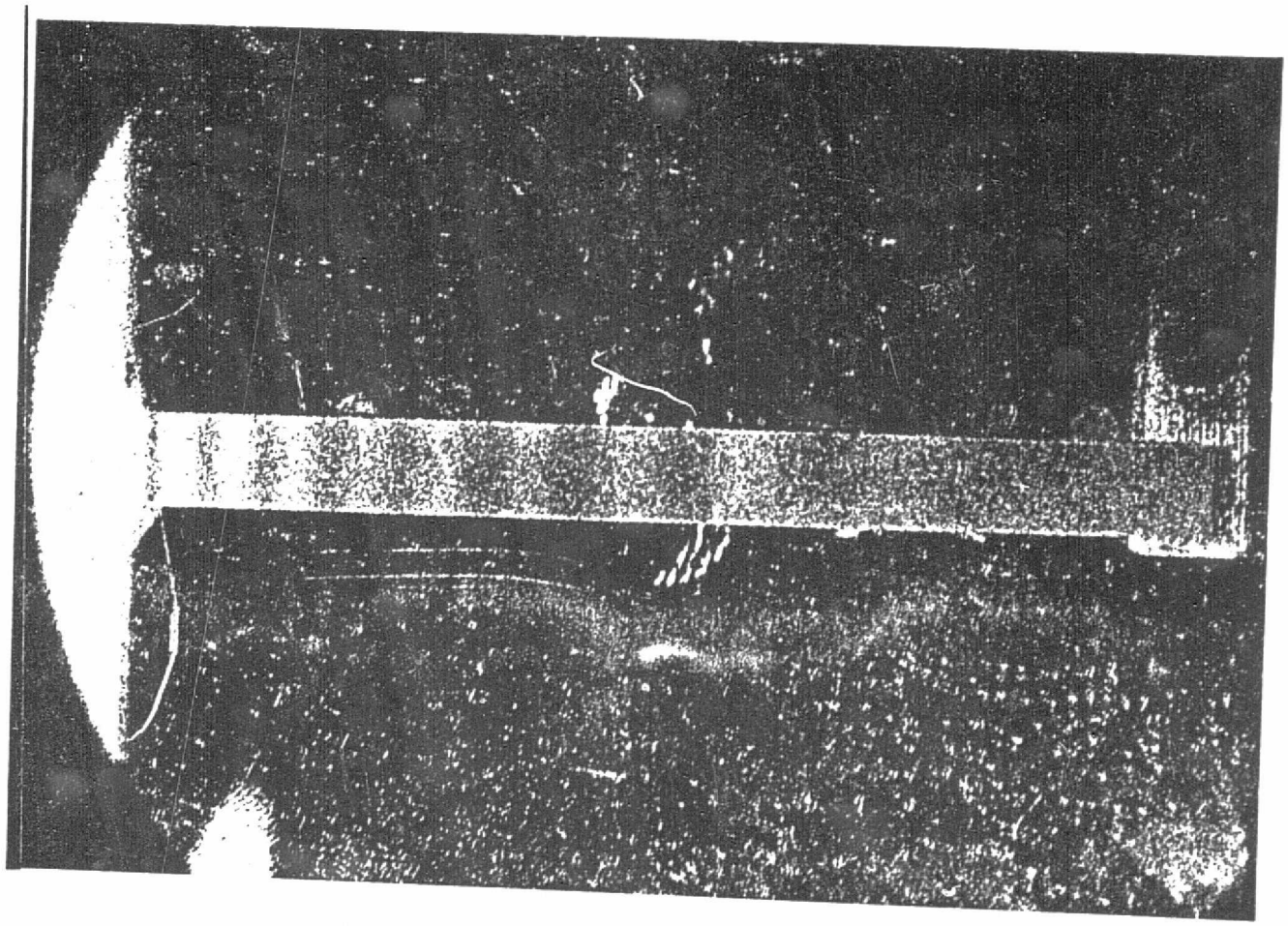

Figure 15. Shearing speckle photograph after Fourier filtering.

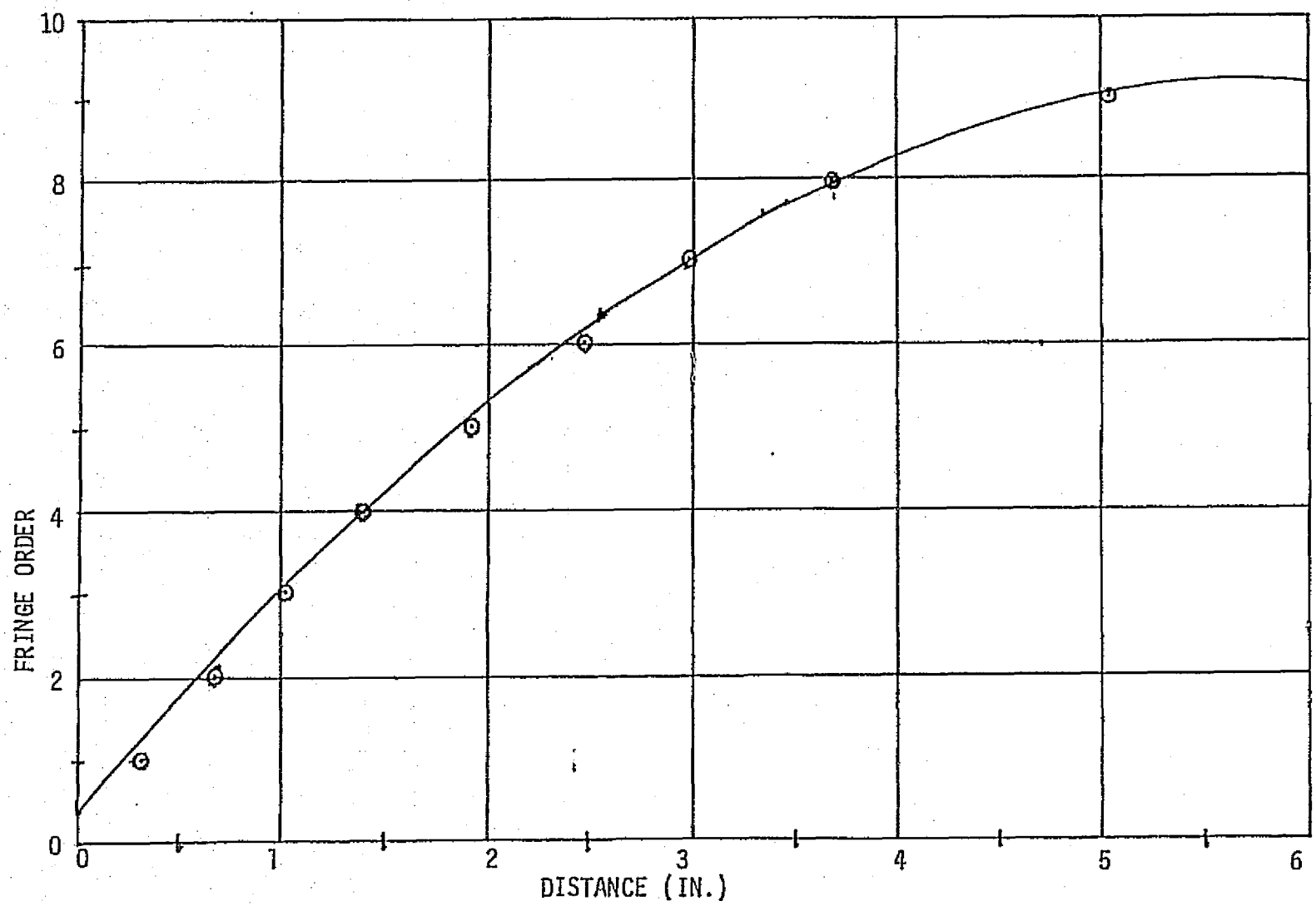

Figure 16. Comparison of theoretical curve and experimental points for double exposure shearing speckle interferometry.

Where

W is the amplitude

C is a constant

$$U(\lambda_r z) = \frac{\cosh\lambda_r z - \cos\lambda_r z}{2}$$

$$V(\lambda_r z) = \frac{\sinh\lambda_r z - \sin\lambda_r z}{2}$$

$$S(\beta_r) = \frac{1}{2}(\cosh\beta_r + \cos\beta_r)$$

$$T(\beta_r) = \frac{1}{2}(\sinh\beta_r + \sin\beta_r)$$

λ_r is wavelength due to vibration

$\beta_r = \lambda_r l$

The transcendental equation for a vibrating cantilever beam is [19]

$$\cosh\beta_r \cos\beta_r = -1 \tag{4.12}$$

The solutions are tabulated in Table 2. For the first mode of vibration r=1 and at z=1

$$W_1(1) = \delta = C[\, U(\beta_1) - \frac{S(\beta_1)}{T(\beta_1)} V(\beta_1)] \tag{4.13}$$

So

$$\frac{W_1}{\delta} = U(\lambda_1 z) - .734\ V(\lambda_1 z) \tag{4.14}$$

for the first mode.

TABLE 2

Solutions for Transcendental Equation for Vibrating Cantilever Beam

β_r
1.875
4.694
7.855
10.996
14.137

Taking the derivative of W_1 (1) the $\frac{\partial u}{\partial z}$ term can be found.

$$\frac{1}{\delta}\frac{\partial u}{\partial z} = \frac{\lambda_1}{2}[(\sinh(\lambda_1,z) + \sin(\lambda_1,z)) - (.734(\cosh(\lambda_1,z) - \cos(\lambda_1,z))] \tag{4.15}$$

A cantilever beam with dimensions and properties shown in Figure 17 was vibrated in the first mode, with two different tip deflections, and shearing speckle photographs were taken. These photographs were Fourier filtered and drawings are shown in Figure 18.

From Equation (2.47)

$$\frac{1}{\delta}\frac{\partial u}{\partial z} = \frac{\Phi_i \quad \lambda}{2\pi(1+\cos\beta)\Delta z} \tag{4.16}$$

From the theoretical equation (4.15) a curve is drawn in Figure 19; the data points are plotted on this curve. The agreement is obvious.

l = 7 in.
b = .75 in.
Δz= 0.2456 in.
λ_1= 50 cycles per second

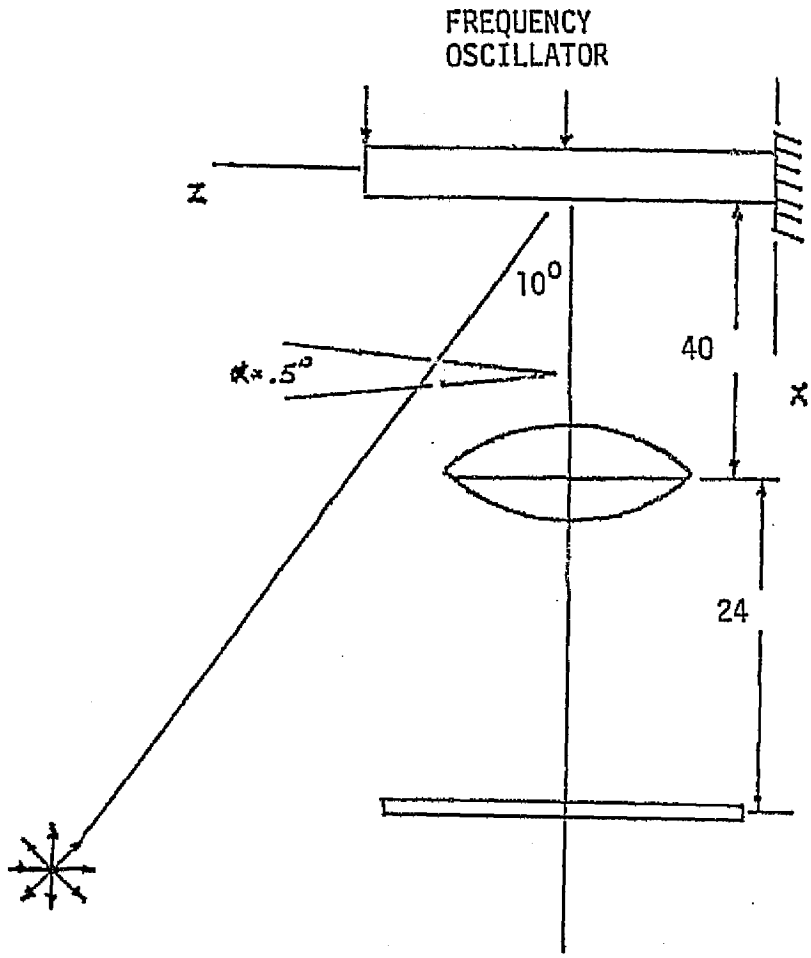

Figure 17. Experimental arrangement for vibration shearing speckle.

PRECEDING PAGE BLANK NOT FILMED

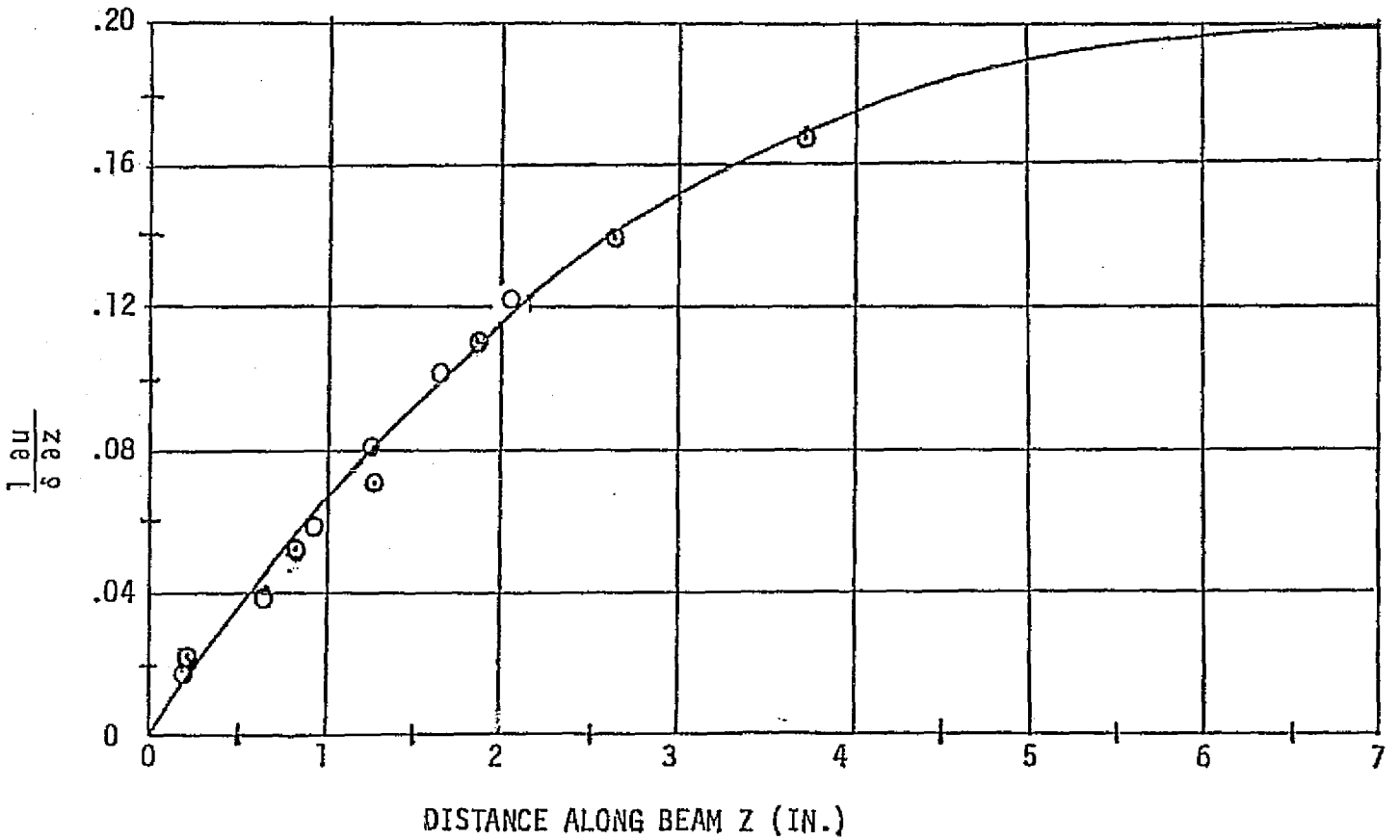

Figure 19. Plot of theoretical curve and experimental points for vibration shearing speckle. O $\delta=1.2\times10^{-3}$ ⊙ $\delta=8.8\times10^{-3}$

PRECEDING PAGE BLANK NOT FILMED

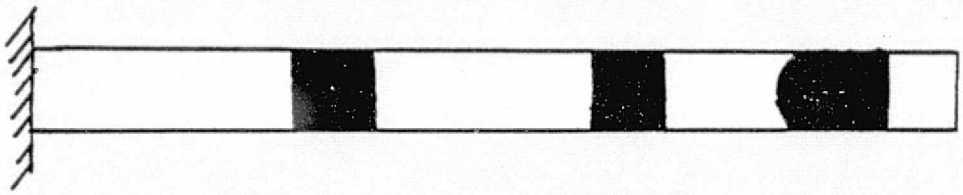

δ = .003

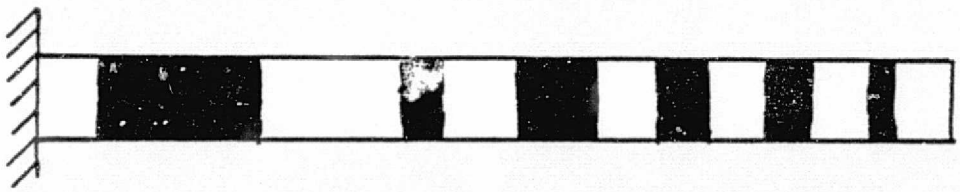

δ =.006

Figure 21. Drawing of the Fourier transformed image for single beam speckle double exposure.

PRECEDING PAGE BLANK NOT FILMED

4.4 Single Beam Speckle Vibration

Figure 23 shows the experimental configuration used. Again using the solution by Nowacki [18] for the first mode

$$\frac{W}{\delta} = U(\lambda_1, z) - .734\ V(\lambda_1, z) \tag{4.20}$$

This gives a theoretical curve for the vibration amplitude. Recall Equation (3.23)

$$J_0(2\pi p u_f/\lambda z) = 0 \tag{4.21}$$

For the point-by-point data reduction (Figure 24), the distance between the first two fringes is the zero of the Bessel function giving

$$2\pi p u_f/\lambda z = 2.40 \tag{4.22}$$

For the distance between the second outer fringes, the second zero of the Bessel function gives

$$2\pi p u_f/\lambda z = 5.52 \tag{4.23}$$

Table 3 gives the results of the data reduction. Notice at $z = 4.95$ in. through 6.67 in., the second outer fringes were used, thus the change in the constant relating displacement to fringe spacing.

Figure 25 shows a plot of the experimental and the theoretical displacement curve. Again the agreement is obvious .

PRECEDING PAGE BLANK NOT FILMED

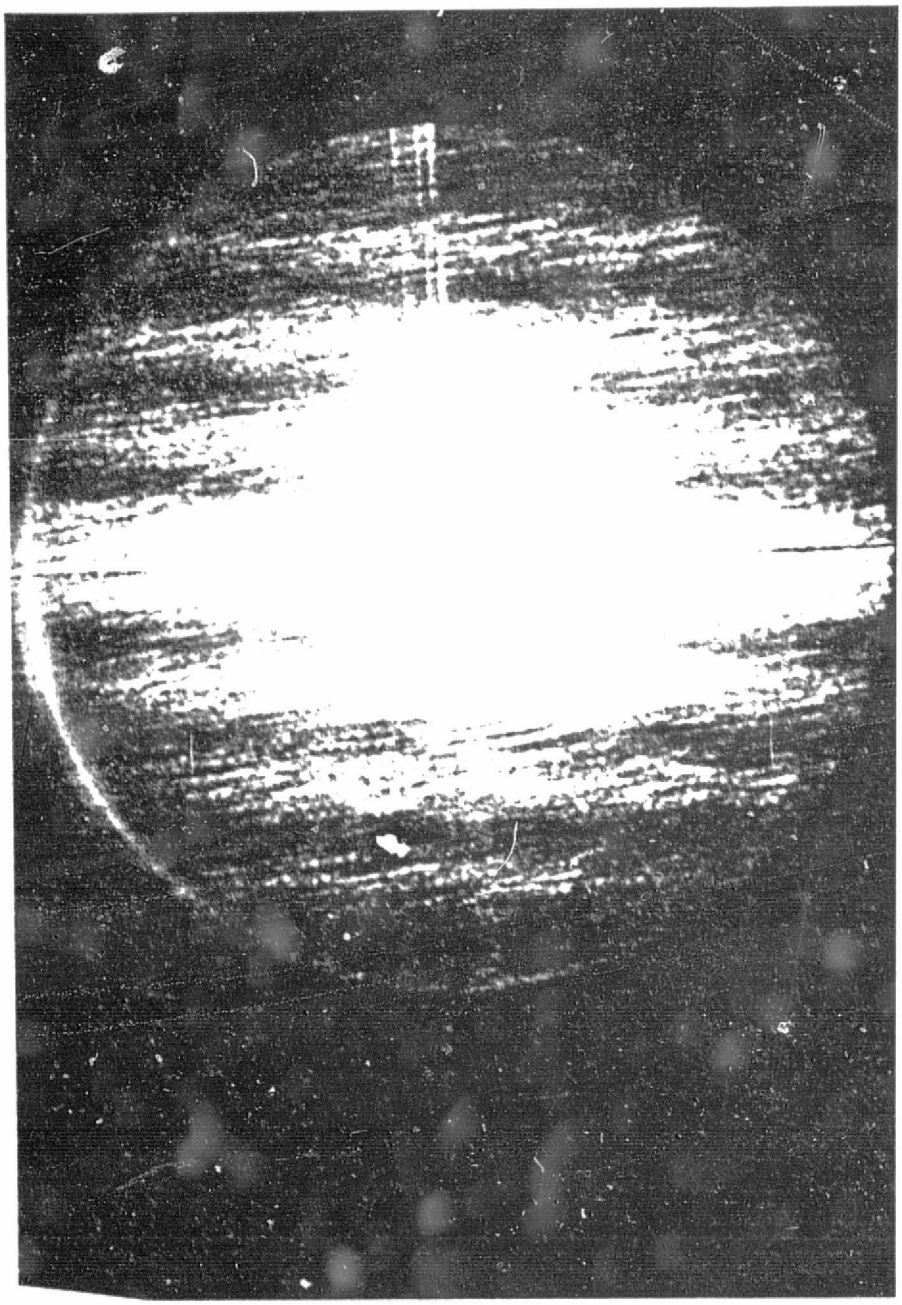

Figure 24. Sample of Point by Point Data.

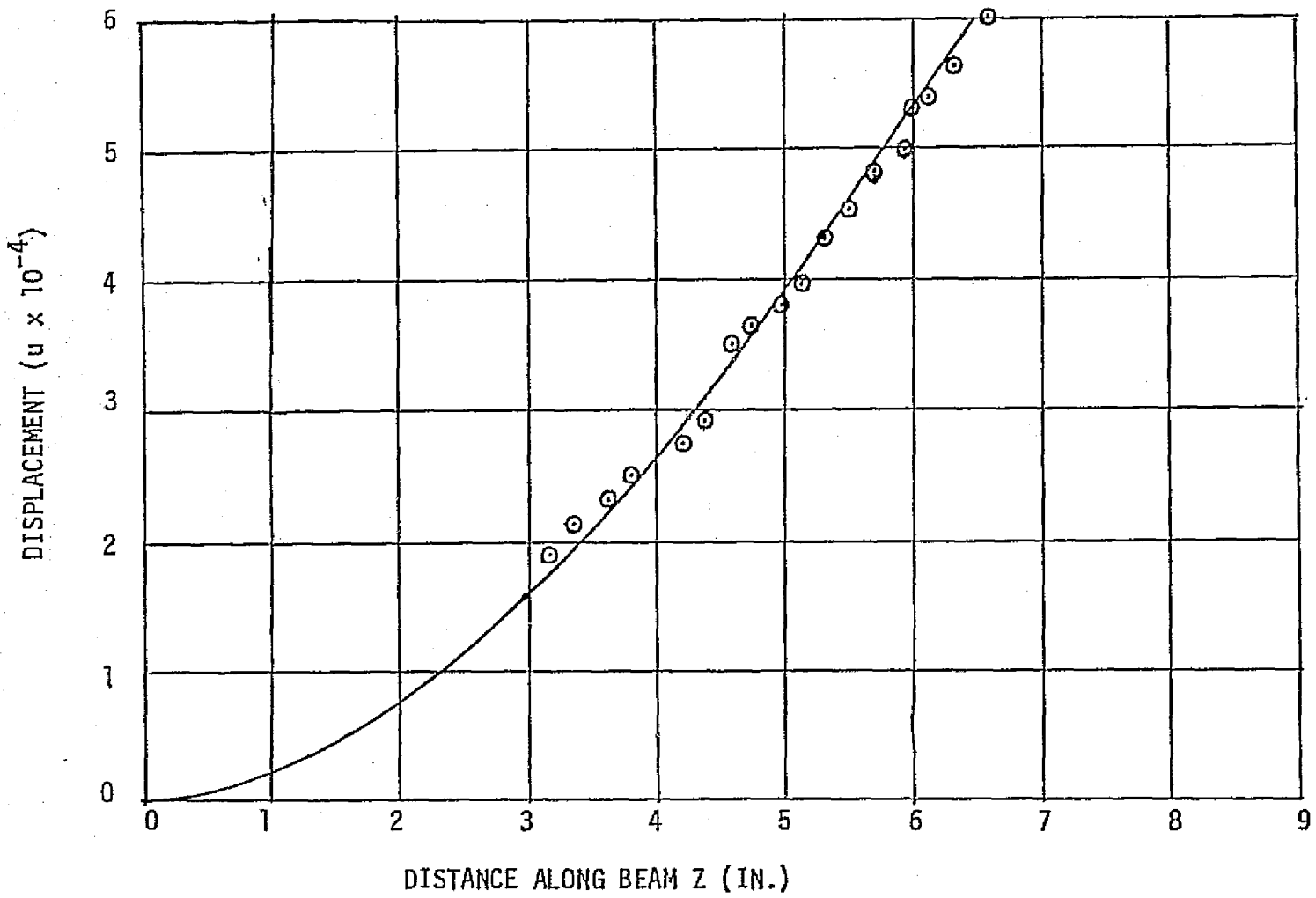

Figure 25. Theoretical curve and experimental points for vibration single beam speckle.

TABLE 3

DATA REDUCTION FOR VIBRATION SPECKLE

Model Location	X Model	u_f Model
2.86	4.50	1.56×10^{-4}
3.14	3.56	1.98×10^{-4}
3.33	3.14	2.24×10^{-4}
3.62	2.95	2.39×10^{-4}
3.81	2.78	2.53×10^{-4}
4.00	2.57	2.74×10^{-4}
4.19	2.5	2.82×10^{-4}
4.38	2.38	2.96×10^{-4}
4.57	1.92	3.67×10^{-4}
4.76	1.85	3.80×10^{-4}
4.95	4.08	3.97×10^{-4}
5.14	3.89	4.16×10^{-4}
5.33	3.60	4.50×10^{-4}
5.52	3.39	4.78×10^{-4}
5.71	3.20	5.06×10^{-4}
5.90	3.10	5.23×10^{-4}
6.09	2.90	5.59×10^{-4}
6.29	2.76	5.87×10^{-4}
6.47	-	-
6.67	2.70	6.00×10^{-4}

V. CONCLUSIONS AND RECOMMENDATIONS

The speckle effect has been noticed for several years by many investigators. The theory for shearing speckle and single beam interferometry was developed.

Shearing speckle, like holography, is dependent upon a phase change. In general, for a shear in one direction at least two derivations of displacement terms are combined in the fringe pattern. Experimentally shearing speckle is simple to set up, and for double exposure the fringes are easy to transform. For time average analysis, the fringes are difficult to transform. For this type of experimental work time average holography yields much clearer fringes, and with photopolymer recording, natural frequencies of complex vibrating objects can be found.

Single beam speckle interferometry is dependent upon an amplitude change. This technique is very simple to set up experimentally, yielding two in-plane displacement components. For time average, single beam speckle can be used to determine the amplitude of motion, even for thin structures.